MECHANISM OF SULFUR POISONING BY H_2S AND SO_2 OF NICKEL AND COBALT BASED CATALYSTS FOR DRY REFORMING OF METHANE

A Thesis Submitted to the College of

Graduate Studies and Research

in Partial Fulfillment of the Requirements

for the Degree of Master of Science

in the Department of Chemical and Biological Engineering

University of Saskatchewan

Saskatoon

By

Francisco Javier Pacheco Gómez

PERMISSION TO USE

In presenting this thesis in partial fulfillment of the requirements for a Postgraduate degree from the University of Saskatchewan, I agree that the Libraries of this University may make it freely available for inspection. I further agree that permission for copying of this thesis/dissertation in any manner, in whole or in part, for scholarly purposes may be granted by Professor Hui Wang who supervised my thesis work. It is understood that any copying or publication or use of this thesis or parts for financial gain shall not be allowed without my written permission. It is also understood that due recognition shall be given to me and to the University of Saskatchewan in any scholarly use which may be made of any material in my thesis.

DISCLAIMER

The University of Saskatchewan was exclusively created to meet the thesis and/or exhibition requirements for the degree of Master of Science at the University of Saskatchewan. Reference in this thesis to any specific commercial products, process, or service by trade name, trademark, manufacturer, or otherwise, does not constitute or imply its endorsement, recommendation, or favouring by the University of Saskatchewan. The views and opinions of the author expressed herein do not state or reflect those of the University of Saskatchewan, and shall not be used for advertising or product endorsement purposes. Requests for permission to copy or to make other uses of materials in this thesis in whole or part should be addressed to:

Department Head

Department of Chemical and Biological Engineering

University of Saskatchewan

College of Engineering

57 Campus Drive

Saskatoon, SK S7N 5A9

Canada

Or

Dean

College of Graduate Studies and Research

University of Saskatchewan

107 Administration Place

Saskatoon, Saskatchewan S7N 5A2

Canada

ABSTRACT

Nickel catalysts employed in the production of syngas throughout CO_2 reforming of CH_4 can be poisoned and deactivated by the presence of H_2S or SO_2 found in the feedstock. It is necessary to understand the poisoning mechanism to develop more resistant catalysts. The effect of sulfur poisoning by H_2S and SO_2 on the mechanism of carbon dioxide reforming of methane was studied for Ni/AlMgOx, Ni-Co/AlMgOx and Co/AlMgOx catalysts prepared by coprecipitation and impregnation methods. The method employed for mechanism study was Diffuse Reflectance Infrared Fourier Transform Spectroscopy (DRIFTS). DRIFTS made possible to observe that the mechanism of carbon dioxide reforming of methane reaction involved: 1) methane adsorption and possibly dissociation into C, CH_x and H_2; 2) carbon dioxide adsorption and dissociation into CO; 3) formation of carbonates that could occur after CO_2 attaches to an oxygen atom or after CO binds to two oxygen atoms present in the catalyst surface. It was found a relation ship between the concentration of carbonates and adsorbed CO.

The presence of H_2S in reacting gasses caused a decrease in the intensity of the methane and CO_2 absorption bands on the nickel (Ni)-monometallic catalysts, suggesting that H_2S blocks the nickel active sites. Also, H_2S caused a decrease in the OH^- species, suggesting that NiS was formed. The band at 2077 cm^{-1}, attributed to linear carbonyl, was replaced by two bands located at 2071 and 2051 cm^{-1}, which are assigned to carbonyl sulfide produced by the reaction $H_2S + CO_2 \rightleftharpoons COS + H_2O$ on the catalyst surface. When SO_2 interacted with the catalysts, a band at about 1358 cm^{-1} was observed, which is assigned to sulfate species. SO_2 also caused a decline in the concentration of carbonates and adsorbed CO. This study allowed a better understanding of the poisoning mechanism by H_2S and SO_2.

ACKNOWLEDGEMENTS

I want to thank all the people and organizations that made the completion of this thesis possible. Firstly, I want to deeply thank my supervisor Dr. Hui Wang for accepting my application to the Master of Science in Chemical Engineering program at the University of Saskatchewan. I appreciate his guidance throughout this journey and also his financial support.

I recognize the valuable suggestions received from the members of the advisory committee, Dr. Lifeng Zhang and Dr. Yongfeng Hu. Additionally, I thank Dr. Stephen Foley for accepting to be the external examiner for my thesis defense.

I appreciate the scholarship provided by CONACYT throughout the official length of my studies. It allowed me to focus on my studies without financial concerns.

I feel grateful for the help received from Kelly Bader to complete my application. She was the first staff member from the University of Saskatchewan I had communication with. Her help and kindness were very valuable to complete the application to the program.

I also acknowledge Wahab Alabi, Mohsen Shakouri and Armin Moniri for helping me to answer questions and showing me their knowledge in the laboratory.

My gratitude also goes to Richard Blondin for providing technical support for devices and instruments and to RLee Prokopishyn for helping to fix devices whenever it was needed.

DEDICATION

I dedicate this thesis to my parents for supporting me financially and for encouraging me to study and take important decisions in life. Also, I dedicate this thesis to myself for having the strength to begin, continue and finish this journey in spite of hard and sometimes discouraging challenges.

TABLE OF CONTENTS

PERMISSION TO USE.....i

ABSTRACT.....iii

ACKNOWLEDGMENTS.....iv

DEDICATION.....v

TABLE OF CONTENTS.....vi

LIST OF TABLES.....x

LIST OF FIGURES.....xi

NOMENCLATURE AND ABBREVIATIONS.....xv

CHAPTER 1. INTRODUCTION.....1

1.1 OVERVIEW.....1

1.2 PREVIOUS RESEARCH MADE BY DR. HUI WANG'S GROUP.....3

1.3 MOTIVATION TO CARRY OUT THIS THESIS.....5

1.4 ORGANIZATION OF THE THESIS.....6

CHAPTER 2. LITERATURE REVIEW.....8

2.1 REFORMING OF METHANE.....8

2.2 COMMERCIAL PROCESSES FOR THE PRODUCTION OF SYNGAS.....11

2.2.1 CALCOR process.....11

2.2.2 SPARG process.....12

2.3 DRY REFORMING OF METHANE.....13

2.3.1 Environmental aspects for dry reforming of methane.....13

2.3.2 Obtainment of reactants for dry reforming of methane.....14

2.3.3 Thermodynamic analysis.....16

2.3.4 Mechanisms reported for dry reforming of methane.....18

2.3.5 Catalysts used for dry reforming of methane.....22

2.3.5.1 Nickel-based catalysts.....22

2.3.5.2 Cobalt-based catalysts.....24

2.3.6 Catalyst deactivation.....25

2.3.6.1 H_2S poisoning.....27

2.3.6.2 SO_2 poisoning.....29

2.3.7 Regeneration of catalysts after sulfur poisoning.....31

2.4 KNOWLEDGE GAPS, HYPOTHESES AND RESEARCH OBJECTIVES.....32

2.4.1 Knowledge gaps.....32

2.4.2 Research objectives.....32

2.4.3 Hypotheses.....32

CHAPTER 3. EXPERIMENTAL SET-UP AND PROCEDURE.....33

3.1 SAFETY PRECAUTIONS.....33

3.2 CATALYST PREPARATION METHODS.....34

3.2.1 Coprecipitation method.....34

3.2.2 Impregnation method.....35

3.3 CATALYST CHARACTERIZATION.....36

3.4 PROCEDURE OF DRIFTS EXPERIMENTS.....37

CHAPTER 4. RESULTS AND DISCUSSION.....40

4.1 MECHANISM OF CH_4 ADSORPTION AND DISSOCIATION.....40

4.2 MECHANISM OF CO_2 ADSORPTION AND DISSOCIATION.....44

4.3 MECHANISM OF DRY REFORMING OF METHANE.....52

4.4 EFFECT OF H_2S ON DRY REFORMING OF METHANE.....56

4.4.1 Independent interactions of H_2S with the catalysts.....56

4.4.2 Adsorptions of CH_4 and CO_2 in the presence of H_2S.....59

4.4.3 Formation of carbonyl sulfide in the presence of H_2S.....70

4.4.4 Proposed mechanism for H_2S poisoning.....71

4.5 EFFECT OF SO_2 ON DRY REFORMING OF METHANE.....72

4.5.1 Independent interactions of SO_2 with the catalysts.....73

4.5.2 Adsorptions of CH_4 and CO_2 in the presence of SO_2.....77

4.5.3 Proposed mechanism for SO_2 poisoning.....89

CHAPTER 5. CONCLUSIONS AND RECOMMENDATIONS.....91

5.1 CONCLUSIONS.....91

5.1.1 Mechanism of dry reforming of methane……..…...91

5.1.2 Effect of H_2S on dry reforming of methane……..……..…..92

5.1.3 Effect of SO_2 on dry reforming of methane…….……...……..93

5.2 RECOMMENDATIONS 93

REFERENCES.....95

APPENDIX A: FUNDAMENTALS OF FTIR SPECTROSCOPY……..…….....108

APPENDIX B: WAVENUMBERS OF FUNCTIONAL GROUPS……..…….....116

LIST OF TABLES

1-1. Metal and metal oxide content after reduction measured by the curve fitting of XANES…….....……5

2-1. Reforming of methane reactions to produce syngas…….……...…..……..…….9

2-2. Side reactions during reforming of methane……...……..……11

2-3. Mechanisms reported in the literature for dry reforming of methane……..…….**.....**19

2-4. Chemical composition of natural gas……..……..…….....27

2-5. Mechanism steps for H_2S chemisorption and dissociation…….……...…….…....28

3-1. Comparison of methods for catalyst preparation…..……...……...35

3-2. Catalysts tested in this research work……..……...……...…….36

3-3. BET properties of the catalysts tested in this research work……..……..…..…37

3-4. Metal compositions of the catalyst precursors measured by ICP……...……..….37

B-1. Vibrations attributed to OH^- functional groups…….....…....116

B-2. Vibrations attributed to carbonates…….....……116

B-3. Vibrations attributed to H_2S or species produced by H_2S……...……..…..116

B-4. Vibrations attributed to SO_2 or species produced by SO_2……...……...…..117

B-5. Vibrations attributed to carbonyl sulfide……..……...……117

B-6. Vibrations attributed to CH_4……...……...……..……117

B-7. Vibrations attributed to CO_2……..……...…….……..118

B-8. Vibrations attributed to CO……..……118

LIST OF FIGURES

2-1. Simplified process flow of CALCOR standard process…….....…….…....12

2-2. Process flow of SPARG process……..…….…….....13

2-3. Greenhouse gas emissions in the US in 2013……...……..…..……14

2-4. US Carbon dioxide emissions by source……...……..…….14

2-5. US methane emissions by source…….……...……15

2-6. Reaction equilibrium constants as a function of temperature for some of the reactions related to dry reforming of methane……..……..…...……..17

2-7. Possible SO_2 interactions with alumina…….…….....30

3-1. Pictorial representation of DRIFTS experimental setup……...…..…..39

3-2. Top view of the DRIFTS accessory showing the trajectory of the infrared light……..…..39

4-1. Comparison of bands produced by CH_4 on coprecipitated catalysts and support……...42

4-2. Comparison of bands produced by CH_4 on impregnated catalysts and support……...43

4-3. Antisymmetric mode of CO_2……..……..45

4-4. Bands produced by adsorbed CO_2 on coprecipitated catalysts and support…….....46

4-5. Bands produced by adsorbed CO_2 on impregnated catalysts and support…….....47

4-6. Broad band attributed to carbonates for coprecipitated and impregnated catalysts after the interaction with CO_2…….……..…..48

4-7. Carbonates formed after CO interacted with the catalysts at 600 ^oC……..……50

4-8. Band at 2077 cm^{-1} attributed to linear carbonyl for coprecipitated and impregnated catalysts in the presence of CO_2…….……..……...…….51

4-9. Coadsorption of CH_4 and CO_2 before the introduction of H_2S…….....53

4-10. Coadsorption of CH_4 and CO_2 before the introduction of SO_2……..……54

4-11. OH^- consumption in the presence of H_2S…….....…..…….…..58

4-12. Bands attributed to CO_2 (a) and CH_4 (b, c, d) displayed before introducing H_2S, 3 hours after introducing H_2S and 1 hour after stopping the H_2S flow for CopCat-Ni4…….....61

4-13. Bands attributed to CO_2 (a) and CH_4 (b, c, d) displayed before introducing H_2S, 3 hours after introducing H_2S and 1 hour after stopping the H_2S flow for ImpCat-Ni5……..…….62

4-14. Bands attributed to CO_2 (a) and CH_4 (b, c, d) displayed before introducing H_2S, 3 hours after introducing H_2S and 1 hour after stopping the H_2S flow for CopCat-Co6…….....63

4-15. Bands attributed to CO_2 (a) and CH_4 (b, c, d) displayed before introducing H_2S, 3 hours after introducing H_2S and 1 hour after stopping the H_2S flow for ImpCat-Co5……...……64

4-16. Bands attributed to CO_2 (a) and CH_4 (b, c, d) displayed before introducing H_2S. 3 hours after introducing H_2S and 1 hour after stopping the H_2S flow for CopCat-Ni2Co4…….....65

4-17. Bands attributed to CO_2 (a) and CH_4 (b, c, d) displayed before introducing H_2S, 3 hours after introducing H_2S and 1 hour after stopping the H_2S flow for ImpCat-Ni2Co3…….....66

4-18. Bands attributed to CO_2 (a) and CH_4 (b, c, d) displayed before introducing H_2S, 3 hours after introducing H_2S and 1 hour after stopping the H_2S flow for $MgAlO_x$ support…….....67

4-19. Decrease in the concentration of carbonates in the presence of H_2S…….…….....68

4-20. Carbonyl sulfide instead of carbonyl produced in the presence of H_2S……..……..……70

4-21. Bands attributed to physisorbed SO_2 and sulfate species……..…….....74

4-22. Negative peak at the OH^- region seen after the interaction of SO_2…….…….**.....**76

4-23. Bands attributed to CO_2 (a) and CH_4 (b, c, d) displayed before introducing SO_2, 3 hours after introducing SO_2 and 1 hour after stopping the SO_2 flow for ImpCat-Ni5…….....**.....**78

4-24. Bands attributed to CO_2 (a) and CH_4 (b, c, d) displayed before introducing SO_2, 3 hours after introducing SO_2 and 1 hour after stopping the SO_2 flow for CopCat-Ni4…….…...79

4-25. Bands attributed to CO_2 (a) and CH_4 (b, c, d) displayed before introducing SO_2, 3 hours after introducing SO_2 and 1 hour after stopping the SO_2 flow for CopCat-Co6……...80

4-26. Bands attributed to CO_2 (a) and CH_4 (b, c, d) displayed before introducing SO_2, 3 hours after introducing SO_2 and 1 hour after stopping the SO_2 flow for ImpCat-Co5……...……81

4-27. Bands attributed to CO_2 (a) and CH_4 (b, c, d) displayed before introducing SO_2, 3 hours after introducing SO_2 and 1 hour after stopping the SO_2 flow for CopCat-Ni2Co4…….**.....**82

4-28. Bands attributed to CO_2 (a) and CH_4 (b, c, d) displayed before introducing SO_2, 3 hours after introducing SO_2 and 1 hour after stopping the SO_2 flow for ImpCat-Ni2Co3…….83

4-29. Bands attributed to CO_2 (a) and CH_4 (b, c, d) displayed before introducing SO_2, 3 hours after introducing SO_2 and 1 hour after stopping the SO_2 flow for $MgAlO_x$ support……..……84

4-30. The impact of the presence of SO_2 on CO species for various catalysts…….……85

4-31. Concentration of carbonates before, in and after the presence of SO_2……...……..86

4-32. Decrease of the concentration of carbonates after the introduction of SO_2……..…88

A-1. The electromagnetic spectrum……...…….**.....**108

A-2. Stretching vibrations (symmetrical and asymmetrical) of the CO_2 molecule…….**.....**110

A-3. Bending vibrations for a CH_2 group ……..……..…..111

NOMENCLATURE AND ABBREVIATIONS

BET: Brunauer–Emmett–Teller.

CopCat-Ni4: Coprecipitated monometallic nickel catalyst.

CopCat-Ni2Co4: Coprecipitated bimetallic Ni-Co catalyst.

CopCat-Co6: Coprecipitated monometallic cobalt catalyst.

C_p: Heat capacity at mole-constant pressure.

DRIFTS: Diffuse Reflectance Infrared Fourier Transform Spectroscopy.

DRM. Dry reforming of methane.

FTIR: Fourier-Transform Infrared Spectroscopy.

ICP: Inductively Coupled Plasma.

ImpCat-Ni5: Impregnated monometallic nickel catalyst.

ImpCat-Ni2Co3: Impregnated bimetallic Ni-Co catalyst.

ImpCat-Co5: Impregnated monometallic cobalt catalyst.

***K*:** Reaction equilibrium constant.

MSDS: Material Safety Data Sheets.

OH^-: Hydroxyl functional group.

XANES: X-ray Absorption Near Edge Spectroscopy.

R: Gas constant (J/mol K).

ΔG^o**:** Standard Gibbs free-energy change (J/mol).

ΔH^o: Standard enthalpy change (J/mol).

ΔS^o: Standard entropy change (J/mol K).

$\sum(\nu_i C_{p,i})$**:** Sum of heat capacities of chemical species multiplied by their stoichiometric coefficients.

CHAPTER 1. INTRODUCTION

1.1 OVERVIEW

Carbon dioxide reforming of methane, also known as dry reforming of methane or DRM ($CO_2 + CH_4 \rightarrow 2CO + 2H_2$), generates syngas, which is a gaseous mixture appropriate for the production of valuable chemicals (Bitter et al., 2000). The complete process to convert natural gas into valuable liquid products such as methanol and dimethyl ether is called Gas to Liquids (GTL) Technology. In this process, the production of syngas is the part of the process that requires more capital investment, ranging from 50 to 75% of the plant investment (Christensen et al., 1998).

Syngas can be produced from any feedstock containing carbon such as coal, petroleum, coke, hydrocarbons, and biomass. Among these options, the cheapest processes to produce syngas use natural gas as feedstock (Wilhelm et al., 2001). The reactants for dry reforming of methane can also be obtained from biogas, which is a mixture of methane and carbon dioxide with trace quantities of nitrogen, hydrogen sulfide, ammonia and other compounds. Biogas is produced by anaerobic digestion of biomass. The CO_2 reforming of CH_4 reaction is environmentally friendly because it turns two greenhouse gases into useful and valuable chemicals (Ruckenstein and Hu, 1995). The utilization of biogas would help to decrease a wide variety of contaminants that are dangerous to human health. Therefore, a significant motivation exists to use biogas as soon as it is generated for energy applications (Saha et al., 2014).

Catalysts made with most of the metals from Group VIII are active for the reaction according to Fischer and Tropsch in 1928. Transition metals such as Ru, Rh, Ni, Pd and Pt have also been tested (Bitter et al., 2000).

Nickel-based catalysts are seen with interest from the industrial perspective due to their low cost and high availability (Cui et al., 2007). However, sulfur poisoning is one of the biggest challenges for nickel catalysts that interferes with their activity (Sehested, 2003).

Both carbon formation and sulfur poisoning can block active sites in the catalyst. Sulfur molecules can inhibit the catalyst at concentrations as low as in the ppb order (Hashemnejad and Parvari, 2011). The capacity to adsorb sulfur is an important characteristic of the catalyst (Sehested, 2003). Different variables such as the sulfur-containing compound, the composition of the catalyst and, the conditions of operation determines the degree of sulfur poisoning. (Ashrafi et al., 2008).

There are two options to overcome sulfur poisoning: 1) to purify the feed to low levels of sulfur compounds (even as small as in the ppb order) or 2) to develop catalysts that maintain their activity in the presence of sulfur compounds. The separation of sulfur from the gas stream before the reforming reaction would represent a high percentage of operating costs and therefore, the second approach is preferred (Rangan et al., 2011).

It is reported that sulfur adsorbs on the catalysts as metal sulfides, but suitable identification of sulfur species on the deactivated catalysts has been of great importance (Chen et al., 2010). The catalysts can be deactivated not only by the formation of metal sulfides but also by the formation

of sulfates on the support. The formation of sulfates can change the crystal arrangement, thus impacting the metal-support synergy. The capacity for every catalyst to reverse this mechanism depends on its composition (Jones et al., 2003).

This study will help to determine the effect of H_2S and SO_2 on Ni-Co/AlMgOx, Ni/AlMgOx and Co/AlMgOx catalysts during dry reforming of methane. The catalysts will be tested for dry reforming of methane before, in and after the presence of H_2S and SO_2. Diffuse Reflectance Infrared Fourier Transform Spectroscopy (DRIFTS) will be used to determine the species adsorbed on the surface of the catalysts.

1.2 PREVIOUS RESEARCH MADE BY DR. HUI WANG'S GROUP

Previous work done under Dr. Hui Wang's supervision at the University of Saskatchewan has generated deep insight into the catalyzed CO_2 reforming of methane.

It was reported by Zhang et al. (2007) that, among bimetallic coprecipitated catalysts containing nickel with either Co, Fe, Cu and Mn supported on AlMgOx, the Ni-Co/AlMgOx catalyst was the best regarding activity, stable operation and low carbon formation. This superior performance was attributed to its high surface area, small pore size, high-extent reducibility and strong metal-support interaction. Carbon Sciences Inc, in Santa Barbara, USA obtained an exclusive license from University of Saskatchewan to use the Ni-Co/AlMgOx catalyst in 2010. Additionally, the catalyst was patented in July 2011 for the production of syngas (US patent 7, 985, 710).

Zhang et al. (2008a) tested different Ni/Co ratios for the dry reforming of methane reaction and found that the best ratios are between 0.6 and 1.5. Also, the best metal dispersion and smaller

metal particles are found in lower Ni-Co content. They concluded that Ni-Co catalysts with a ratio approximate to 1 and lower metal content had higher activity and stability and insignificant carbon formation since they have smaller particles that suppress carbon deposition.

On the basis that particle sizes and metal-support interaction are the most influential factors for carbon resistance in catalysts, Zhang et al. (2008a) studied the calcination temperature to determine its effect on particle size and metal-support interaction. They discovered that low calcination temperature such as 400 ^{o}C allowed the formation of particles with small sizes but lacking strong metal-support interaction. On the contrary, by increasing the temperature up to 1100 ^{o}C, larger particles were produced and the catalyst had stronger metal-support interaction. It was concluded that a calcination temperature between 700-900 ^{o}C was better for Ni-Co/AlMgOx for dry reforming of methane.

Finally, Zhang et al. (2008b) studied the kinetics of dry reforming of methane using Ni-Co/AlMgOx in the range 650-750 ^{o}C. It was suggested that the dissociation of methane and the reaction between carbon and adsorbed CO_2 are the rate-determining steps.

Shakouri (2011) studied the effect of Ni-Co ratios and H_2S poisoning on the performance of catalysts for dry reforming of methane. He prepared bimetallic Ni-Co/AlMgOx catalysts as well as monometallic Ni/AlMgOx and Co/AlMgOx catalysts using coprecipitation and impregnation methods. Catalysts with higher nickel content showed higher resistance to H_2S poisoning. Moreover, the bimetallic and nickel monometallic catalysts prepared by impregnation regenerated better after the interaction of H_2S than the catalysts prepared by coprecipitation.

X-Ray Absorption Near-Edge Spectroscopy (XANES) determined the reduction extent of nickel and cobalt oxides. The reduction took place at 750 ^{o}C for 4 hours by a H_2/He mixture. This technique determined the composition of nickel and cobalt in its reduced and oxidized forms as shown in Table 1-1.

Table 1-1. Metal and metal oxide content after reduction measured by the curve fitting of XANES (Wang et al., 2013).

Catalyst	Ni/Co	Ni%	NiO%	Co%	CoO%
CopCat-Ni4	-	87	13	-	-
CopCat-Ni2Co4	0.6	52	48	20	80
CopCat-Co6	-	-	-	0	100
ImpCat-Ni5	-	84	16	-	-
ImpCat-Ni2Co3	0.5	82	18	37	63
ImpCat-Co5	-	-	-	43	57

Reduction at higher temperatures (850 ^{o}C) produced larger particle sizes (more than 100 angstroms) whereas reduction at 750 ^{o}C produced particles smaller than 100 angstroms. Also, the amount of reduced metal on impregnated catalysts was almost twice the amount on coprecipitated catalysts. Nickel was easier to reduce than cobalt, regardless of the preparation method. The impregnated Ni monometallic catalysts had the highest conversion. On the other side, the Co monometallic catalyst did not show good activity. (Wang et al., 2013).

1.3 MOTIVATION TO CARRY OUT THIS THESIS

As previously discussed, the CO_2 reforming of methane is important because it produces syngas that can be used in the production of liquid hydrocarbons by the Fischer-Tropsch reaction and at the same time it consumes two of the more abundant greenhouse gases in the atmosphere.

Many studies focus only on the gas phase or the species desorbed from the catalysts. It is necessary to study the species adsorbed on the catalyst surface to understand the mechanism or the reaction pathway (Hauchecorne and Lenaerts, 2013). It is important to understand the reaction mechanism for dry reforming of methane without H_2S and SO_2. Additionally, since the reactants for DRM usually contain gases such as H_2S in biogas and SO_2 in the mixture of gases produced by the combustion of coal, it is paramount to study the response of Ni-Co/AlMgOx catalysts when there is H_2S or SO_2 in the feed. The knowledge of the mechanism of a reaction is one of the steps involved in the design of a catalyst and helps to determine the properties that a satisfactory catalyst should possess. (Dowden et al., 1968). Another purpose of the study of the mechanisms is the optimization of reaction conditions for rate and selectivity.

1.4 ORGANIZATION OF THE THESIS

The thesis is organized according to the University of Saskatchewan guidelines for master degree thesis.The arrangement of this work is as follows:

Chapter 1: Introduction describes the background of dry reforming of methane and the challenges this area has faced. The previous research made on catalyst development for dry reforming of methane under the supervision of Dr. Hui Wang is also presented.

Chapter 2: Literature review gives information about the different forms of reforming of methane. Attention is then focused on dry reforming of methane and its characteristics (environmental aspects, thermodynamics and mechanism). Research on different catalysts (especially nickel and cobalt based catalysts) for DRM reaction is also presented. Finally, this

chapter shows causes of deactivation of catalysts, especially H_2S and SO_2 poisoning. Knowledge gaps in the literature review are identified at the end of this chapter.

Chapter 3: Experimental set-up and procedure describes the process of preparation of the catalysts used in this research work. Some of the physical and chemical properties of the catalysts such as surface area, pore size, pore volume and metal composition are presented. Finally, this chapter explains the fundamentals of infrared spectroscopy and the procedure of the experiments using this technique.

Chapter 4: Results and discussion shows the results of the experiments and the analysis to reach the conclusions. First, the mechanism on the catalyst surface when methane interacts with the catalysts without the presence of carbon dioxide, and then the other way around, is discussed. Then, the mechanism on the catalyst surface is described when both methane and CO_2 interact with the catalysts at the same time (during dry reforming of methane reaction). Finally, the effect of either H_2S or SO_2 on the mechanism for DRM is analyzed.

Chapter 5: Conclusions and recommendation summarizes the main contributions or findings in this research work and suggests further research that could be performed in the area.

CHAPTER 2. LITERATURE REVIEW

The intention of this chapter is to revisit existing literature to enable both the reader and researcher to learn from previous studies.

In this chapter, firstly, some of the reactions to produce syngas (as well as the side reactions) using methane as feedstock will be presented. Secondly, a review of the carbon dioxide reforming of methane and the catalysts used for this reaction (especially nickel and cobalt-based catalysts) will be introduced. Finally, the mechanism of dry reforming of methane and the poisoning of catalysts by hydrogen sulfide and sulfur dioxide during the reaction using FTIR spectroscopy will be presented.

At the end of the literature review, some knowledge gaps are identified to justify the research.

2.1 REFORMING OF METHANE

The reforming of methane is the reaction of methane with either water, carbon dioxide or oxygen (or a combination of them) to produce syngas. Table 2-1 illustrates the methane reforming reactions.

Table 2-1. Reforming of methane reactions to produce syngas (Zhang et al., 2007 and 2008).

Reaction	Equation	ΔH_{298K} (KJ/mol)
Steam reforming of methane	$CH_4+H_2O \quad CO+3H_2$	206
Partial oxidation of methane	$CH_4+0.5O_2 \quad CO+2H_2$	-36
Dry reforming of methane	$CH_4+CO_2 \quad 2CO+2H_2$	247

Steam Reforming is a reaction that produces syngas from natural gas and water. However, endothermicity is one of the disadvantages of steam reforming, making the reaction expensive due to heat requirements (Rodrigues et al., 2012). This reaction is carried out industrially at around 800 ^oC using nickel catalysts supported on alumina (Matsumura and Nakamori, 2004).

The partial oxidation of methane is attractive since it is mildly exothermic (Rodrigues et al., 2012). Also, it is better than steam reforming since it offers more selectivity to syngas and better H_2/CO ratio (Ashcroft et al., 1991). However, since the partial oxidation of methane produces a H_2/CO ratio equal to 2, it is not desired for the further production of higher hydrocarbons (Bradford & Vannice, 2007).

Dry reforming of methane is interesting since it produces a lower H_2/CO ratio than steam reforming and partial oxidation of methane. This reduced ratio, which is equal to or less than 1, is required for processes such as the synthesis of long-chain hydrocarbons by the Fischer-Tropsch reaction (Ruckenstein and Wang, 2000). Also, DRM is relatively inexpensive due to the high availability of the reactants methane and carbon dioxide (Bradford and Vannice, 2007). Some of the drawbacks of this reaction are its high endothermicity and its inclination for carbon formation (Ashcroft et al., 1991).

Syngas can also be produced by a combination of steam and dry reforming of methane or by tri-reforming of methane, which is reacting methane with oxygen, CO_2 and steam (Gangadharan et al., 2012; Song and Pan, 2004). The combination of reactions, also known as "mixed" reforming, allows H_2/CO ratios from 1 to 3 simply by adjusting the $CO_2/H_2O/O_2$ ratios (Bradford & Vannice, 2007). One example of "mixed" reforming is the autothermal reforming of methane, which is the combination of partial oxidation of methane with either carbon dioxide or steam (Ayabe et al., 2003). In the autothermal mode, the heat provided by the exothermic reaction (partial oxidation of methane) supplies the energy for the endothermic reactions (steam or dry reforming of methane) (Barrai et al., 2007). The preferred option to produce syngas industrially in an economical, safe and large-scale manner is autothermal reforming (Aasberg-Petersen et al., 2003).

Synthesis gas has a wide variety of applications. Hydrogen can be used for the production of electricity using fuel cells (Choudhary et al., 2003), as well as in many processes in the petrochemical industry such as hydrotreating and hydrocracking. Syngas can also be used for the production of liquid fuels such as diesel, methanol, gasoline and dimethyl ether (DME) (Rostrup-Nielsen, 2000). Carbon monoxide can be utilized for the production of valuable products such as chemicals used in agriculture, organic acids and polycarbonates (Teuner et al., 2001). Syngas can be produced from any feedstock containing carbon such as coal, petroleum, coke, hydrocarbons, and biomass. Among these options, the cheapest processes to produce syngas use natural gas as feedstock (Wilhelm et al., 2001).

The reforming of methane has side reactions which deactivate the catalyst or alter the H_2/CO ratio. Table 2-2 shows some of these reactions.

Table 2-2. Side reactions during reforming of methane.

Reaction	Equation
CH_4 decomposition	$CH_4 \quad C+2H_2$
Boudouard reaction	$2CO \quad C+CO_2$
Reverse water gas shift reaction	$CO_2+H_2 \quad CO+H_2O$
Water gas reaction	$H_2O+C \quad H_2+CO$
Water-gas shift reaction	$CO+H_2O \quad CO_2+H_2$

2.2 COMMERCIAL PROCESSES FOR THE PRODUCTION OF SYNGAS

There are at least two commercial processes for the production of syngas, the CALCOR and SPARG processes:

2.2.1 CALCOR process

The CALCOR process comprises the steps (Teuner et al., 2001) shown in Figure 2-1:

-Heating a stream composed of natural gas as feed and recirculated hydrogen coming from syngas purification.

-Desulfurization of this mixture by hydrogenation and adsorption on ZnO.

-Mixing of the mixture with recirculated carbon dioxide.

-Reforming of the mixture in reforming tubes filled with catalysts and heated with a high-speed burner.

-Cooling of the syngas product before passing it into a purification unit in which hydrogen is separated as well as traces of CH_4 and CO_2.

-CO is produced by low-temperature or membrane purification, depending on the concentration or purity required.

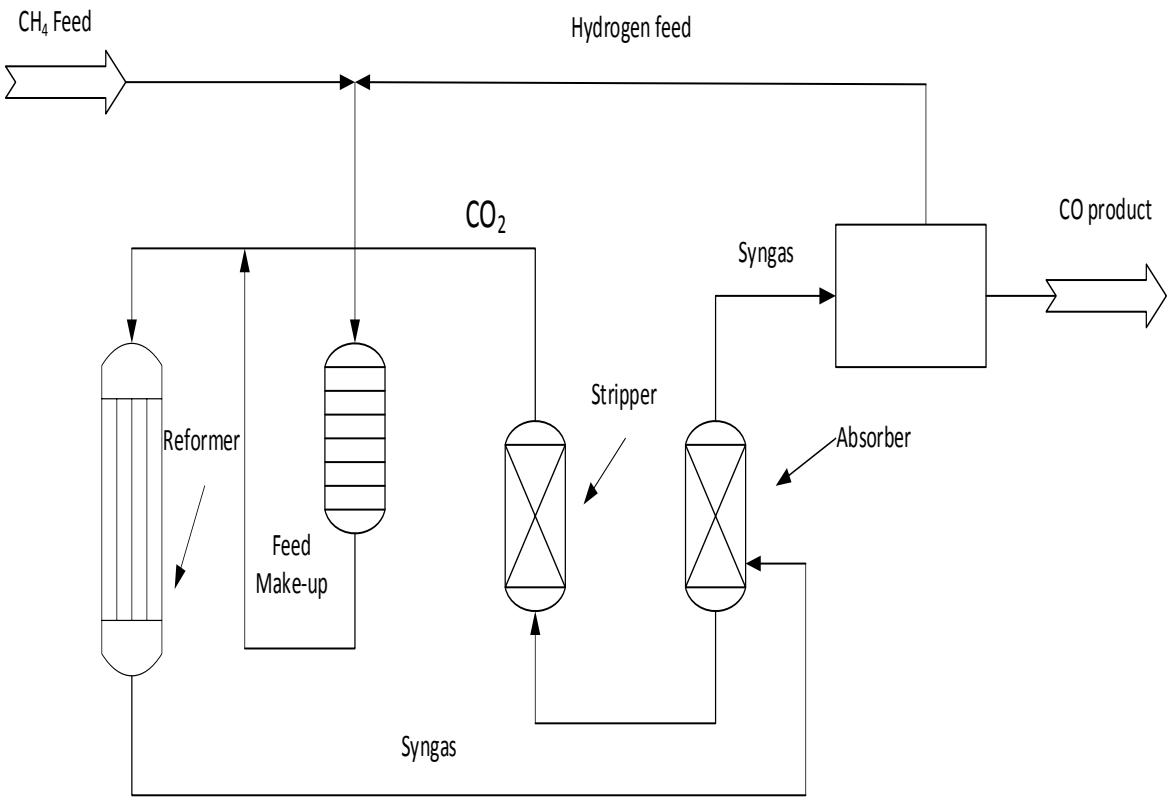

Figure 2-1. Simplified process flow of CALCOR standard process (Teuner et al., 2001).

2.2.2 SPARG Process

One characteristic of this process is that the catalysts are covered by sulfur (sulfur passivation) to prevent carbon deposition (Udengaard et al., 1992). This process produces a ratio of H_2/CO equal to 1.8 which is suitable for the production of valuable chemicals such as dimethyl ether, oxo-alcohols, and acetic acid. This process combines steam reforming with CO_2 reforming of methane, producing a lower H_2/CO ratio than steam reforming alone (Udengaard et al., 1992). The developers of this process have reported the absence of coke for almost three years at the prereformer. The flow diagram of SPARG process is shown in Figure 2-2.

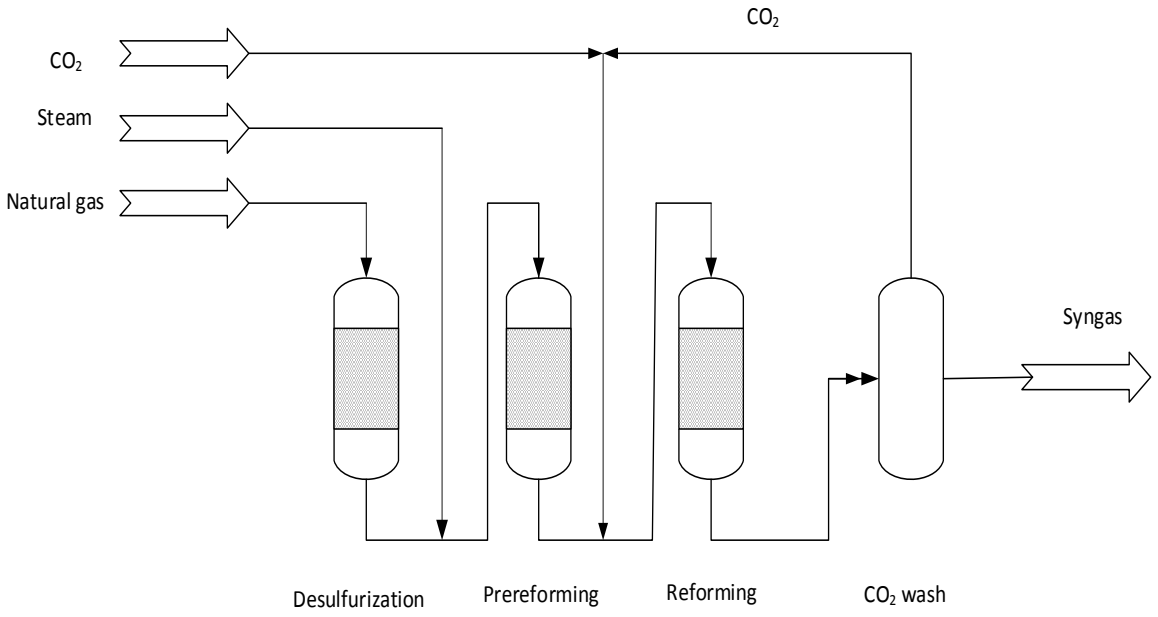

Figure 2-2. Process flow of SPARG process (Udengaard et al., 1992).

2.3 DRY REFORMING OF METHANE

2.3.1 Environmental aspects for dry reforming of methane

From the environmental point of view, dry reforming of methane is beneficial since it consumes two abundant greenhouse gasses (Pichas et al., 2010). More concern should be taken about methane since it was reported to have a global warming potential 28 times higher than that of carbon dioxide (epa.gov). It is debated whether the dry reforming of methane reduces carbon dioxide in the atmosphere since the energy consumption during reaction produces more carbon dioxide than the carbon dioxide consumed in the chemical reaction (Centi and Perathoner, 2009).

The main greenhouse gasses emitted to the atmosphere are methane and carbon dioxide as Figure 2-3 shows:

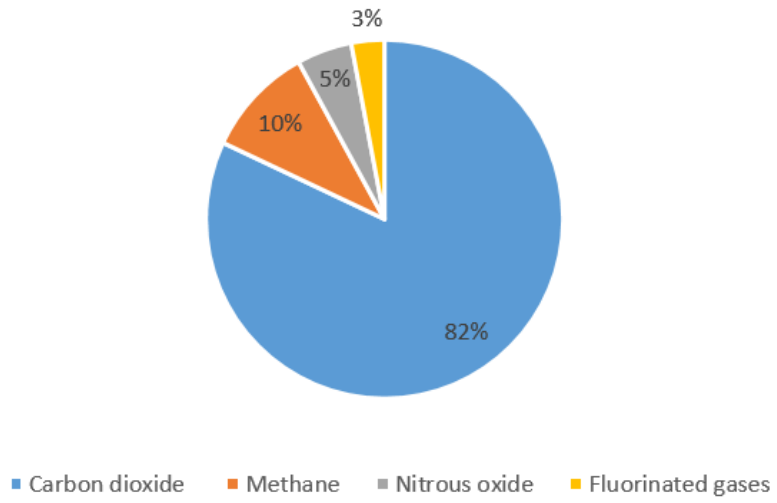

Figure 2-3. Greenhouse gas emissions in the US in 2013 (epa.gov).

2.3.2 Obtainment of reactants for DRM

The main sources that generate carbon dioxide are shown in Figure 2-4:

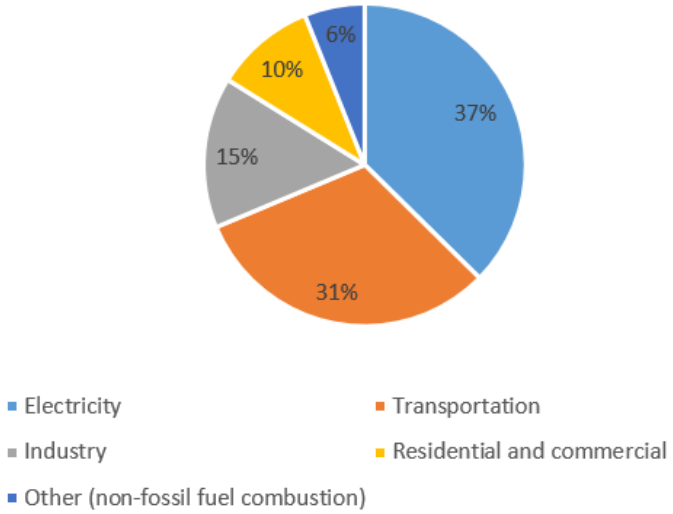

Figure 2-4. US Carbon dioxide emissions by source in 2013 (epa.gov).

Methane can be emitted and obtained from many sources as displayed in Figure 2-5.

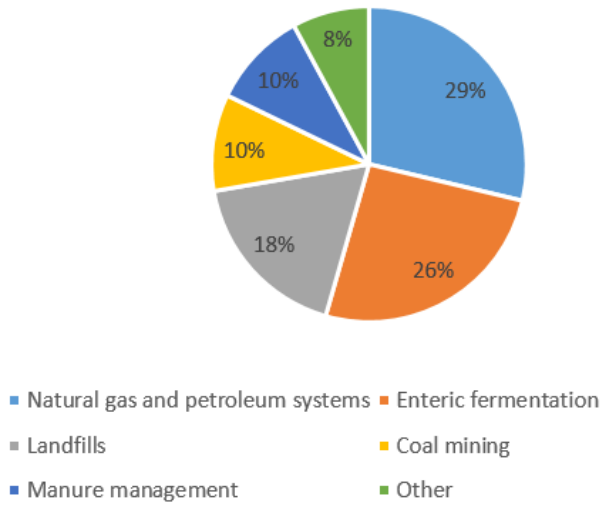

Figure 2-5. US methane emissions by source in 2013 (epa.gov).

Most of the methane emitted come from organic waste, as Figure 2-5 shows. The organic waste can be originated from animals, crops, wastewater, sewage sludge and municipal residues. Biogas is produced when bacteria break down organic waste by anaerobic digestion (Buekens, 2005).

The composition of biogas varies depending on its source but generally, it is composed mainly of methane (45-75%) and carbon dioxide (25-50%). It also contains sulfur compounds such as hydrogen sulfide (up to 100-1000 ppm), mercaptans (up to 100 ppm) and minuscule amounts of carbonyl sulfide, sulfur dioxide and CS_2 (Mescia et al., 2011).

The utilization of biogas for the production of syngas has been reported in the literature as dry reforming of biogas (Barrai et al., 2007). It would help to decrease a wide variety of contaminants that are dangerous to human health including methane, which is a greenhouse gas. That is why there is a great motivation to use biogas as soon as it is generated for energy applications. (Saha et al., 2014). Biogas, compared to other sources of renewable energy such as

solar, wind and hydropower, has the advantage of not having geographical limits, and its production neither requires sophisticated technology nor is it monopolistic (Taleghani and Kia, 2005).

2.3.3 Thermodynamic analysis

For a chemical reaction, ΔG^o represents the standard Gibbs free-energy change for the conversion of reactants in their standard states to products in their standard states. ΔG^o is a function of temperature and it is defined as:

$$\Delta G^o = -RT\ln K \tag{2-1}$$

$$\Delta G^o = \Delta H^o - T\Delta S^o \tag{2-2}$$

where R is the gas constant, T is the temperature, K is the reaction equilibrium constant, ΔH^o and ΔS^o are the standard enthalpy change and standard entropy change, respectively. Equation (2-1) can be rearranged as follows:

$$K = e^{\frac{-\Delta G^o}{RT}} \tag{2-3}$$

ΔH^o and ΔS^o are defined as:

$$\Delta H^o = \Delta H^o{}_{289\text{K}} + \int_{298K}^{T} \sum(v_i C_{p,i})\, dT \tag{2-4}$$

$$\Delta S^o = \Delta S^o{}_{298\text{K}} + \int_{298K}^{T} \frac{\sum(v_i C_{p,i})}{T}\, dT \tag{2-5}$$

C_p is the heat capacity at mole-constant pressure and can be determined with the formula:

$$C_p = a + bT + cT^2 + dT^3 \quad (2\text{-}6)$$

where a, b, c and d are constants that are reported on thermodynamic books such as Cengel and Boles, 2011. ΔH^o_{298K} and ΔS^o_{298K} are reported as well. $\sum(v_i C_{p,i})$ is the sum of heat capacities of chemical species multiplied by their stoichiometric coefficients. By combining equations (2-2), (2-4) and (2-5) into (2-3), it is possible to find the equilibrium constants for the dry reforming of methane reaction and its side reactions as a function of temperature, as shown in Figure 2-6 (Zhang et al., 2008).

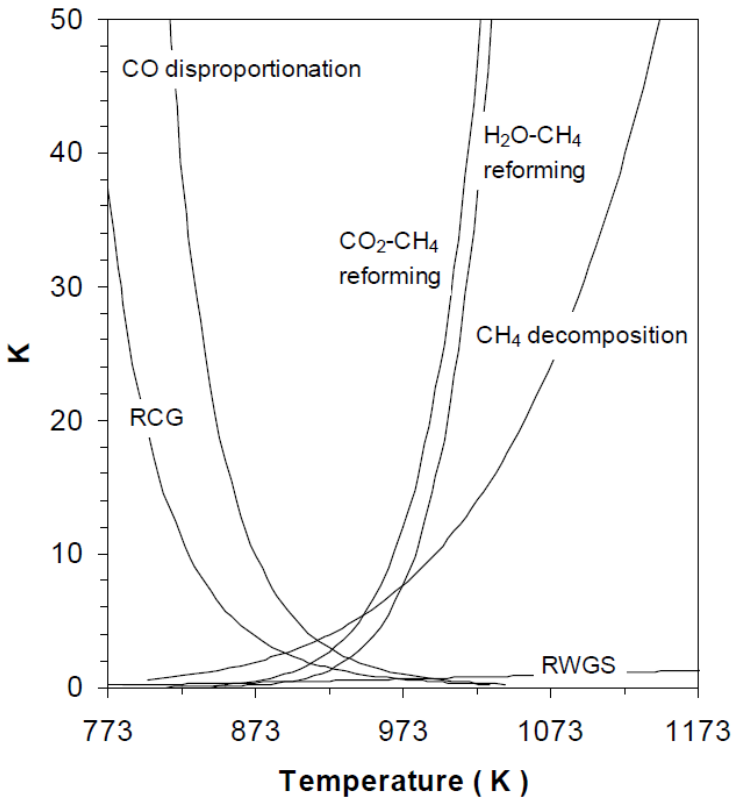

Figure 2-6. Reaction equilibrium constants as a function of temperature for some of the reactions related to dry reforming of methane (Zhang et al., 2007).

2.3.4 Mechanisms reported for dry reforming of methane

The mechanism of dry reforming of methane can be studied by Diffuse Reflectance Infrared Fourier Transform Spectroscopy (DRIFTS). This technique helps to characterize in situ intermediates of reaction adsorbed on the surface of heterogeneous catalysts at actual conditions of operation such as high pressure and temperature. The DRIFTS cell is like a "window" that allows the observation of the mechanism of reaction on the surface of the catalyst at reaction conditions (Highfield et al., 1991). Some examples of the information obtained by different authors related to the dry reforming of methane and sulfur poisoning using infrared spectroscopy will be presented in the following paragraphs.

Kroll et al. (1997) studied the mechanism of dry reforming of methane catalyzed by nickel supported on silica using in-situ DRIFT spectroscopy. They found that right after methane and CO_2 interact with the catalyst, dehydrogenated carbon species adsorb on nickel. Bands were found at 2012 and 1855 cm^{-1}, which were attributed to linear and multibonded CO adsorbed species, respectively. They found CO infrared bands at 500 ^oC but not at 700 ^oC and they assigned this to a very short residence time and, therefore, negligible accumulation of CO on the catalyst surface.

Erdőhelyi et al. (1997) determined that CH_4 has a promoting effect on the dissociation of CO_2. This promoting effect was concluded by observing CO bands at higher intensities and at lower temperatures when CH_4 was also introduced.

Kitla et al. (2013) detected a band at 2075 cm^{-1} which they attributed to linear carbonyl chemisorbed on Ni^0. When Cu was added to the nickel catalyst it was observed a redshift, which

is lower energy to produce the vibration or lower wavenumber, of about 50-70 cm^{-1} for the CO peak, this was attributed to copper donating electrons to nickel. The vibration frequency of carbon monoxide experienced a blue shift (higher energy of vibration or higher wavenumber) of about 34 cm^{-1} on Ni-rich bimetallic catalysts.

Redshifts and blueshifts can be explained in terms of bond length. For example, in X-H (in which X is a more electronegative atom or functional group than H), bond lengthening is related to redshift or lower wavenumber in infrared spectrometry (Joseph and Jemmis, 2007). On the contrary, X-H bond contraction is believed to produce a blueshift or higher wavenumber on the spectra.

Bitter et al. (1997) documented that upon CO_2 adsorption, the presence of linear CO on Pt as well as carbonates were detected on Al_2O_3, TiO_2 and ZrO_2 catalyst supports using infrared spectroscopy. However, they could not observe carbonates on SiO_2. They concluded that catalysts that can form carbonates on the support have superior activity to catalysts which do not have this feature. Among the previous catalyst supports, the formation of carbonates was much higher on Al_2O_3, this was confirmed by infrared spectroscopy.

Other mechanistic steps for DRM are reported in Table 2-3.

Table 2-3. Mechanisms reported in the literature for dry reforming of methane.

Mechanism	Reaction	Comments and references
Carbonates on the support react with C to produce CO (Tsipouriari and Verykios, 1999).	CO_2-O_s+C→2CO (where s means oxygen on the support)	Tsipouriari and Verykios (2001) reported this step to be rate determining.

Table 2-3. Mechanisms reported in the literature for dry reforming of methane (continued).

Mechanism	Reaction	Comments and references
CO_2 adsorption and further dissociation into gaseous CO and adsorbed oxygen (Schuurman et al., 1998; Bitter et al., 1997)	$CO_2 + 2S^* \rightleftharpoons CO\text{-}S^* + O\text{-}S^*$	Schuurman et al. (1998) and Kroll et al. (1997) showed by their experiments that no oxygen release was detected after CO_2 dissociation and CO was immediately detected in the gas phase. This step is greatly reversible and swift (Kroll et al., 1997).
Adsorbed oxygen reacting to carbon produced by methane dissociation, yielding more CO. (Schuurman et al., 1998)	$CO_2 \rightleftharpoons CO + O\text{-}S^*$ $Ni\text{-}O_{ads} + NiC \rightarrow 2Ni + CO$ Overall reaction: $CO_2 + NiC \rightleftharpoons 2CO + Ni$ Or in simpler terms: $CO_2 + C \rightleftharpoons 2CO$	The inverse of the previous reaction is called Boudouard reaction (Tsipouriari and Verykios, 1999). This step was reported as rate limiting on Ni/SiO2 catalyst (Schuurman et al., 1998; Kroll et al., 1997).
Methane dissociation after adsorption on the catalyst (Hickman and Schmidt, 2015; Schuurman et al., 1998)	$CH_4 \rightarrow C\text{-}S^* + 4H\text{-}S^*$ $CH_4 + Ni \rightleftharpoons NiC + 2H_2$	On nickel catalysts, methane dissociation leads to hydrogen production and carbon accumulation on nickel (Schuurman et al., 1998). The methane conversion decreases when the oxygen on the catalytic surface is unavailable or when the surface is saturated with carbon (Schuurman et al., 1998). It also decreases on a highly oxidized catalyst (Schuurman et al., 1998). Tsipouriari and Verykios (1999) concluded that dissociation of CH4 to form CHx species is a slow step. Bitter et al. (1997) concluded that the activation of methane occurs on the metal.
Water produced after hydrogen reacts with oxygen produced by CO_2 dissociation (Schuurman et al., 1998).	$CO_2 + 2S^* \rightleftharpoons CO\text{-}S^* + O\text{-}S^*$ $H_2 + Ni\text{-}Oads \rightleftharpoons H_2O + Ni$ (Schuurman et al., 1998)	The water-gas shift reaction is a combination of these steps
Formation of formate and/or carbonate on alumina support (Schuurman et al., 1998; Erdohelyi et al., 1997).	$O^{2-} + CO_2 \rightleftharpoons CO_3^{2-}$ $OH^- + CO \rightleftharpoons OCHO$	Bitter et al. (1997) reported that catalysts containing MgO, Al_2O_3, TiO_2 or ZrO_2 allow carbonates formation. Formation of carbonates does not occur on SiO_2 support.

Table 2-3. Mechanisms reported in the literature for dry reforming of methane (continued).

Mechanism	Reaction	Comments and references
Oxidation of carbon to CO_2 (Goula et al., 1996).	$O_2+2S^* \rightleftharpoons 2O\text{-}S^*$ $C+O\text{-}S^* \rightarrow CO\text{-}S^*$ $CO\text{-}S^*+O\text{-}S^* \rightarrow CO_2+2S^*$	There is not a report of a kinetic model for the oxidation of filamentous carbon

Erdőhelyi et al. (1997) concluded that the concentration of the reactants has an effect on the composition of the mixture of products on alumina supported catalysts. An increase in the concentration of CH_4 leads to lower CO/H_2 ratio and an increase in the concentration of carbon dioxide produces more CO and less H_2. Additionally, it was reported that when methane is in excess on the reacting mixture, the amount of carbon deposited also increased.

In the reforming of methane reaction, carbon dioxide, oxygen or water have as purpose to regenerate the catalysts and removing carbon produced by the cracking of methane with the following mechanism (Choudhary and Goodman, 2006):

$$C+H_2O/O_2/CO_2 \rightarrow CO_x+H_2 + \text{regenerated catalyst surface} \quad (2\text{-}7)$$

It might be reasonable to think that the carbon deposition could be prevented by an excess of carbon dioxide during DRM reaction. However, this is not preferred in the industry due to the high costs that the further separation of CO_2 would incur (Zhang et al., 2012).

The dissociation of methane is very small on metal surfaces and it is promoted by oxygen produced by the dissociation of carbon dioxide. Synergistically, the dissociation of CO_2 is favored by adsorbed hydrogen resulting from the cracking of methane (Erdőhelyi et al., 1997).

Tsipouriari and Verykios (1999) documented that the dissociation of methane on nickel to produce NiC and H_2 is a slow step while activation of CO_2 in the support used (La_2O_3) to produce carbonates ($La_2O_2CO_3$) is a fast step.

Zhang et al. (2008b) studied the kinetics of dry reforming of methane using Ni-Co/AlMgOx at the range 650-750 ^oC. He suggested that the dissociation of methane and the reaction between carbon and adsorbed CO_2 are the rate-determining steps.

2.3.5 Catalysts used for dry reforming of methane

Many metals have been employed to produce catalysts for the reforming of methane. For example, Rostrup-Nielsen and Hansen (1993) tested Ni, Ru, Rh, Pd, Pt and Ir and they found that Ru and Rh allow carbon-free operation and they concluded the succeding order in activity: Ru, Rh > Ir > Ni, Pt and Pd.

Even though catalysts composed of noble metals have shown a stable operation for dry reforming of methane and low carbon deposition, they are not the preferred option in the industry due to their high price and limited availability. Therefore, the research community has widely focused on nickel catalysts due to their high availability (Zhang et al., 2007).

2.3.5.1 Nickel-based catalysts

Nickel catalysts have been prepared both monometallic and bimetallic for dry reforming of methane. An example of this was the study made by Zhang et al. (2008). Ni-Metal/$AlMgO_x$ (where metal could be Co, Cu, Fe, or Mn) catalysts were compared and Ni-Co/$AlMgO_x$ was more active and stable than the others. The performance of Ni-Co/$AlMgO_x$ was different after varying Ni/Co ratio and loading. Coke was not detected with a Ni/Co ratio around 1 and Ni-Co

loading between 4-10% (Zhang et al., 2008). The Ni-Co bimetallic catalyst performed steadily for 2000 h with CH_4 and CO_2 conversions = 90 and 91%, respectively. (Zhang et al., 2007). This superior activity of the catalysts was attributed to its high surface area and high metal dispersion, small particle size, strong metal-support interaction and synergy between nickel and cobalt.

Sun (2005) prepared Ni-Ti and Ni-Ti-Al catalysts. The activity of the Ni-Ti catalyst for DRM increased with Ni loading between 1-10 wt%. The reduction temperature had a big effect on the activity of the reduced catalyst. The activity increased when reduction temperature was increased until 973 K, and after that point, the activity decreased until disappearance at 1023 K. Also, the author obtained a Ni-Ti catalyst with a high surface area equal to 426 m^2/g when calcined at 473 K and it was noted that calcination at higher temperature made surface area to decrease notably.

Another aspect that influences the performance of the catalysts is the method of preparation. An example of this was the work made by Shakouri (2011). He prepared bimetallic Ni-Co/AlMgOx, as well as monometallic Ni/AlMgOx and Co/AlMgOx catalysts by coprecipitation and impregnation methods with different Ni/Co ratios. His findings were that Ni/Co obtained ratios in the impregnated catalyst were closer to the intended ratio, contrary to the catalysts prepared by coprecipitation. Also, with equal Ni/Co ratios, the impregnated catalysts were reduced more than the ones made by coprecipitation. In terms of activity, the nickel monometallic catalyst prepared by impregnation had the higher conversion at 710 ^oC.

Tang et al., (2000) developed nickel-based catalysts with 3 different methods of preparation and with the same nickel content (10 wt%): 1) impregnation of γ-Al_2O_3 support ($NiAl_{CO-IM}$), 2) sol–gel-made γ-Al_2O_3 ($NiAl_{SG-IM}$) and 3) direct sol–gel method from organometallic compounds

($NiAl_{SG}$). In his tests, the catalysts had similar activity but a significant difference in coking resistivity. $NiAl_{SG-IM}$ catalyst had great resistance to coke even after 80 hours at 700 ^{o}C. Followed by $NiAl_{SG}$, with an average coke rate deposited of 0.003 $g_{carbon}\ g_{cat}^{-1}h^{-1}$. On contrast, quick coke deposition occurred on $NiAl_{CO-IM}$, with an average rate of 0.095 $g_{carbon}\ g_{cat}^{-1}h^{-1}$, blocking the reactor after 3.5 hours.

The support on which nickel is deposited also plays a significant role on the catalyst performance. Ruckenstein and Hu (1995) found that reduced NiO/MgO catalyst had higher CH_4 conversion and selectivity than NiO/CaO, NiO/SrO and NiO/BaO. Additionally, NiO/MgO had excellent stability and good resistivity to coking. The author attributed the resistant to coking to the suppression of CO disproportionation caused by a solid solution between NiO and MgO.

Goula et al. (1996) showed that the CaO/Al_2O_3 ratios in Ni/CaO-Al_2O_3 catalysts influenced the amount of carbon species formed during dry reforming of methane. The catalyst with CaO/Al_2O_3=1/2 was more resistant to the formation of coke and slightly more active than that with CaO/Al_2O_3=12/7.

2.3.5.2 Cobalt-based catalysts

Ruckenstein and Wang (2000) prepared cobalt catalysts supported on MgO, CaO, SrO and BaO and they found that MgO was the best support. Co/MgO had higher and more stable activity for dry reforming of methane. Additionally, it resisted carbon formation and sintering and they attributed this to a solid solution formed between MgO and CoO.

Takanabe et al. (2005) prepared titania-supported catalysts composed of nickel and cobalt, both bimetallic and monometallic. Catalysts containing only cobalt showed a high resistance to carbon deposition but they deactivated due to copper oxidation. The addition of 10 mol% of nickel resulted in the resistance of cobalt to oxidation and high stability, whereas an excess of nickel, higher than 80 mol%, provoked carbon formation. It was reported that cobalt has a stronger affinity for species containing oxygen whereas nickel has higher attraction for carbon species.

While Takanabe et al. (2005) found that catalysts containing only cobalt had a high resistance to carbon formation, San-Jose-Alonso et al. (2009) determined that among Ni-Co catalysts with different ratios, the catalysts with the highest amount of cobalt had the greatest amount of carbon deposited after 6 hours of reaction.

2.3.6 Catalyst deactivation

One of the main problems that nickel catalysts face is the formation of carbonaceous deposits that eventually decreases catalyst activity (Priya et al., 2012). Haldor Topsoe reported that in order for a catalyst to operate without carbon formation, it must have less acidic sites since they are known to cause cracking reactions. Therefore, they used magnesium aluminate in the composition of their catalysts because it is less acidic than pure alumina.

Other factors responsible for catalyst deactivation are sintering, which is defined as the decrease in catalytic area caused by the growth of smaller particles (Sehested, 2004) and, sulfur poisoning (Ashrafi et al., 2008; Erdohelyi et al., 2004).

While some authors consider the presence of sulfur compounds as a problem, other authors have considered their presence as beneficial. For example, it was demonstrated by Priya et al. (2012) that the addition of ethyl disulfide decreased the rate of formation of carbon more than the reforming rate. Also, Jones et al. (2003) showed that sulfur-containing compounds at certain levels produce alterations in the metal or the support that could be favorable for certain reactions such as the catalyzed combustion of certain alkanes. Rostrup-Nielsen (1984) found the when the catalysts where partially passivated by sulfur it was possible to carry out steam reaction free of carbon deposition.

This mechanism of sulfur passivation is used in the SPARG process (Udengaard et al., 1992). Rostrup-Nielsen (1991) compared this beneficial effect to the principle of homeopathy in which an evil can be treated by a poison in small doses. It was assumed that sulfur is chemisorbed on sites that are active for carbon formation and at the same time leaving the reaction sites unchanged.

However, at higher concentration, sulfur-containing compounds have demonstrated to lower the catalytic activity for dry reforming of methane. Natural gas contains small amounts of sulfur-containing compounds (about 5.5 mg/m^3), including the mercaptan added (4.9 mg/m^3) to warn about leakages (Uniongas.com). Table 2-4 shows the composition of natural gas as reported by Union Gas. However, this composition can vary depending on the location where the gas is obtained from.

Table 2-4. Chemical composition of natural gas (uniongas.com/about-us/about-natural-gas/chemical-composition-of-natural-gas).

Component	Typical analysis (mole %)	Range (mole %)
Methane	95.00	87-97
Ethane	3.20	1.5-7.0
Propane	0.20	0.1-1.5
iso-Butane	0.03	0.01-0.3
normal-Butane	0.03	0.01-0.3
iso-Pentane	0.01	trace-0.04
normal-Pentane	0.01	trace-0.04
Hexane	0.01	trace-0.06
Nitrogen	1.00	0.2-5.5
Carbon dioxide	0.50	0.1-1.0
Oxygen	0.02	0.01-0.1
Hydrogen	trace	trace-0.02

There are two different ways to overcome the issue of sulfur poisoning. The first solution is to develop catalysts with high tolerance to sulfur poisoning. The second one is the separation of sulfur from the gas stream before the reaction but this would represent a high cost of operating costs and therefore the first option is preferred (Rangan et al., 2011).

Sulfur poisoning is caused when metal sulfides, either reversibly or irreversibly, are formed on a metal surface (Sato and Fujimoto, 2007). Also, in the surface of a metal oxide they can form sulfates (Rodriguez et al., 1999). Sulfur chemisorption on the metal surface reduces methane conversion (Bartholomew, 2001).

2.3.6.1 H_2S poisoning

H_2S can be removed by many methods to lower its concentration to about 10 ppm. Harsh sulfur poisoning on catalysts can occur even at this low concentration (Agrawal, 1979). H_2S causes poisoning and deactivation of nickel-based catalysts even at extremely low ppb levels. H_2S

decomposes to sulfur on the Ni catalyst surface throughout the steps shown in Table 2-5: (Rangan et al., 2011).

Table 2-5. Mechanism steps for H_2S chemisorption and dissociation (Rangan et al., 2011).

Step	Equation
H_2S adsorption	$H_2S_{(gas)} \rightarrow H_2S_{(ads)}$
1^{st} dissociation	$H_2S_{(ads)} \rightarrow SH_{(ads)} + H_{(ads)}$
2^{nd} dissociation	$SH_{(ads)} \rightarrow S_{(ads)} + H_{(ads)}$

Some examples of the effects of H_2S poisoning on catalyst activity for dry reforming of methane and related reactions are shown in the following paragraphs.

Ashrafi et al. (2008) experimented with steam reforming of methane using Ni-based catalysts. The catalysts were poisoned by H_2S concentrations ranging from 15 to 145 ppm at 700 ^oC. They found out that the CH_4 conversion decreased from 90 to 10% in 3 hours at 145 ppm and from 90 to 30% in 10 hours at 15 ppm. They observed that the temperature has a strong effect on the catalyst to resist sulfur poisoning. For example, in the presence of H_2S, the activity had a slight decrease at 900 ^oC. In contrast, at 800 and 700 ^oC, there was a marked decrease in activity. The same pattern was shown at 31 and 108 ppm. However, at 108 ppm, the activity loss was much faster than at 31 ppm.

Finally, Ashrafi et al. (2008) tested the catalytic activity before H_2S, during hydrogen sulfide and after its removal. They observed that the catalysts partially recovered their initial activity just by removing hydrogen sulfide. The activity was not decreased significantly when the reaction was carried out at 900 ^oC compared to at 700 ^oC.

Shakouri (2011) examined the effect of H_2S on the activity of monometallic catalysts of nickel and cobalt as well as bimetallic catalysts composed of the two metals. He found out that in contrast to Ni-Co/AlMgOx, Ni/AlMgOx had more H_2S tolerance in all experiments, either prepared by impregnation or coprecipitation methods. Moreover, catalysts made by impregnation were more active and had higher regeneration after H_2S poisoning than the coprecipitated catalysts.

2.3.6.2 SO_2 poisoning

In the autothermal reforming of diesel using Pt/Ceria catalyst, it was found that the addition of SO_2 increased the concentration of methane and carbon dioxide but decreased the hydrogen yield (Cheekatamarla and Lane, 2005).

On cesium and Cs/ZnO catalysts, it was determined that sulfur dioxide produced SO_3 and SO_4 upon reaction with atomic oxygen. Also, the presence of sulfur dissociated on the metal was very low (Rodriguez et al., 1999).

In the study of SO_2 poisoning over $Pt/Ba/Al_2O_3$ catalysts for NOx storage. Sulfur dioxide caused a decrease in NOx capacity, suggesting that it forms SO_x species that compete for adsorption against NO_2. The presence of sulfur dioxide also inhibited carbon formation (Anderson et al., 2006). Poulston and Rajaram (2003) showed that when Pt/Ba-based catalysts are sulfated they were almost totally deactivated and were not able to be completely regenerated using H_2. On the contrary, using a mixture containing CO_2 made the catalysts recover its storage activity.

The catalysts can be deactivated not only by the formation of metal sulfides but also by the occurrence of sulfating on the support. This formation of sulfates can change the crystal arrangement, thus impacting the metal-support synergy. The capacity of every catalyst to reverse this mechanism depends on its composition (Jones et al., 2003). Hubbard et al. (1993) reported that sulfation increases the acid strength of gamma alumina. However, large deposits of sulfates in catalysts can block access of reactants to the catalytic active sites.

Datta and Cavell (1985) studied the sequential adsorption of sulfur dioxide and hydrogen sulfide on alumina catalysts. Using FTIR, they found no infrared bands ascribed to bending of stretching modes of hydrogen sulfide but they did not interpret this as a lack of adsorption of H_2S on the alumina catalysts. They concluded that H_2S adsorbs to the catalyst and dissociates immediately. However, the occurrence of dissociation and formation of Al-S bonds cannot be detected by infrared spectroscopy. Also, they identified peaks at about 1324 cm^{-1} which were attributed to sulfur dioxide physically adsorbed on alumina. This band decreased in intensity after H_2S was also introduced. They found other peaks after SO_2 was fed, which they attributed to different SO_2 interactions on alumina as shown in Figure 2-7.

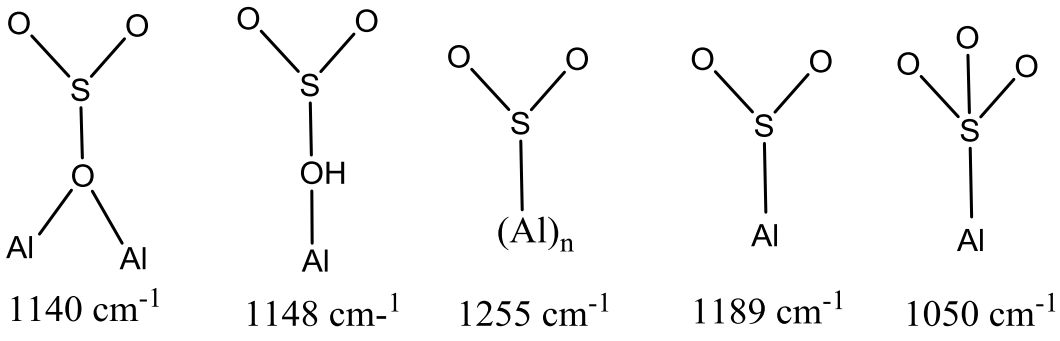

Figure 2-7. Possible SO_2 interactions with alumina. (Datta and Cavell, 1985).

2.3.7 Regeneration of catalysts after sulfur poisoning

Since H_2S adsorbs on the catalyst surface by the reaction: $H_2S+Ni_{surface} \leftrightarrow Ni_{surface}-S+H_2$, the regeneration of the catalyst can be achieved with hydrogen (the reverse of previous reaction) and also by oxidation. (Ashrafi et al., 2008). The regeneration is favored at temperatures ranging from 800 to 900 ^oC for steam reforming of methane.

Sulfur can be removed from the catalyst surface by exposing it to oxygen or to species that dissociate to oxygen, forming SO_2 (Bartholomew, 2001).

After nickel-based catalysts used in the steam reforming of methane had been sulfur poisoned, they were regenerated by a mixture of CO_2, H_2O and O_2 and using nitrogen as a carrier gas. The process was carried out for 2 hours at 700 ^oC due to the risk of sintering at higher temperatures (Hashemnejad & Parvari, 2011). It was shown that the sulfur and carbon removed is greater at higher H_2O/H_2 ratios.

Ashrafi et al. (2008) tried to regenerate nickel-based catalysts with an air/N_2 mixture after they were poisoned by H_2S at 700 ^oC. It was found that activity was not increased, so they concluded that sulfur chemisorption was irreversible by air treatment.

Figoli and Argentiere (1996) studied the regeneration of Ni/Silica catalysts after submitted to poisoning by carbon disulfide. The regenerating compounds used were hydrogen and a mixture of 2-butyne with hydrogen. They found out that some sulfur was removed from the surface of the catalyst and the rest of sulfur was irreversibly adsorbed on the catalyst.

2.4 KNOWLEDGE GAPS, HYPOTHESES AND RESEARCH OBJECTIVES

2.4.1 Knowledge gaps

- The effect of H_2S and SO_2 on the mechanism of dry reforming of methane on Ni-Co/$AlMgO_x$, Ni/$AlMgO_x$ and Co/$AlMgO_x$ catalysts prepared by our research group has been neither studied by Dr. Wang's research group nor reported in the literature (to the best of my knowledge).

2.4.2 Research objectives

The objective of this research is to determine the following:

-The mechanism of the DRM reaction on Ni-Co/AlMgOx, Co/AlMgOx and Ni-Co/AlMgOx.

-The chemical species formed on the catalysts in the presence of H_2S or SO_2 as well as the poisoning mechanism.

-The influence of the preparation methods, Ni and Co on the poisoning mechanisms.

2.4.3 Hypotheses

The following hypothesis were tried to be proved or disproved by this research.

-The presence of SO_2 forms sulfates.

-The presence of H_2S forms metal sulfides.

-Bimetallic catalysts are more resistant to poisoning by H_2S and SO_2 due to the synergy between Ni and Co (formation of alloys that prevent sulfur chemisorption).

-There should be differences in the chemical species and its concentration formed between catalysts prepared by impregnation and impregnation due to the reduction extent.

-Species attributed to the dissociation of methane must not be found on MgAlOx support.

CHAPTER 3. EXPERIMENTAL SET-UP AND PROCEDURE

This chapter will introduce the material, instrumentation and procedure employed to conduct the research. Subsection 3.1 briefly introduces the safety guidelines, one of the most important aspects in this research. Subsections 3.2 and 3.3 in this chapter will describe the methods employed to prepare the catalysts and some properties of the catalysts such as surface area, pore size, pore volume and metal composition, as reported in Wang et al. (2013). Finally, subchapter 3.4 presents the procedure used for the experiments.

3.1 SAFETY PRECAUTIONS

For this research, it was necessary to employ hazardous and poisonous gases. Therefore, safety guidelines according to the individual Material Safety Data Sheets (MSDS) and in adherence to the policies of the Department of Chemical Engineering of the University of Saskatchewan were followed. All the gases leaving the reaction were vented and a GasAlertMicro 5 detector was used to determine if the concentration of the gases used was above allowed safety limits.

3.2 CATALYST PREPARATION METHODS

The catalysts were prepared by and received from Mohsen Shakouri, member of Dr. Hui Wang's research group at University of Saskatchewan. The catalysts were prepared by coprecipitation

and impregnation methods as described in Shakouri (2011) and Wang et al (2013). Subsequent paragraphs show a brief explanation about the steps of each preparation method.

3.2.1 Coprecipitation method

In this method, an aqueous solution containing metal salts is mixed with another substance to cause precipitation. Then, the precipitated material is washed, dried and calcined. A brief description of the steps involved in the coprecipitation method is presented in the following paragraphs.

Preparation of the solution: Nitrates of metals (nickel, cobalt, aluminum and magnesium) are dissolved in deionized water in quantities that depend on the composition of the catalyst wanted.

Coprecipitation: This occurs when ammonium hydroxide (NH_4OH) is added to the previous solution, changing the pH and provoking the metals to precipitate.

Filtering and washing: The purpose of this step is to remove unwanted ions. The solution with the solid coprecipitation is filtered and washed with water at room temperature until the pH of the water is 7. After this step, a cake-like solid is produced.

Drying: The solid obtained in the previous step is heated in oven at 120 ^{o}C for at least 16 hours to remove water content.

Calcination: In this step, the dried catalyst is heated in tube furnace exposed to air at 850 ^{o}C for 6 hours.

Selection of particle size: Lastly, the catalyst is ground and sieved to particle sizes between 250 and 355 micrometers using U.S.A standard testing sieves No. 45 and 60 (A.S.T.M. E-11 specification).

3.2.2 Impregnation method

This method involves dipping the support into a solution of metal salts or spraying a metal solution on the support, following by drying and calcination as explained in the previous section. After this process, the metal remains in the pores of the support as well as on the surface of the support.

The advantages and disadvantages of each method are displayed in Table 3-1 (Shakouri, 2011).

Table 3-1. Comparison of methods for catalyst preparation (Zhang et al., 2012).

Feature	Impregnation	Precipitation
Mixing of catalytic components at molecular level	Difficult to achieve	Easy to achieve
Distribution of multi-active components	Less uniform	Uniform
Surface area higher than 200 m^2/g	Easy to achieve	Difficult to achieve
High metal loading	Difficult to achieve	Easy to achieve
High metal dispersion	Easy to achieve	Easy to achieve
Relative cost	Lower	Higher

The catalysts were prepared and separated into two groups: catalysts prepared by coprecipitation and by impregnation methods. Every group was composed of three different catalysts (two monometallic catalysts made of nickel or cobalt and one bimetallic catalyst consisting of nickel and cobalt). The purpose of preparing these six different catalysts was to determine the influence

of the preparation method and the metal composition on the mechanism of dry reforming of methane and sulfur poisoning by H_2S and SO_2. Aluminum and magnesium oxide ($AlMgO_x$) made by precipitation is the support for impregnated catalysts. Therefore, the support was also studied in this thesis.

Properties or characterization results of the catalysts prepared and used in this study have been reported in a previous paper with specific names (Wang et al., 2013; Shakouri, 2011). Therefore, they will be reviewed in further sections by the names shown in Table 3-2.

Table 3-2. Catalysts tested in this research work.

Label	Description	Formula
CopCat-Ni4	Coprecipitated nickel monometallic catalyst	Ni/AlMgOx
CopCat-Ni2Co4	Coprecipitated bimetallic (Ni-Co) catalyst	Ni-Co/AlMgOx
CopCat-Co6	Coprecipitated cobalt monometallic catalyst	Co/AlMgOx
ImpCat-Ni5	Impregnated nickel monometallic catalyst	Ni/AlMgOx
ImpCat-Ni2Co3	Impregnated bimetallic (Ni-Co) catalyst	Ni-Co/AlMgOx
ImpCat-Co5	Impregnated monometallic cobalt catalyst	Co/AlMgOx.
$MgAlO_x$ support	AlMgOx without nickel or cobalt	AlMgOx

3.3 CATALYST CHARACTERIZATION

The BET properties of the catalysts such as surface area, porous volume and average pore size are listed in Table 3-3.

Table 3-3. BET properties of the catalysts tested in this research work.

Catalyst	BET area m^2/g	Porous volume mL/g	Average pore size A
CopCat-Ni4	113	0.227	81
CopCat-Ni2Co4	111	0.287	104
CopCat-Co6	106	0.277	105
ImpCat-Ni5	114	0.34	119
ImpCat-Ni2Co3	124	0.359	116
ImpCat-Co5	102	0.296	116
$MgAlO_x$ support	85	0.226	106

The metal composition of the catalysts is reported in Table 3-4. The data was extracted from Wang et al. (2013) and Shakouri, (2011).

Table 3-4. Metal compositions of the catalyst precursors measured by ICP.

Catalyst	Ni%	Co%	Mg%	Al%	Ni/Co	Mg/Al
CopCat-Ni4	4	0	69	27	-	2.6
CopCat-Ni2Co4	2	4	68	26	0.6	2.6
CopCat-Co6	0	6	69	26	-	2.7
ImpCat-Ni5	5	0	65	30	-	2.2
ImpCat-Ni2Co3	2	3	68	27	0.5	2.5
ImpCat-Co5	0	5	65	30	-	2.1
$MgAlO_x$ support	-	-	69	31	-	2.2

3.4 PROCEDURE OF DRIFTS EXPERIMENTS

PRAXAIR provided the gases employed in the experiments. CH_4, CO_2 and N_2 cylinders were provided in purity higher than 99.9%. Nitrogen and helium diluted the rest of the gases: 5% H_2 in N_2; 522 ppm H_2S (balance helium) and; 1000 ppm SO_2 (balance nitrogen). Rotameters controlled the flow of the gases. A PIKE Technologies temperature controller was used to increase the temperature of the adsorbed and reacting gases up to 600 ^oC, which is the temperature at which

the DRIFTS experiments were carried out. The schematic of the experimental setup and the DRIFTS cell are shown in Figures 3-1 and 3-2, respectively.

All the spectra were collected using a Perkin Elmer Spectrum 100 spectrometer with a DiffuseIR Accessory with KBr windows from PIKE Technologies (Figures 3-3 and 3-4). The boiling point of the KBr windows is 630 ^{o}C. For this reason, experiments were not conducted at temperature higher than 600 ^{o}C. The spectra were obtained in situ or when the reaction was taking place. Firstly, 15 mg of catalyst was inserted into the sample holder of the Diffuse IR cell. The temperature was set at 600 ^{o}C for all the experiments. All the catalysts were reduced first by a mixture of 5% of H_2 in N_2 for 2.5 hours. After reduction, a background spectrum was collected. This background spectrum was subtracted from each of the further spectra obtained. By doing so, it was possible to eliminate the influence of the environmental noise, spectrometer noise and bands present on the catalysts. Therefore, only the chemical species adsorbed on the catalytic surface as a result of the dry reforming of methane reaction and sulfur poisoning were displayed on the spectra.

The spectra were manipulated with the Spectrum software. The spectra were collected with a resolution of 8 cm^{-1}. 30 scans were averaged for every spectrum in order to have a higher signal to noise ratio. Most of the spectra are presented in absorbance units. However, some peaks could not be clearly detected in absorbance units and therefore Kubelka-Munk units were used. An explanation about these two different units is presented in Appendix A.

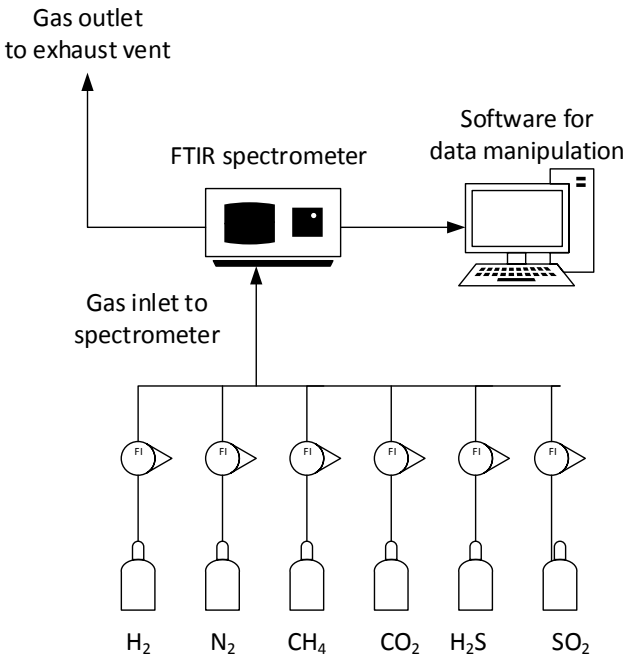

Figure 3-1. Pictorial representation of DRIFTS experimental setup

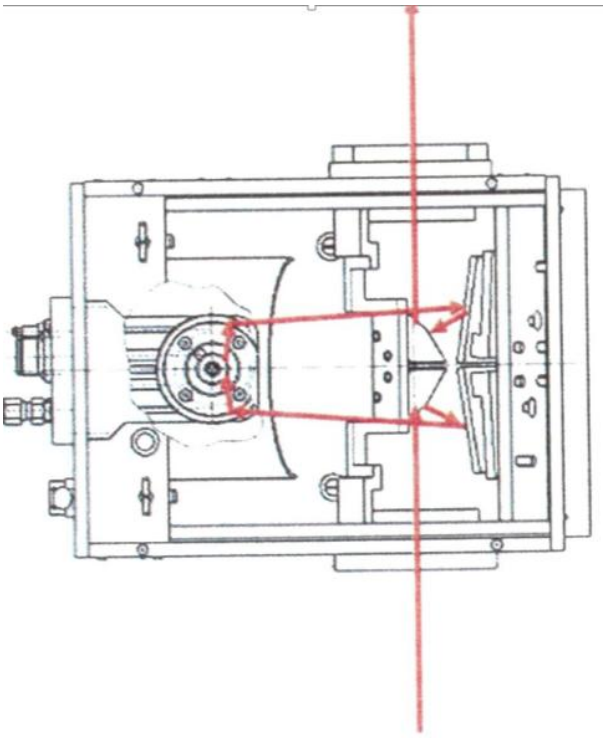

Figure 3-2. Top view of the DRIFTS accessory showing the trajectory of the infrared light

CHAPTER 4. RESULTS AND DISCUSSION

As explained in the previous chapter, the focus of this research is to determine the mechanism of the CO_2 reforming of methane reaction on nickel and cobalt based catalysts, under and without H_2S or SO_2 poisoning conditions.

Firstly, to understand the interactions of CH_4 and CO_2 with the catalysts, the independent adsorptions of methane and CO_2 were assessed. Secondly, the simultaneous interactions of CH_4 and CO_2 were studied to observe differences between independent adsorptions and concomitant adsorptions and to elucidate the reaction mechanism for dry reforming of methane. Finally, the effect of either H_2S or SO_2 before and during dry reforming of methane was investigated to understand the poisoning mechanism.

4.1 MECHANISM OF CH_4 ADSORPTION AND DISSOCIATION

To understand how methane interacts with the catalysts, the following steps were carried out. Firstly, the catalysts were reduced as explained earlier and then methane was introduced. After 15 minutes, a spectrum was collected. When methane interacted with any of the catalysts used (including the support), the spectra showed bands corresponding to the fundamental vibrations of

methane at the following wavenumbers: 3012, 1540 and 1302 cm^{-1}. Bands at near wavenumbers are attributed to asymmetrical stretching, in-plane bending or scissoring and out-of-plane bending, respectively (Silverstein et al., 2005). The band at about 1540 cm^{-1} is inactive in the free molecule but become active when the interaction of methane with the adsorption sites causes lowering of the symmetry of methane from T_d to C_{3v} (Huber and Knozinger, 1995). Therefore, the presence of this band must indicate methane adsorption.

Additionally to the previous fundamental vibrations, overtones were also displayed. An overtone is a band present at multiples of the wavenumbers of the fundamental vibrations. This overtone, which is about two times the fundamental vibration at 1302 cm^{-1} ($2v_3$), occurred at 2599 cm^{-1}. A band found at 3865 cm^{-1} on coprecipitated catalysts and at 3862 cm^{-1} on impregnated catalysts could be resulted from the $3v_4$ overtone of a CH_2 functional group (Rest et al., 1996) or could be caused by OH^- functional groups formed by hydrogen produced from methane dissociation bonding to oxygen atoms present on the catalysts (Schwach et al., 2015). This band was found in all catalysts as shown in Figures 4-1 (a) and 4-2 (a) except on the $MgAlO_x$ support and CopCat-Co6, this might be due to the lack of metallic sites on MgAlOx support and on CopCat-Co6 (Wang et al., 2013) in which methane can dissociate.

Also, combination bands (peaks at wavenumbers equal or approximately equal to the sum of two or more different fundamental vibrations) appeared at 2824 cm^{-1} (combination band v_2+v_4) (Figures 4-1 and 4-2).

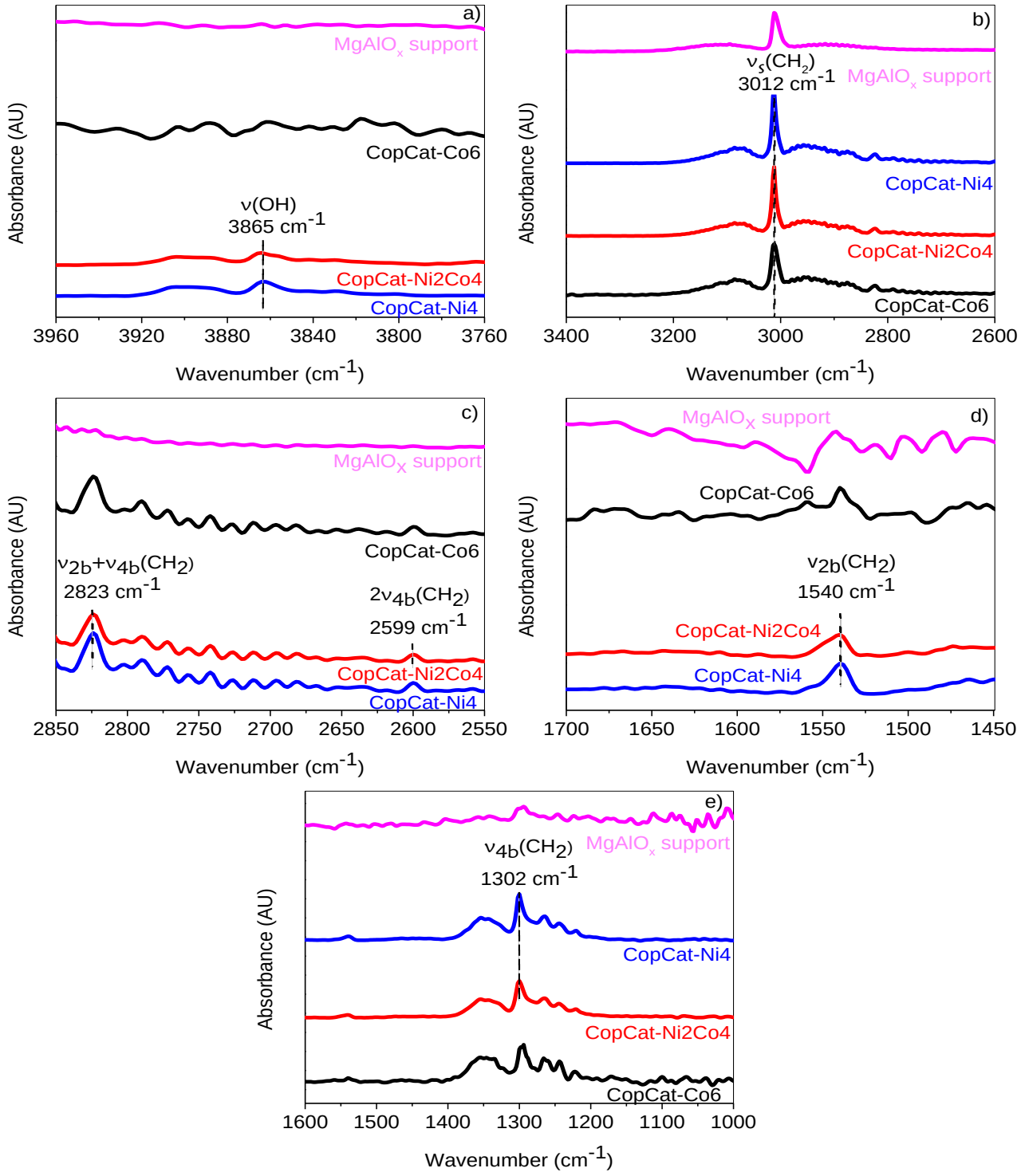

Figure 4-1. Comparison of bands produced by CH_4 on coprecipitated catalysts and support. a) Overtone 3_{v4}, b) v_3 symmetric vibration, c) combination band v_2+v_4 and overtone $2v_4$, d) v_2 bending vibration; e) v_4 bending vibration.

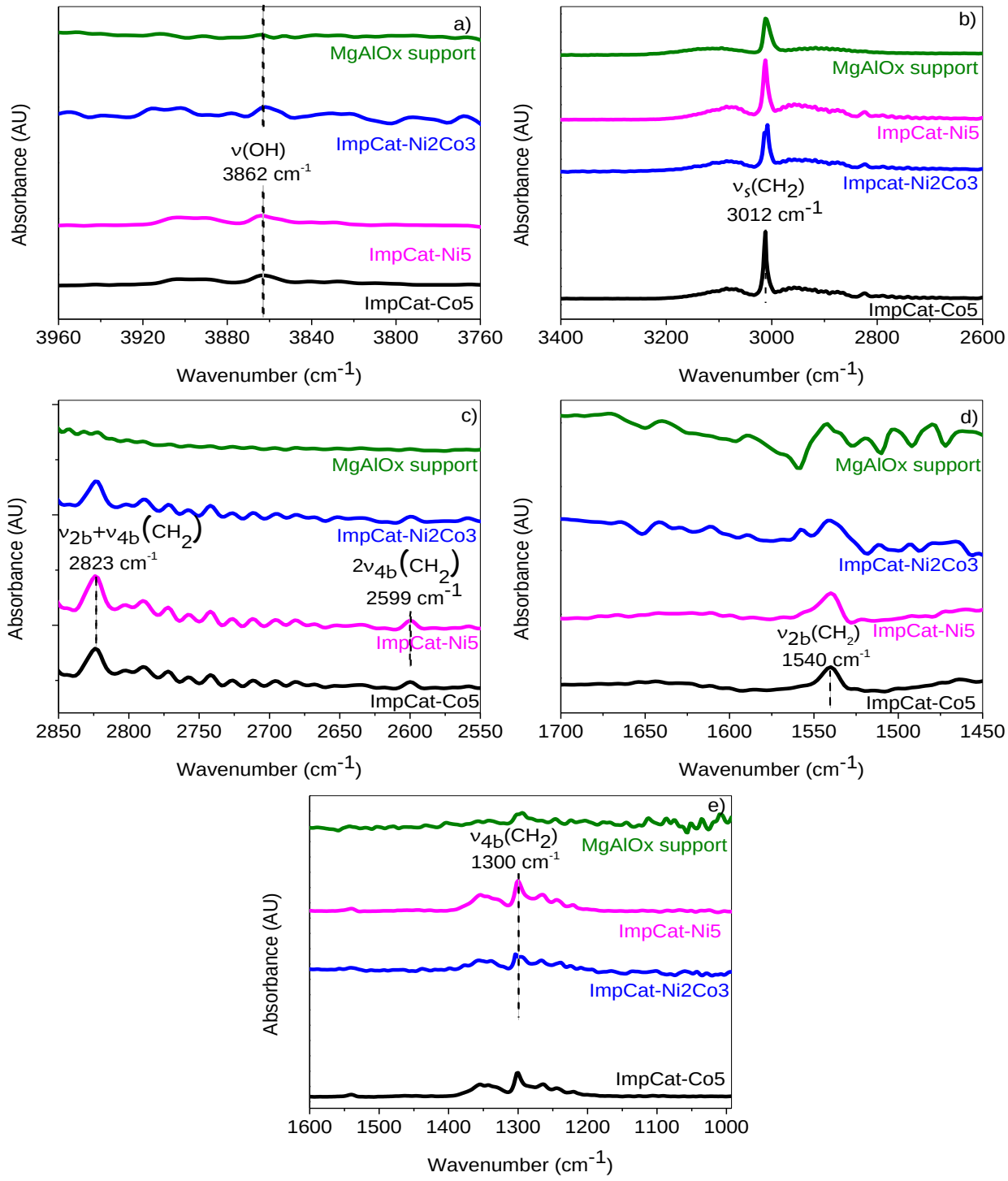

Figure 4-2. Comparison of bands produced by CH_4 on impregnated catalysts and support. a) Overtone 3_{v4}, b) v_3 symmetric vibration, c) combination band v_2+v_4 and overtone $2v_4$, d) v_2 bending vibration; e) v_4 bending vibration.

Spectra on Figures 4-1 and 4-2 show the methane bands after 15 minutes of interaction with the catalysts. The intensities of the bands are lower on the support than those on the rest of the catalysts. This difference in intensities suggests that methane could adsorb preferentially on the metal active sites. Morlanes (2013) reported that hydrocarbons are preferentially adsorbed on metal surfaces.

The dissociation of methane has been reported to occur on nickel catalysts, producing hydrogen and carbon adsorbed on the catalyst surface (Hickman and Schmidt, 2015; Schuurman et al., 1998) according to the Equation 4-1:

$$CH_4+Ni\leftrightarrow NiC+2H_2 \quad (4\text{-}1)$$

In this work, the presence of hydrogen could not be detected by infrared spectroscopy since this molecule is infrared inactive. C and CH_x species could not be detected either. The only possible observations that could indicate that dissociation of methane took place were the bands in the OH^- region previously mentioned. Bradford and Vannice (2007) reported that CH_x species can be detected by transient CH_4/D_2 or by deuteration of adsorbed methane.

4.2 MECHANISM OF CO_2 ADSORPTION AND DISSOCIATION

The molecule of carbon dioxide has 3 fundamental vibrations: symmetric stretching (v_1), bending (v_2) and antisymmetric (v_3) (Aoki et al., 1993). These vibrations occur at the wavenumbers 1388, 667 and 2349 cm^{-1}, respectively (Silverstein et al., 2005). However, only modes v_2 (667 cm^{-1}) and v_3 (2349 cm^{-1}) can be detected by infrared spectroscopy since mode v_1 (1388 cm^{-1}) is infrared inactive (it can be detected by Raman spectroscopy, though).

To elucidate how carbon dioxide interacts with the catalysts, the following steps were performed. Firstly, the catalysts were reduced as described before and then CO_2 entered into the reactor cell. After 15 minutes, a spectrum was collected. In the experiments performed, the mode v_2 located at 667 cm^{-1} was not always observed due to the numerous absorptions present at wavenumbers lower than 1000 cm^{-1}, assigned to metal oxides such as NiO (Rahemi et al., 2013). The band located at 2349 cm^{-1}, although it could be seen, appeared as variable peaks in the wavenumber range around 2280-2380 cm^{-1} (Figure 4-3). For these reasons, the bands at 667 cm^{-1} and 2349 cm^{-1} were not analyzed in the present work.

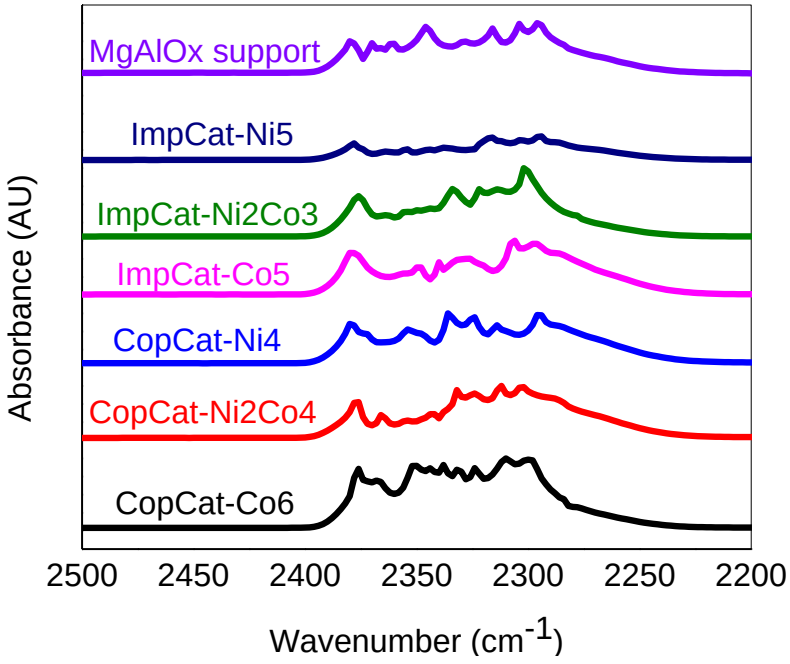

Figure 4-3. Antisymmetric mode of CO_2 (detected as variable peaks in the wavelength range around 2280-2380 cm^{-1}).

Carbon dioxide adsorbed on the catalysts could be clearly distinguished by the presence of 4 combination bands that appeared as four peaks at about 3730 and 3704 cm^{-1} (v_3 + v_1 bending

modes of CO_2); 3622 and 3598 cm^{-1} (v_3+2v_2 modes of CO_2) (Hu et al., 2013). On the support, the bands at about 3622 and 3598 cm-1 occurred at lower wavenumbers than on the rest of the catalysts containing nickel or cobalt (marked by the vertical black lines on Figures 4-4 and 4-5). Bond lengthening is related to lower wavenumber, or red shift, of bands in infrared spectrometry (Joseph and Jemmis, 2007). Bond lengthening could occur when the difference in electronegativity between two atoms in a bond is higher. Using the Pauling scale to calculate these differences yield: Mg-O=2.3 (3.5-1.2); Al-O=2 (3.5-1.5), Ni-O=1.7 (3.5-1.8) and, Co-O=1.7 (3.5-1.8). It is visible that the difference in electronegativity between the two atoms is higher for Mg-O and Al-O than for Ni-O and Co-O. This higher difference could result in bond lengthening and explain the red shift for the support compared to the catalysts that contain nickel, cobalt or both.

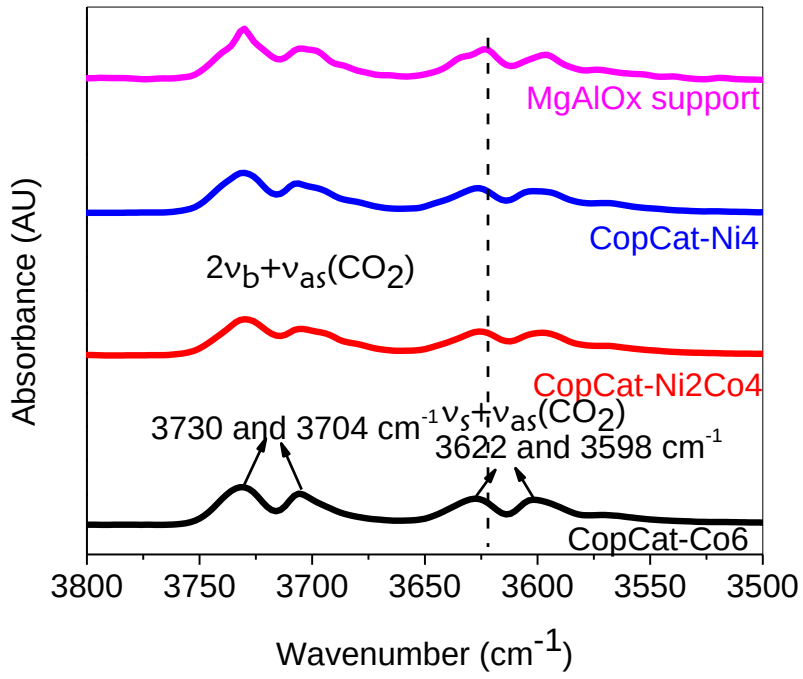

Figure 4-4. Bands produced by adsorbed CO_2 on coprecipitated catalysts and support.

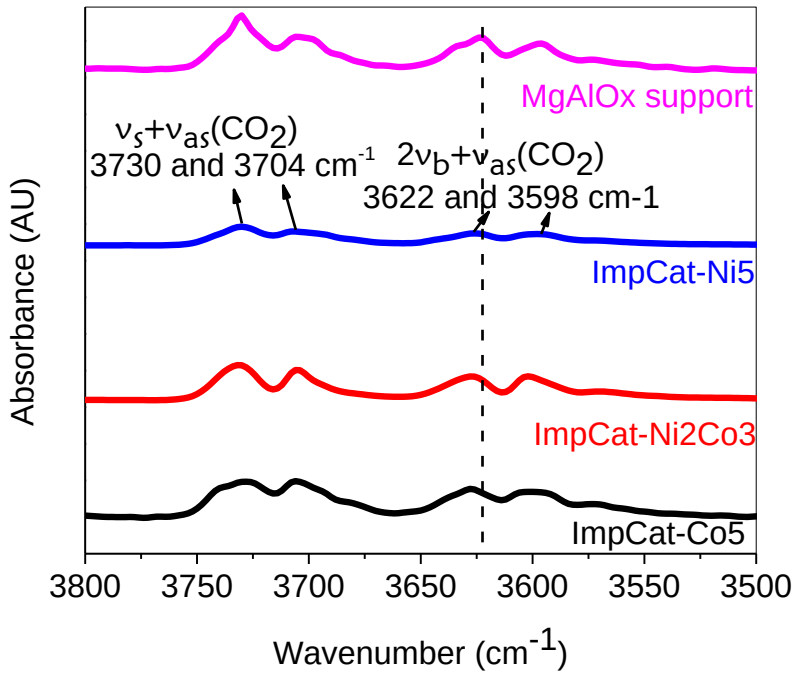

Figure 4-5. Bands produced by adsorbed CO_2 on impregnated catalysts and support.

Besides the fundamental vibrations and combination bands of carbon dioxide, other bands were shown during the interaction of CO_2 with the catalysts. One of these signals was a broad band at about 1640 cm^{-1} (Figure 4-6), which is attributed to the formation of carbonates produced by CO_2 reacting with oxygen in the surface of the catalysts (Pan et al., 2014; Nakamura et al., 1994 and; Morlanés, 2013). All catalysts tested in this work showed the capacity to form carbonates.

Some literature papers report that the catalysts with this attribute perform better for DRM than the catalyst without this characteristic. For example, Bitter et al. (1997) reported that catalysts such as Pt/Al_2O_3, Pt/TiO_2 and Pt/ZrO_2 showed the capacity to have carbonates formed on the support and had much higher activity than catalysts unable to form carbonates on the support, such as Pt/SiO_2.

Nakamura et al. (1994) reported that the catalytic activity for dry reforming of methane is in the order Rh/Al_20_3 >Rh/TiO_2 >Rh/SiO_2. Rh/Al_2O_3 was shown to be 18 times more active than Rh/SiO_2. They reported than CO_2 activates on Al_2O_3, TiO_2 and MgO as carbonates in the presence of hydrogen. Carbonates did not appear on SiO_2. Therefore, it was suggested that the formation of carbonates was responsible for the higher activity for dry reforming of methane.

Morlanés (2013) reported that the formation of carbonates is associated with a better oxygen release capacity for the support and the catalysts that showed carbonates formation had a higher activity for naphtha steam reforming.

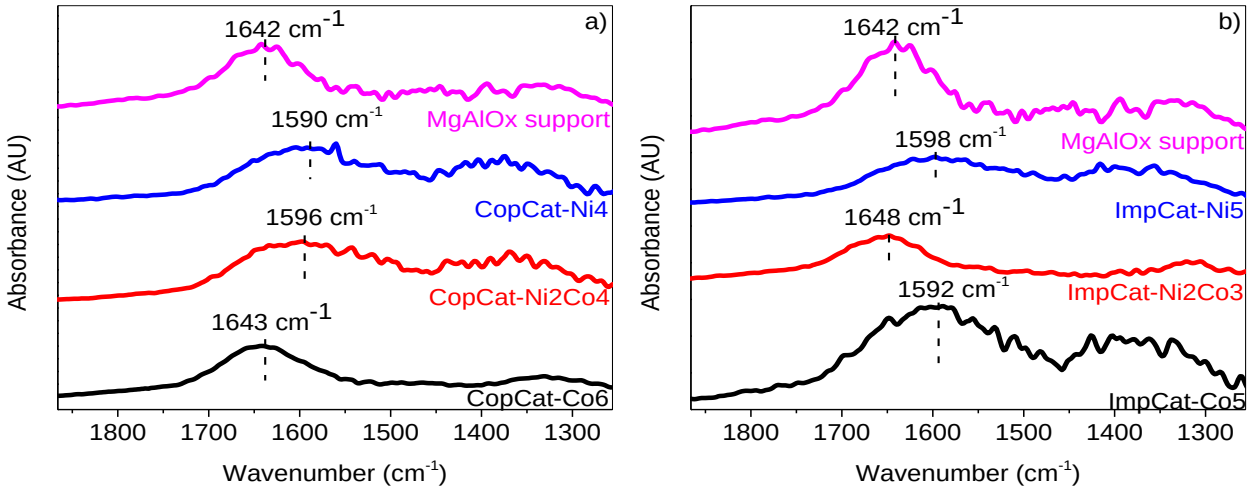

Figure 4-6. Broad band attributed to carbonates for a) coprecipitated and b) impregnated catalysts after the interaction with CO_2.

It can be noted from Figure 4-6 that the carbonate bands are located at different wavenumbers among different catalysts and preparation methods. For example, the band for the cobalt monometallic catalyst prepared by coprecipitation is found at 1643 cm^{-1} and shifted to lower wavenumbers when the cobalt monometallic catalyst was prepared by impregnation. On the

contrary, the bimetallic catalyst prepared by impregnation has a carbonate absorbance band at higher wavenumber than the bimetallic catalyst prepared by coprecipitation. The explanations for this observation is not clear.

The bands attributed to carbonates in Figure 4-6 for the cobalt catalysts, CopCat-Co6 and ImpCat-Co5, have higher intensities compared to the rest of the catalysts containing nickel. This higher intensity could be caused by the low reducibility on cobalt catalysts and higher oxygen content compared to nickel catalysts. It can also be seen that the band is higher for CopCat-Ni4 than for ImpCat-Ni5 which could be explained by the lower reducibility of coprecipitated catalysts compared to impregnated catalysts and, therefore, higher oxygen content to which CO_2 molecules can attach to form carbonates. The $MgAlO_x$ support sample was not treated by reduction because it lacks of nickel and cobalt. Therefore, this sample should have the highest oxygen content, and this might explain the maximum intensity for this sample compared to the rest of the catalysts.

It might be important that the reduction extent is not very high or low. If the reduction extent is very high, the catalyst would have too much Ni^0 and Co^0 and low amount of NiO, CoO and other oxides. This situation would allow activation of methane on Ni^0 and at the same time would permit low formation of carbonates. On the contrary, if the reduction extent is very low, the catalysts would result in low Ni^0 and Co^0 and high content of NiO, CoO and other oxides. In this situation, carbonates would be easily formed but activation in Ni^0 (such as methane activation) would hardly occur. Therefore, the reduction should produce an optimal concentration of Ni^0, Co^0, NiO, CoO and other oxides.

Carbonates could be seen not only in the presence of CO_2 but also when carbon monoxide interacted with the catalysts (Figure 4-7). Therefore, it is possible that two mechanisms explain the formation of carbonates: 1) Dissociation of CO_2 into CO and atomic oxygen and further attachment of CO to two oxygen atoms on the support; 2) Attachment of CO_2 to an oxygen atom on the support. This is in agreement with Morlanés (2013).

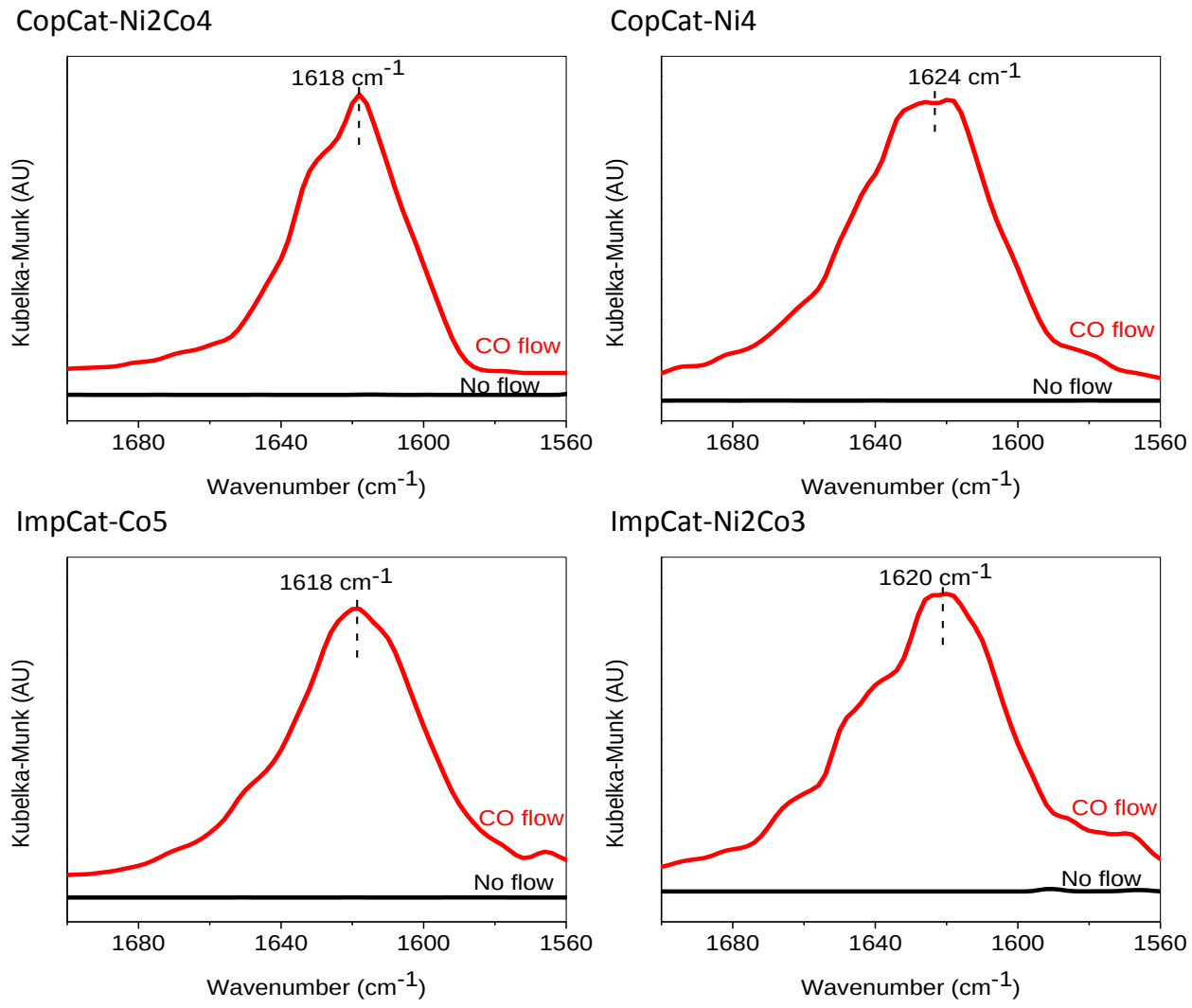

Figure 4-7. Carbonates formed after CO interacted with catalysts at 600 ^{o}C.

The absorbance bands attributed to carbonates seen after the interaction of carbon monoxide (Figure 4-7) is not shifted as obviously among different catalysts compared to the bands seen after the interaction of carbon dioxide with the catalysts on Figure 4-6.

Another band at 2077 cm^{-1} was found when CO_2 interacted with any of the catalysts and the support. This peak was very minuscule compared to the rest of the peaks and it was visible on all catalysts only after zooming in that area (Figure 4-8). This band is attributed to linear carbonyl on different nickel active sites (Morlanés, 2013) produced by dissociation of CO_2 into CO and O^{2-} according to Equation 4-2.

$$CO_2 \rightleftharpoons CO + O \qquad (4\text{-}2)$$

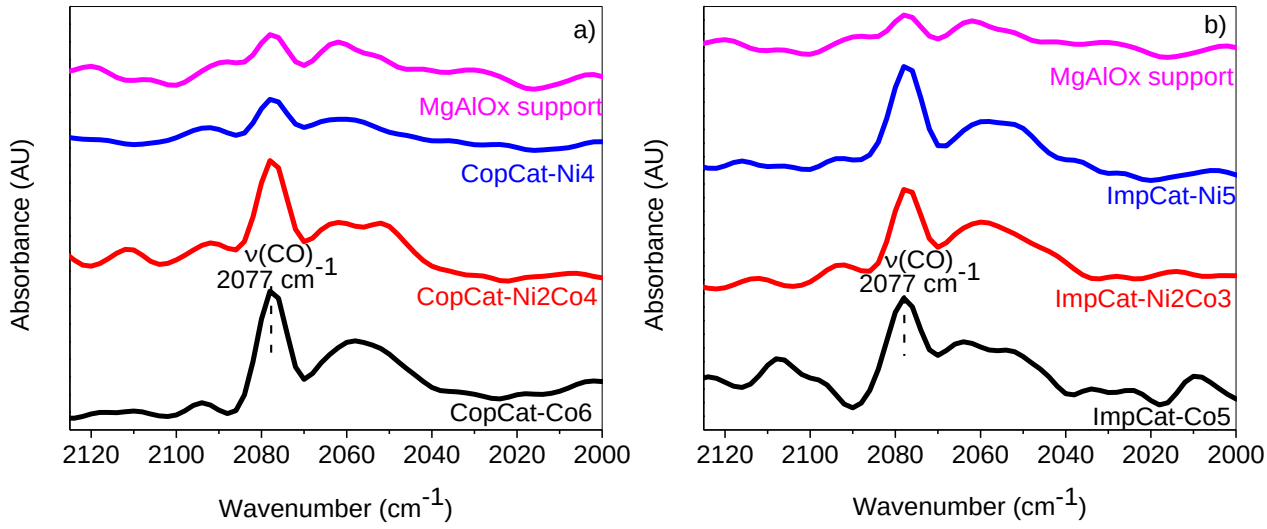

Figure 4-8. Band at 2077 cm^{-1} attributed to linear carbonyl for a) coprecipitated and b) impregnated catalysts in the presence of CO_2.

In this work, the band at 2077 cm^{-1} appeared on catalysts containing nickel and cobalt and also on the support. This band is higher on cobalt catalysts, especially on CopCat-Co6. It was

reported on Wang et al. (2013) that CopCat-Co6 was not able to be reduced, consisting of 100% of CoO and 0% Co, this would allow more activation of CO_2 and, therefore, more dissociation of CO_2. Morlanés (2013) found bigger bands for adsorbed CO on NiMgAlCe catalyst compared to NiMg, NiMgAl, NiMgCoAl. This was attributed to small metal particles with higher oxygen release capacity of NiMgAlCe catalyst.

Summarizing, upon CO_2 interaction with any of the catalysts, it was observed adsorbed CO_2, linear carbonyl produced by dissociation of CO_2 into CO and atomic oxygen and, carbonates formation that could be produced by either CO_2 or CO attachment to oxygen species present in the catalysts.

4.3 MECHANISM OF DRY REFORMING OF METHANE

The following steps were applied to understand how CH_4 and CO_2 interact with the catalysts. Firstly, the catalysts were reduced as explained earlier and then both CH_4 and CO_2 were introduced. After 15 minutes, a spectrum was collected. During the coadsorption of CH_4 and CO_2 at 600 ^oC (or during dry reforming of methane reaction) it was possible to observe the same bands for all the catalysts studied compared to when the independent interactions of CH_4 and CO_2 were studied. CH_4 and CO_2 were coadsorbed on all catalysts before the interaction of H_2S and also prior the interaction of SO_2, as shown in Figures 4-9 and 4-10. These 2 sets of data allowed to test the reproducibility of the results. It can be seen from Figures 4-9 and 4-10 that all bands are located at the same wavenumber, except for the carbonates. This allows to ascertain qualitative repeatability of the results. There are differences in intensities for the same catalysts in the two different figures that could be explained by the way in which the sample is inserted in

the sample holder (such as the pressure applied at the moment of inserting the sample holder). Difference in intensity among different spectra for quantitative information is more reliable when the same catalyst is used to obtain the different spectra.

It can be seen that the bands attributed to adsorbed carbonyl appears in all cases at 2077 cm^{-1}. This band appeared when carbon dioxide interacted with the catalysts independently as well as when both CH_4 and CO_2 were adsorbed at the same time. For carbonates, there are differences in the position of the bands for the same catalyst in Figures 4-9 and 4-10. These differences could be attributed to different types of carbonates coalescing into one single band but this is only a guess. It can also be noted that the adsorbed carbonyl and the carbonates bands are not easily seen in the spectra in the 4000-1000 cm^{-1} range. It was possible to see these bands only by zooming in that region. That is why the three different spectrums are shown in each Figure.

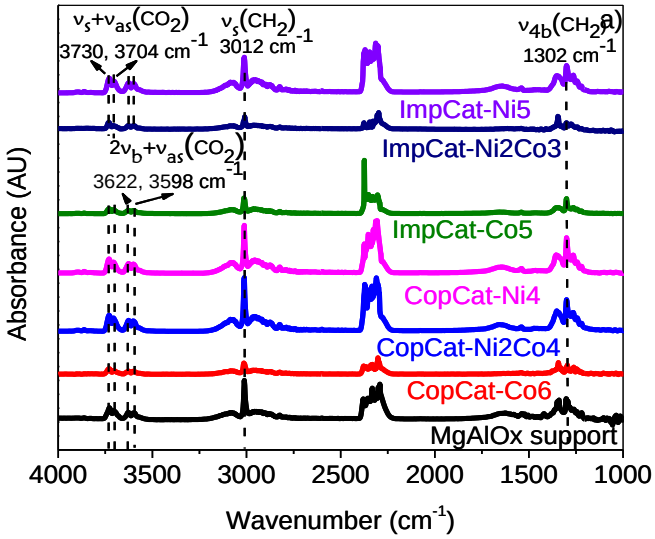

Figure 4-9. Coadsorption of CH_4 and CO_2 before the introduction of H_2S. a) Full range spectra; b) zoom in for carbonyl bands and ; c) zoom in for carbonates.

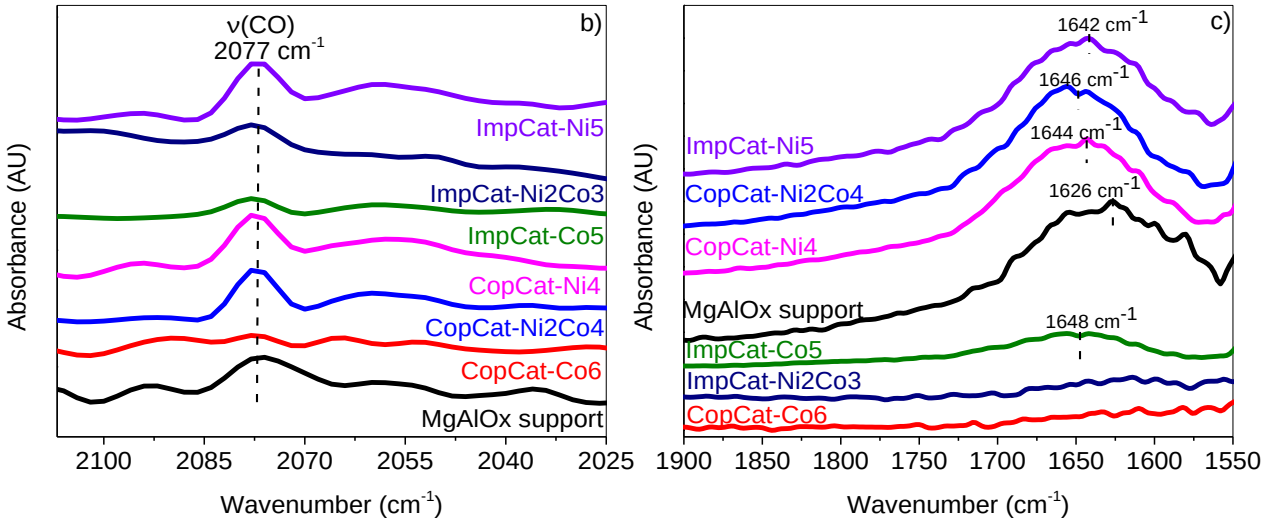

Figure 4-9. Coadsorption of CH_4 and CO_2 before the introduction of H_2S. a) Full range spectra; b) zoom in for carbonyl bands and ; c) zoom in for carbonates (continued).

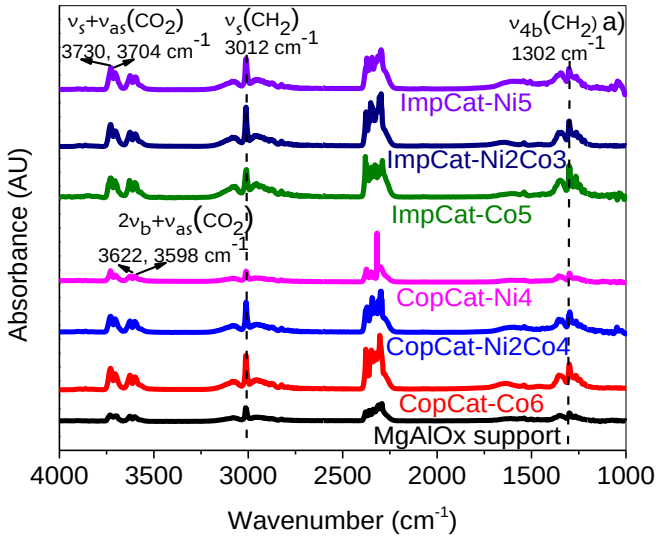

Figure 4-10. Coadsorption of CH_4 and CO_2 before the introduction of SO_2. a) Full range spectra; b) zoom in for carbonyl bands and ; c) zoom in for carbonates.

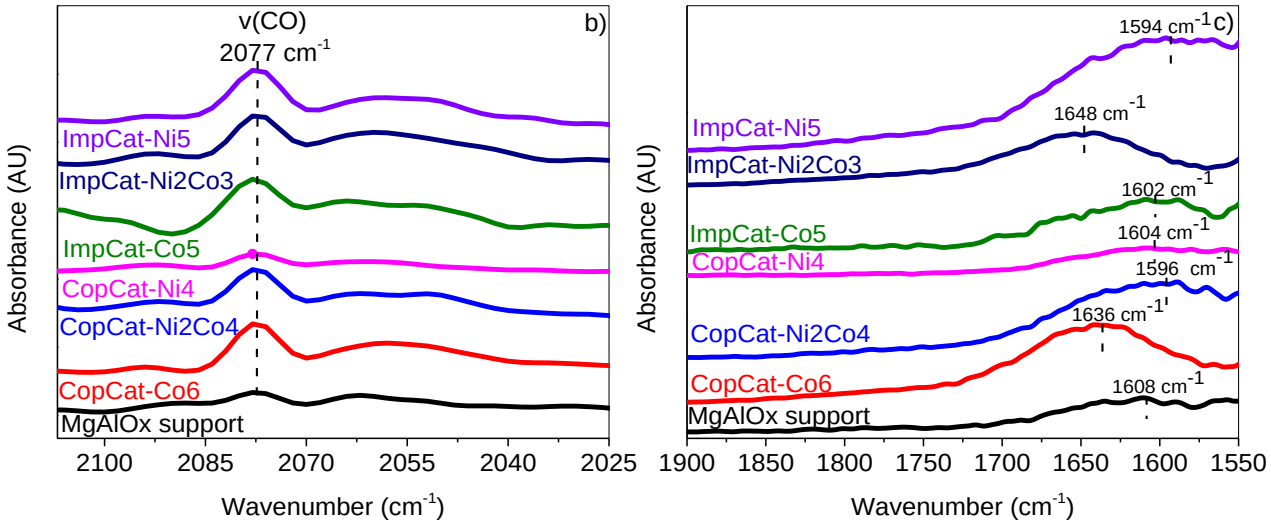

Figure 4-10. Coadsorption of CH_4 and CO_2 before the introduction of SO_2. a) Full range spectra; b) zoom in for carbonyl bands and ; c) zoom in for carbonates (continued).

It can also be seen from Figures 4-9 and 4-10 that the intensity of the carbonyl peaks is related with the intensity of the carbonate peaks. For example, in Figure 4-9 the carbonyl peaks with the lowest intensities are ImpCat-Ni2Co3, ImpCat-Co5 and CopCat-Co6. Similarly, the catalysts with the lowest intensities for the carbonates bands are the same (ImpCat-Ni2Co3, ImpCat-Co5 and CopCat-Co6). From the same prespective, it can be seen in Figure 4-10 that the carbonyl bands with the lowest intensities are the support and CopCat-Ni4. Similarly, the bands for carbonate with the lowest intensities are the support and CopCat-Ni4 as well. This suggest that there is a correlation between the concentration of carbonates and the linear carbonyl.

The bands found during the coadsorption of CH_4 and CO_2 confirm that the mechanism for dry reforming of methane involves formation of carbonates and dissociation of carbon dioxide into adsorbed carbonyl. Carbon monoxide could also be produced by the following mechanisms that were not directly confirmed by this research. 1) Reaction of carbon with an oxygen atom,

forming one molecule of CO (Goula et al., 1996; Tsipouriari and Verykios, 1999). 2) Reaction of carbon with one carbonate group (CO_3^{2-}), forming two molecules of CO and leaving one atom of oxygen available or (Tsipouriari and Verykios, 2001). 3) Reaction of carbon with one molecule of CO_2, forming two molecules of CO, also known as Boudouard reaction (Schuurman et al., 1998; Kroll et al., 1997). If the previous steps did not exist, the catalysts would deactivate due to carbon deposition generated by the following reaction:

$$CH_4 \rightarrow C + H_2 \qquad \Delta H_{1073K} = 90.1 \text{ KJ/mol } CH_4 \tag{4-3}$$

4.4 Effect of H_2S on dry reforming of methane

The purpose of these experiments is to elucidate the poisoning mechanism by H_2S on the dry reforming of methane. To better understand the mechanism, the independent adsorption of H_2S was studied first to try to understand how hydrogen sulfide interacts with the catalysts and determine the chemical species formed on the catalyst surface.

Secondly, in other set of experiments, the dry reforming of methane reaction was carried out first. Then, H_2S was introduced to understand its effect on the mechanism of the dry reforming of methane reaction. Finally the H_2S feed was stopped to understand what happens on the surface of the catalysts after the hydrogen sulfide feed is stopped.

4.4.1 Independent interactions of H_2S with the catalysts

For these experiments, the catalysts were reduced first as explained in chapter 3. Then, the hydrogen feed was stopped and nitrogen started to flow for about 10 minutes. Subsequently, a

background spectrum was collected. After the background scan, H_2S was introduced and some scans were obtained afterwards.

In this work the presence of peaks attributed to the vibrations of hydrogen sulphide or the vibrations of metal sulphides were not observed. Datta and Cavell (1985) pointed out that the adsorption and dissociation of hydrogen sulphide, as well as the formation of nickel sulphide, cannot be detected by infrared spectroscopy. X-ray absorption spectroscopy could determine the formation of nickel sulfide or cobalt sulphide.

However, an interesting observation was found when H_2S interacted with the reduced catalysts without the presence of methane or CO_2. It was visible that soon after H_2S was introduced, a negative peak (pointing downwards) appeared in the OH^- region. The negative peak could suggest hydroxyl consumption by H_2S. Usually, the peaks in absorbance units are pointing upwards, but the presence of this peak pointing downwards could be caused by the background subtraction. At the moment of the background scan, hydroxyl functional groups might be present in the catalysts. This background spectrum is subtracted to further collected spectra. If hydroxyl is consumed, the background subtraction should produce a peak pointing in the opposite direction (Figure 4-11). The previous observation is in agreement with Pakhare et al. (2014).

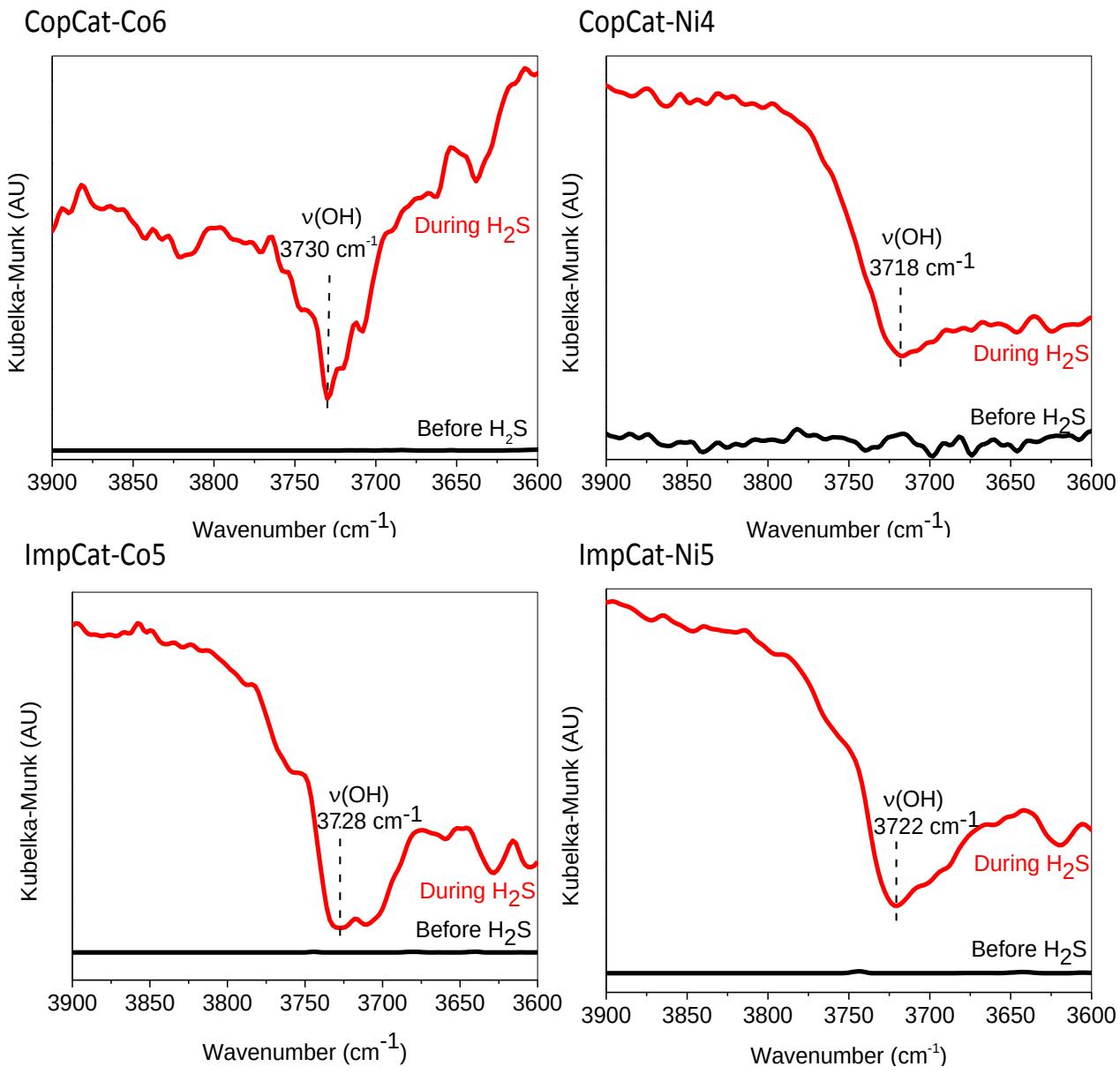

Figure 4-11. OH^- consumption in the presence of H_2S.

The disappearance of OH^- groups is ascribed to hydroxy groups reacting to produce adsorbed water (Toops and Crocker, 2008). This OH^- groups could be in the form of $Ni(OH)_2$. Czekaj et al. (2011) reported that their "as delivered" catalysts contained NiO and $Ni(OH)_2$ particles. The

partial reduction of Ni^{2+} produced Ni^0 and still some NiO and $Ni(OH)_2$ particles remained unreduced.

Davidson and Sohail (1995) documented that hydroxy groups in zinc oxides disappeared due to interaction with hydrogen sulphide, producing water. They suggested that H_2S required chemisorbed OH- to transfer two protons. They concluded that in the creation of sulfides, H_2S does not transfer two protons to oxides on the surface.

For cobalt monometallic catalysts, CopCat-Co6 and ImpCat-Co5, the negative peak occurs at higher wavenumbers (3730 and 3728 cm^{-1}, respectively) compared to the nickel monometallic catalysts CopCatNi-4 and ImpCatNi-5 (3718 and 3722 cm^{-1}, respectively).

4.4.2 Adsorptions of CH_4 and CO_2 in the presence of H_2S

For this set of experiments, the catalysts were reduced first by a mixture of 5% H_2 in N_2 for 2.5 hours. Right after the reduction, a background spectrum was collected. Then, a mixture of methane and CO_2 was introduced to the DRIFTS cell and after 15 minutes the first spectrum was collected. Following the previous step, a mixture of 522 ppm of H_2S in Ar was added and after 3 hours, the second spectrum was scanned. After the second scan, the flow of hydrogen sulfide was stopped and the flow of methane and CO_2 continued for one more hour and then the third spectrum was collected. All the spectra were normalized for easier comparison.

Figures 4-12 to 4-18 show the comparison of bands produced by carbon dioxide: a) and methane: b) 3012 cm^{-1} (asymmetrical stretching); c) 2823 and 2599 cm^{-1} (combination band and overtone respectively) and; d) 1540 and 1302 cm^{-1} (in-plane bending and out-of-plane bending, respectively). These bands are compared at three different intervals: before the introduction of

H_2S (black spectrum), three hours after the introduction of H_2S (red spectrum) and one hour after stopping the H_2S flow (blue spectrum). The purpose of comparing these three spectra at different intervals was to study 1) the CH_4 and CO_2 response to the interaction of H_2S to determine if poisoning occurred or not and; 2) the recovery of the CH_4 and CO_2 bands after stopping H_2S to determine if the catalyst can be recovered after being poisoned by H_2S.

The spectra for the catalysts containing only nickel, both prepared by coprecipitation (CopCat-Ni4)) and impregnation (ImpCat-Ni5) are compared in Figures 4-12 and 4-13, respectively. It can be seen a decrease in intensity in all the absorbance bands of CO_2 and CH_4 after 3 hours of exposure to H_2S. This decline suggests that H_2S blocks active sites for CH_4 and CO_2 adsorptions. It can also be noticed that the decrease caused by H_2S poisoning is lower for the impregnated catalysts ImpCat-Ni5 (Figure 4-13) than that for coprecipitated catalyst CopCat-Ni4 (Figure 4-12).

It can also be noted that the CH_4 and CO_2 bands for all the catalysts increased in intensity after stopping the H_2S flow, suggesting that the poisoning is reversible and that catalyst activity is recoverable. This could be confirmed by Gas Chromatography.

The intensity of the CH_4 and CO_2 bands collected 1 hour after stopping the H_2S feed are much higher than the bands collected before the introduction of H_2S (with the exception of MgAlOx support). This could be explained by the time that the catalysts were not in contact with H_2S, which was 15 minutes for the period before the introduction of H_2S and 60 minutes for the period after stopping the H_2S feed. Therefore, both CH_4 and CO_2 had more time to adsorb on the catalyst surface. An alternative explanation to this phenomena is that H_2S contributed to reduce

the metals, allowing more adsorption of CH_4 and CO_2. This could be further determined by synchrotron experiments.

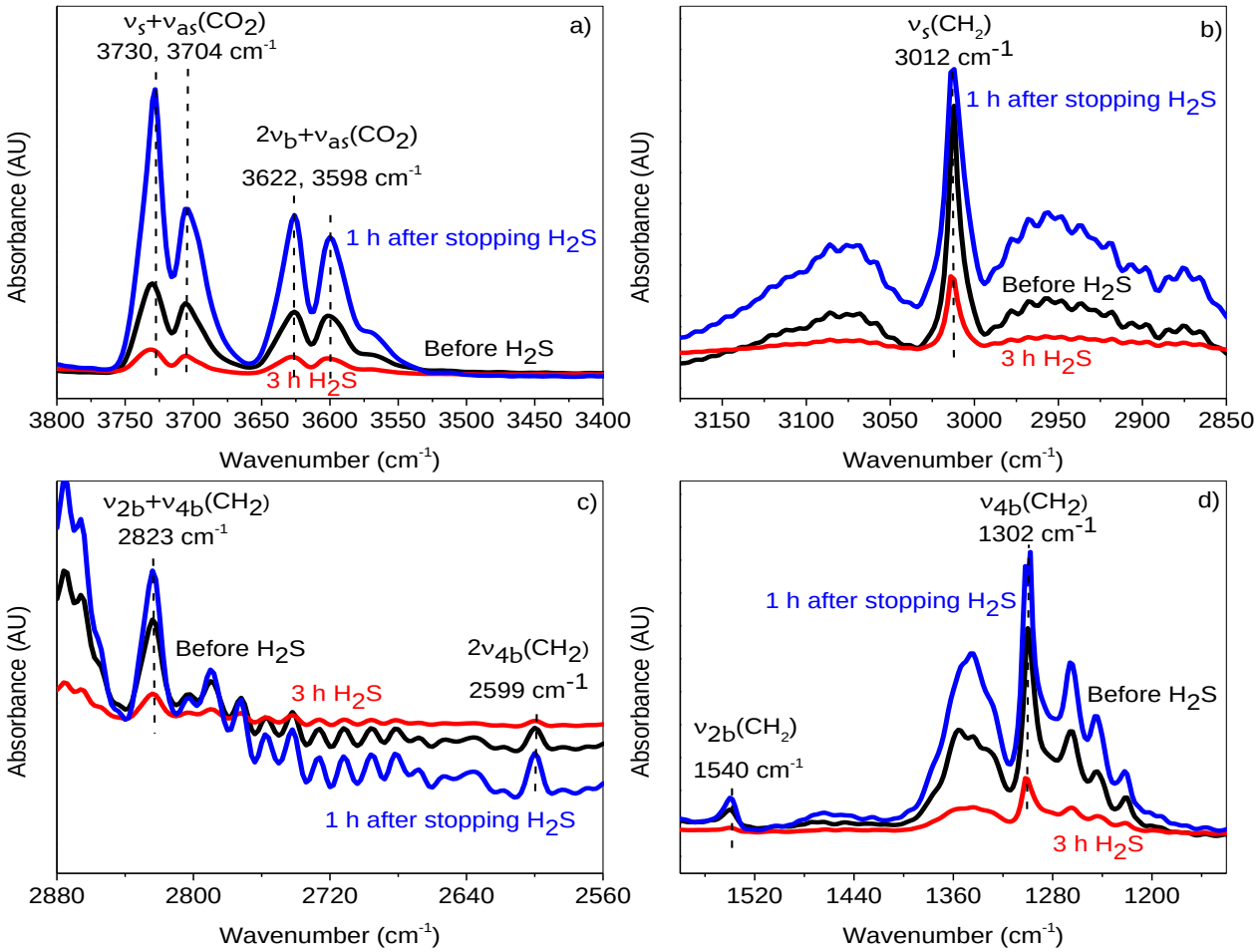

Figure 4-12. Bands attributed to CO_2 (a) and CH_4 (b, c, d) displayed before introducing H_2S, 3 hours after introducing H_2S and 1 hour after stopping the H_2S flow for CopCat-Ni4.

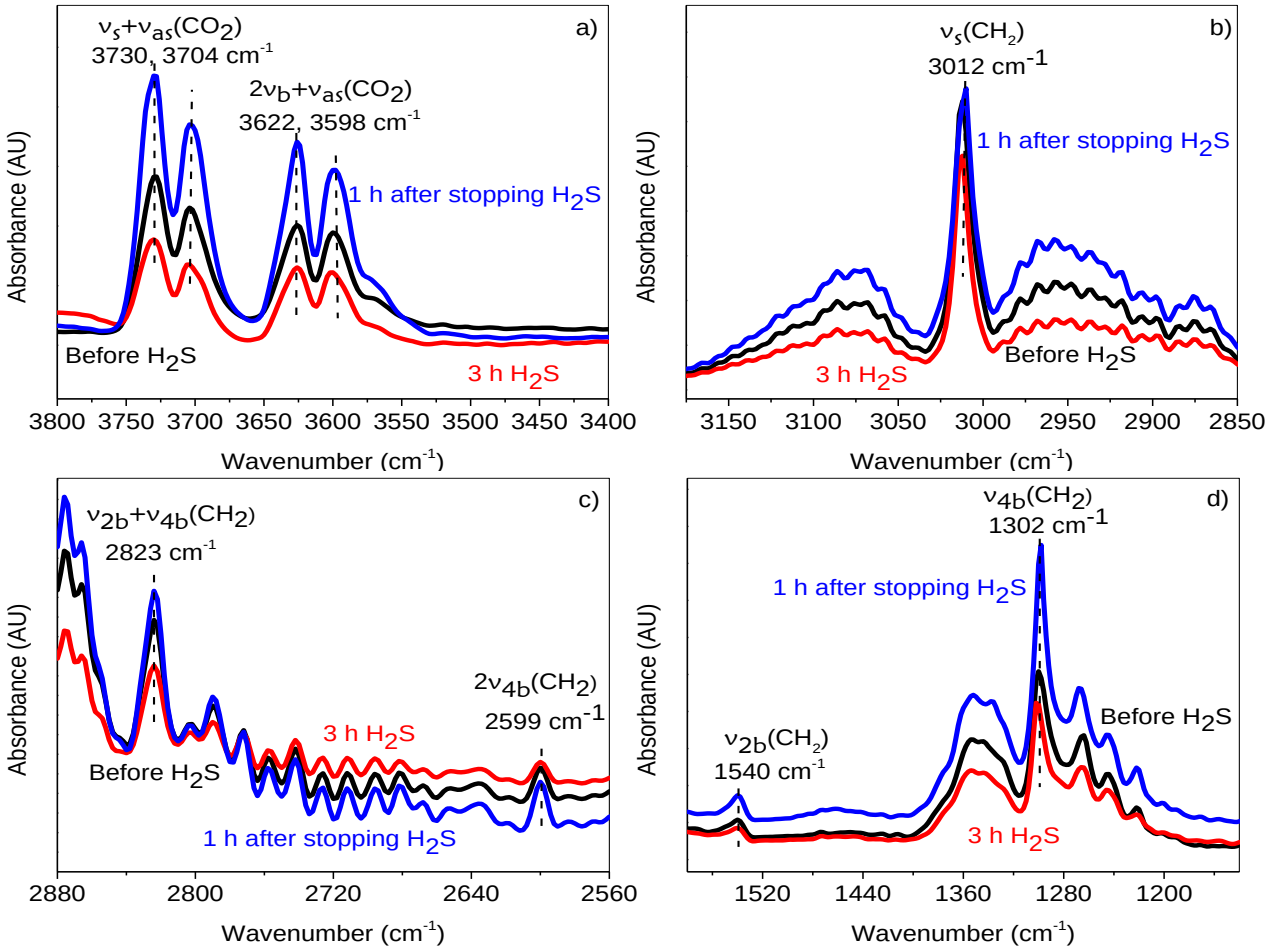

Figure 4-13. Bands attributed to CO_2 (a) and CH_4 (b, c, d) displayed before introducing H_2S, 3 hours after introducing H_2S and 1 hour after stopping the H_2S flow for ImpCat-Ni5 (continued).

Interestingly, the catalysts containing only cobalt (CopCat-Co6 and ImpCat-Co5) showed the opposite trend: the intensities of the methane and CO_2 bands increased in the presence of hydrogen sulphide (Figures 4-14 and 4-15), suggesting that H_2S does not poison the cobalt sites at 600 ^{o}C.

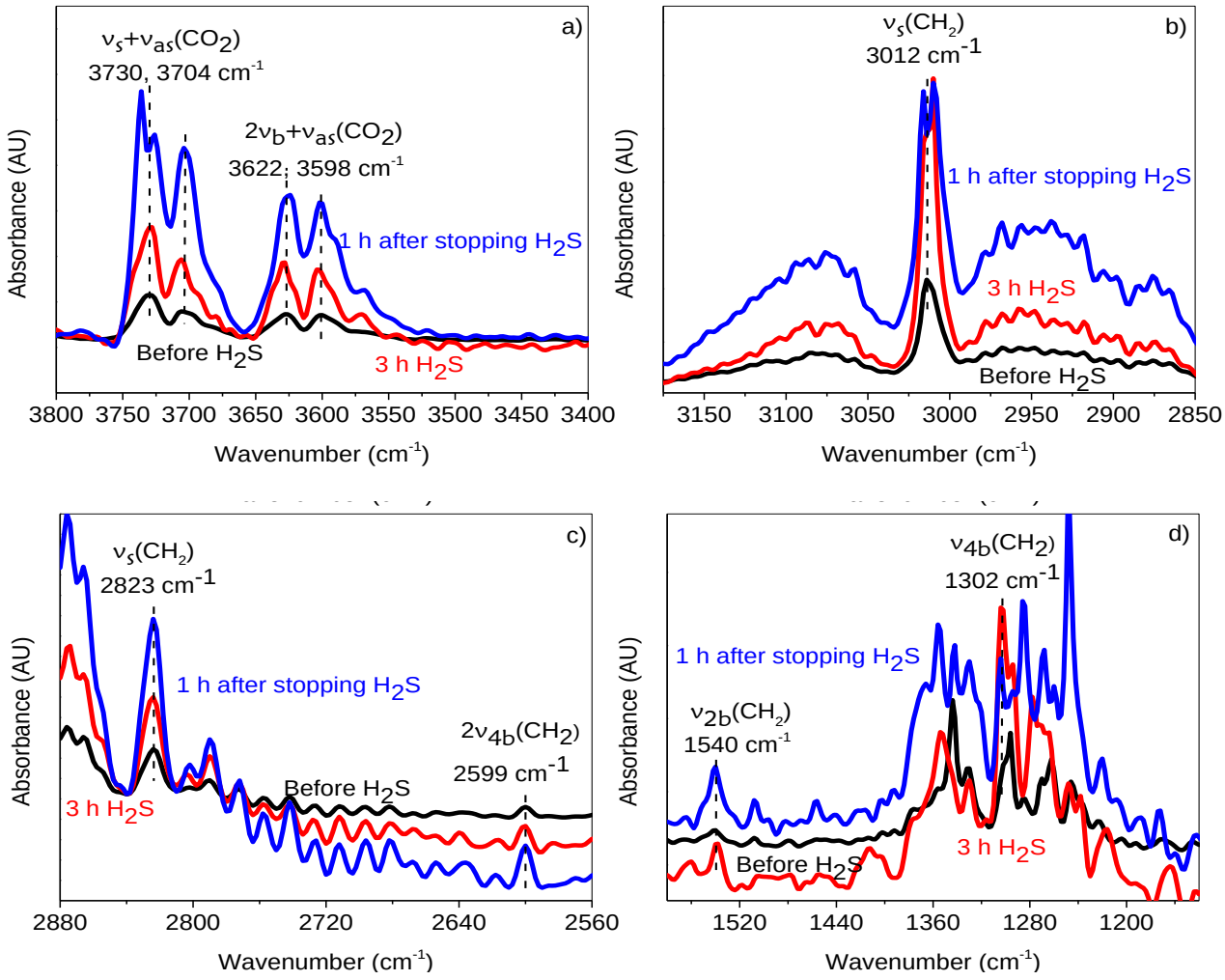

Figure 4-14. Bands attributed to CO_2 (a) and CH_4 (b, c, d) displayed before introducing H_2S, 3 hours after introducing H_2S and 1 hour after stopping the H_2S flow for CopCat-Co6 (continued).

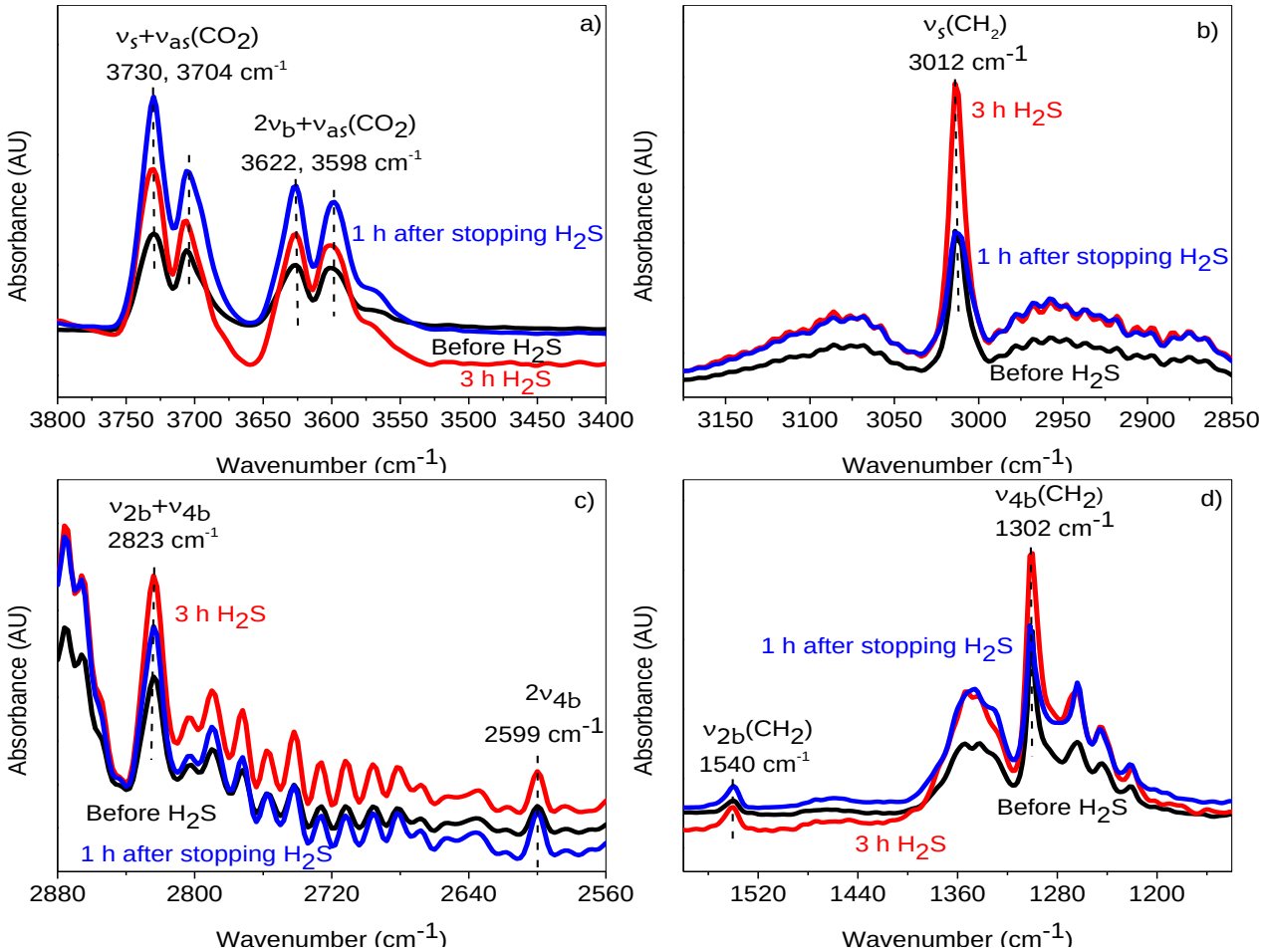

Figure 4-15. Bands attributed to CO_2 (a) and CH_4 (b, c, d) displayed before introducing H_2S, 3 hours after introducing H_2S and 1 hour after stopping the H_2S flow for ImpCat-Co5.

For the coprecipitated bimetallic catalysts CopCat-Ni2Co4 (Figure 4-16) the bands produced by methane and CO_2 significantly decreased in intensity in the presence of H_2S and regained intensity after the removal of hydrogen sulphide. The decline in intensity could be caused by nickel active sites poisoned or blocked by hydrogen sulphide. It can also be noted that the decrease in intensity in the methane and CO_2 bands is lower for the impregnated catalyst ImpCat-Ni2Co3 (Figure 4-17) than for the coprecipitated catalyst CopCat-Ni2Co4 (Figure 4-16).

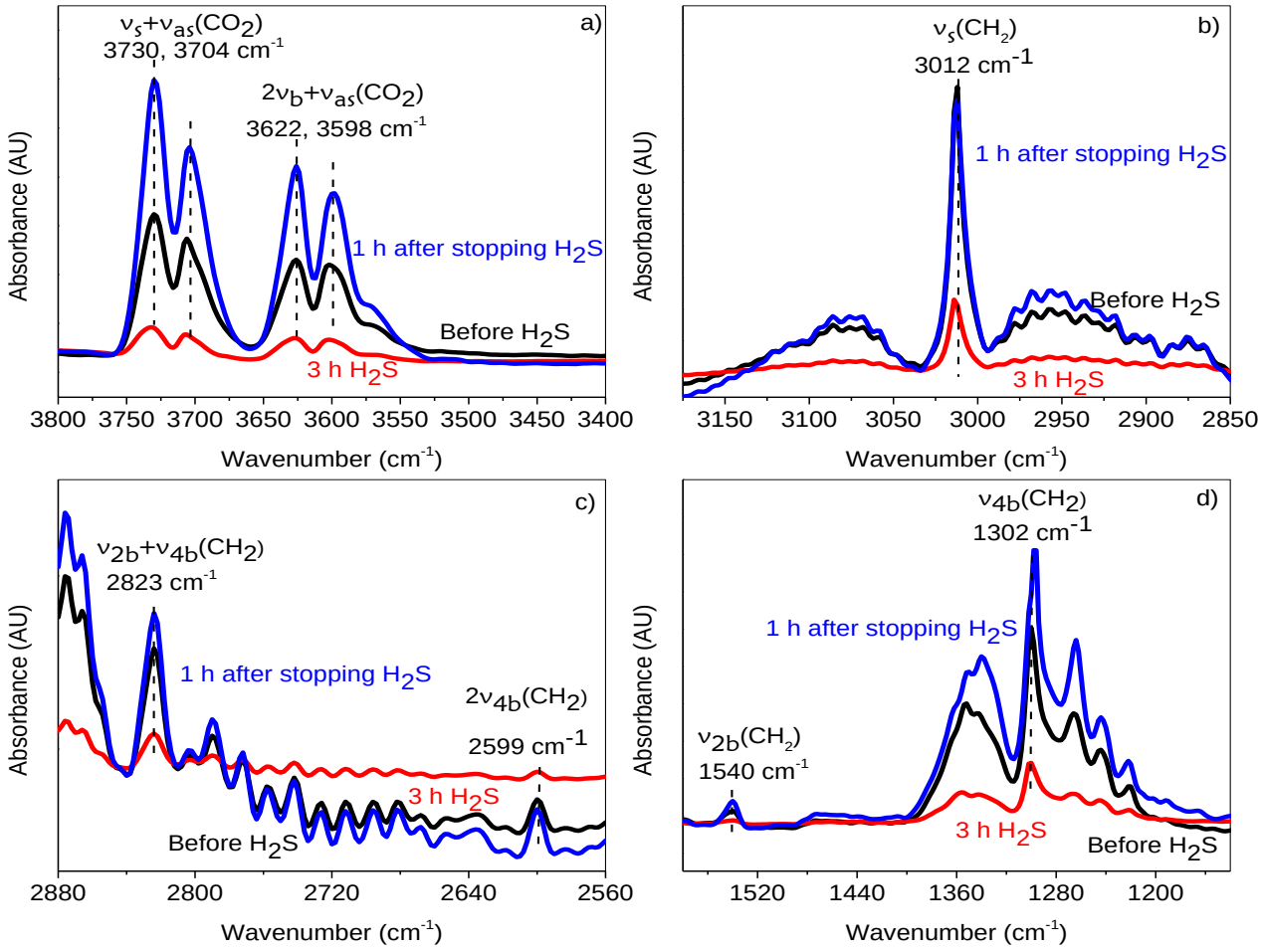

Figure 4-16. Bands attributed to CO_2 (a) and CH_4 (b, c, d) displayed before introducing H_2S, 3 hours after introducing H_2S and 1 hour after stopping the H_2S flow for CopCat-Ni2Co4.

The ImpCat-Ni2Co3 was the only nickel-containing catalysts for which the CO_2 and methane intensities were not highly lowered in the presence of H_2S (the height of the peaks remained almost the same) as shown in Figure 4-17. This could suggest that among all the nickel-containing catalysts tested, this is the catalyst with more tolerance to H_2S poisoning. After the interruption of the H_2S flow, the bands attributed to CH_4 and CO_2 increased in intensity.

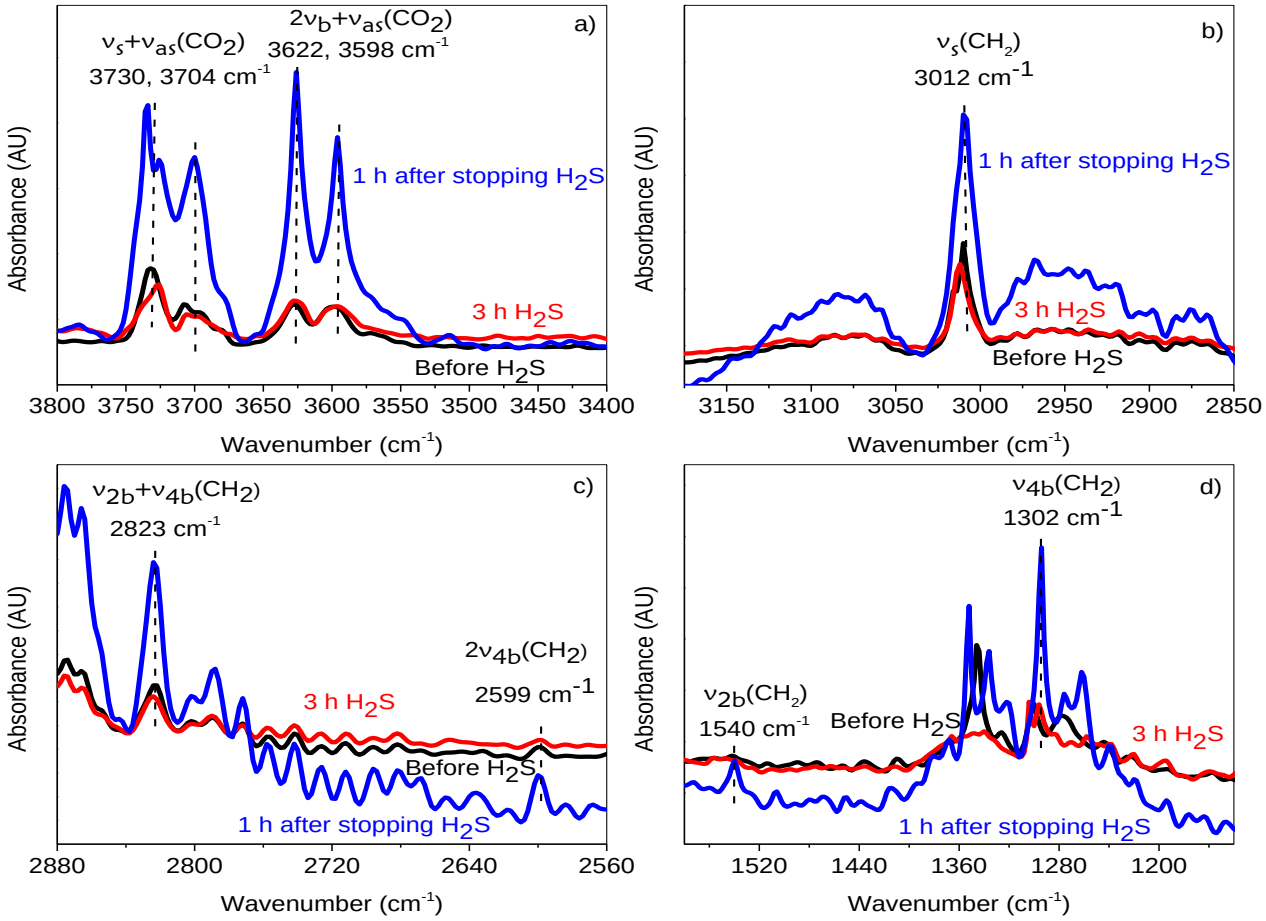

Figure 4-17. Bands attributed to CO_2 (a) and CH_4 (b, c, d) displayed before introducing H_2S, 3 hours after introducing H_2S and 1 hour after stopping the H_2S flow for ImpCat-Ni2Co3.

It can also be observed that the intensities of methane and CO_2 bands decreased more on coprecipitated catalysts (CopCat-Ni2Co4 and CopCat-Ni4) than on impregnated catalysts (ImpCat-Ni2Co3 and ImpCat-Ni5). This lower decline for impregnated catalysts could be caused by their larger pore volume and pore size than coprecipitated catalysts. Also, the particles size resulted from reduction are higher on impregnated catalysts than on coprecipitated catalysts (Shakouri, 2011). The higher tolerance to H_2S on impregnated catalysts could be explained by the higher reducibility of nickel and cobalt on impregnated catalysts (Wang et al., 2013).

For the support, the methane and CO_2 intensities decreased in the presence of H_2S and remained with almost the same intensity after H_2S was stopped, suggesting that H_2S reduced the adsorptions of methane and CO_2 on the support irreversibly.

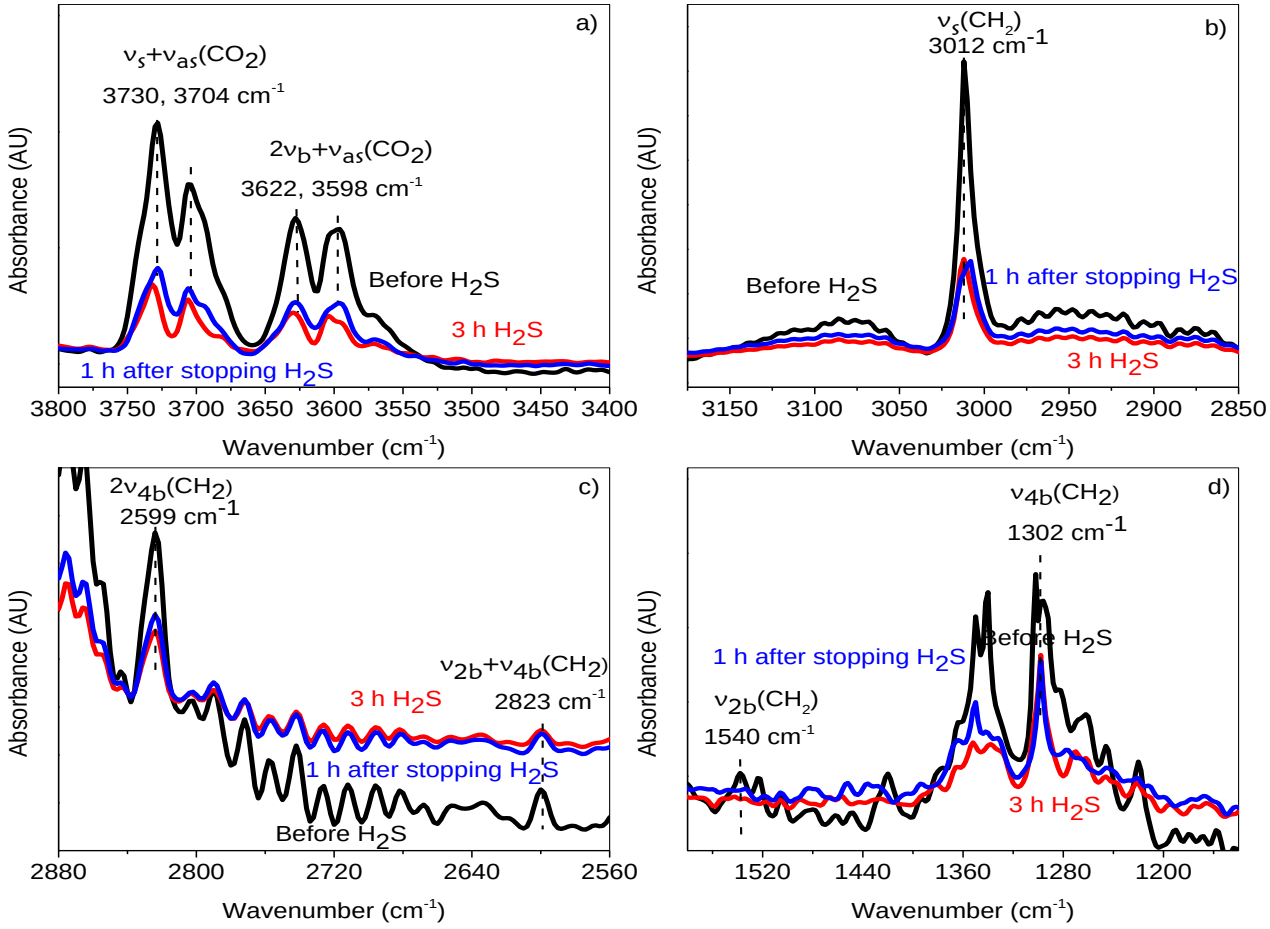

Figure 4-18. Bands attributed to CO_2 (a) and CH_4 (b, c, d) displayed before introducing H_2S, 3 hours after introducing H_2S and 1 hour after stopping the H_2S flow for $MgAlO_x$ support.

The bands collected 1 hour after stopping H_2S feed were the highest for the catalysts containing nickel or cobalt. However, for the support, these bands remained decreased almost at the same intensities than bands collected in the presence of H_2S, suggest that sulfur blocked active sites

that interfered with the methane and CO_2 adsorptions even after the removal of H_2S (Figure 4-18). Czekaj et al. (2011) found that carbonyl sulfide is more stably adsorbed to the support than to nickel particles on Ni/Al_2O_3 catalyst.

One effect produced by H_2S in the mechanism of dry reforming of methane reaction is to decrease the concentration of carbonates as shown in Figure 4.19. Davidson and Sohail (1995) documented that carbonates (CO_3^{2-}) react with hydrogen sulfide to produce H_2O and CO_2 during sulfidation.

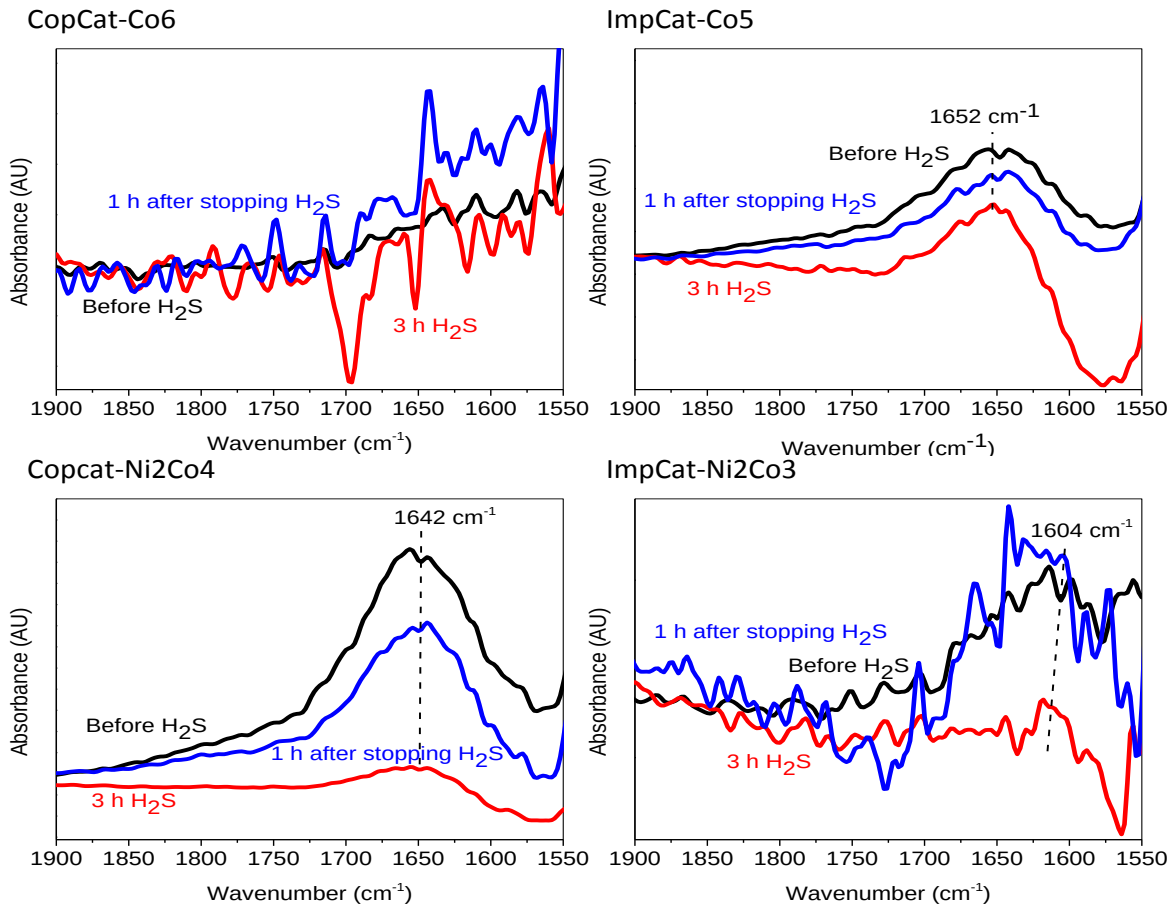

Figure 4-19. Decrease in the concentration of carbonates in the presence of H_2S.

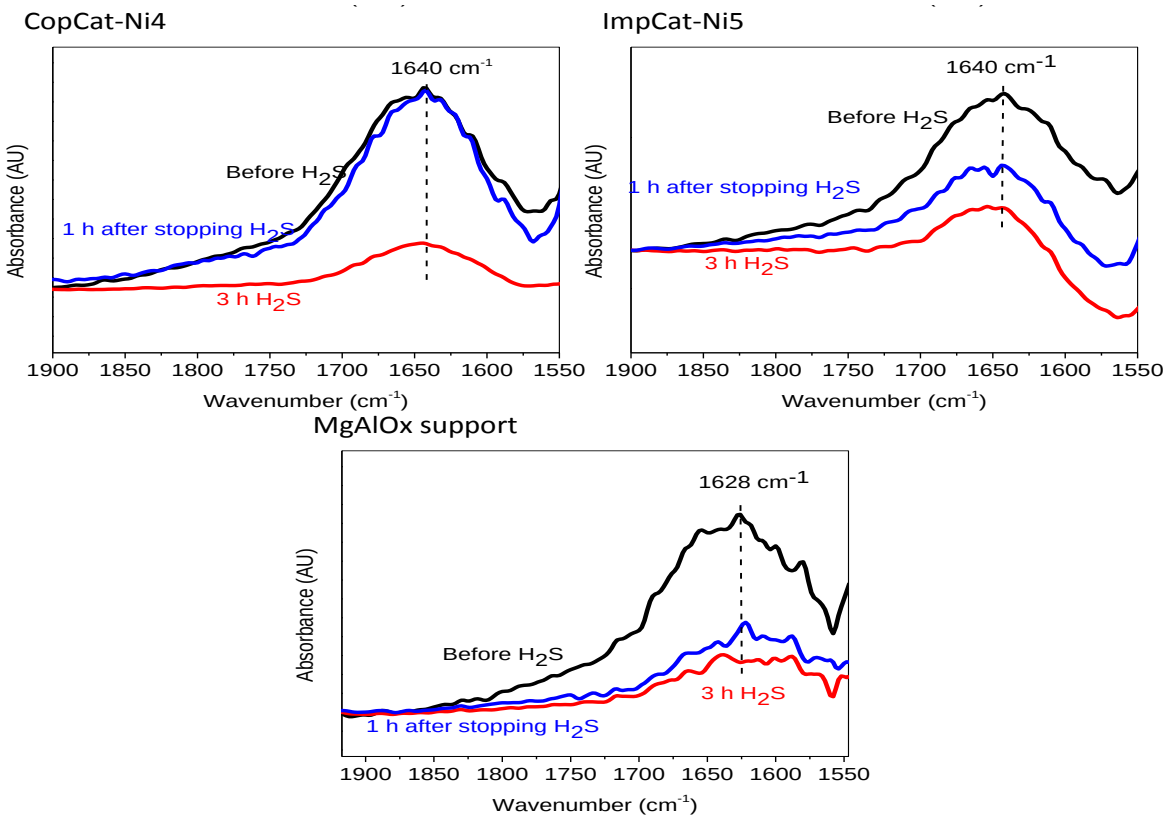

Figure 4-19. Decrease in the concentration of carbonates in the presence of H_2S (continued).

The ability of catalysts to have carbonates formed is related with a better activity for DRM (Bitter et al., 1997; Nakamura et al., 1994). For the cobalt monometallic catalyst, ImpCat-Co5, the decrease in the carbonates band during the H_2S feed was not as obvious as for nickel-containing catalysts CopCat-Ni4, CopCat-Ni2Co4 and ImpCat-Ni5 (Figure 4-19), suggesting that cobalt catalysts are harder to poison by hydrogen sulfide than nickel-containing catalysts.

For the coprecipitated catalysts CopCat-Ni2CO4 and Copcat-Ni4, the reduction in the concentration of carbonates in the presence of H_2S was higher than for the impregnated catalyst ImpCat-Ni5, suggesting that impregnated catalysts are more resistant to H_2S poisoning than coprecipitated catalysts.

4.4.3 Formation of carbonyl sulfide in the presence of H_2S

For all the catalysts tested, including the support, the peak at 2077 cm^{-1}, attributed to linear CO produced by CO_2 dissociation, was replaced by two peaks at 2071 and 2054 (or 2051) cm^{-1}, upon interaction with hydrogen sulfide. These two peaks are attributed to carbonyl sulfide (COS) (Barnes et al., 1995; Hongbo et al., 2004; Hattori et al., 2012). Carbonyl sulfide might have been produced by the reaction $H_2S + CO_2 \rightleftharpoons COS + H_2O$. After the flow of H_2S was stopped, the peak at 2077 cm^{-1} reappeared, and the two peaks produced by COS disappeared (Figure 4-20).

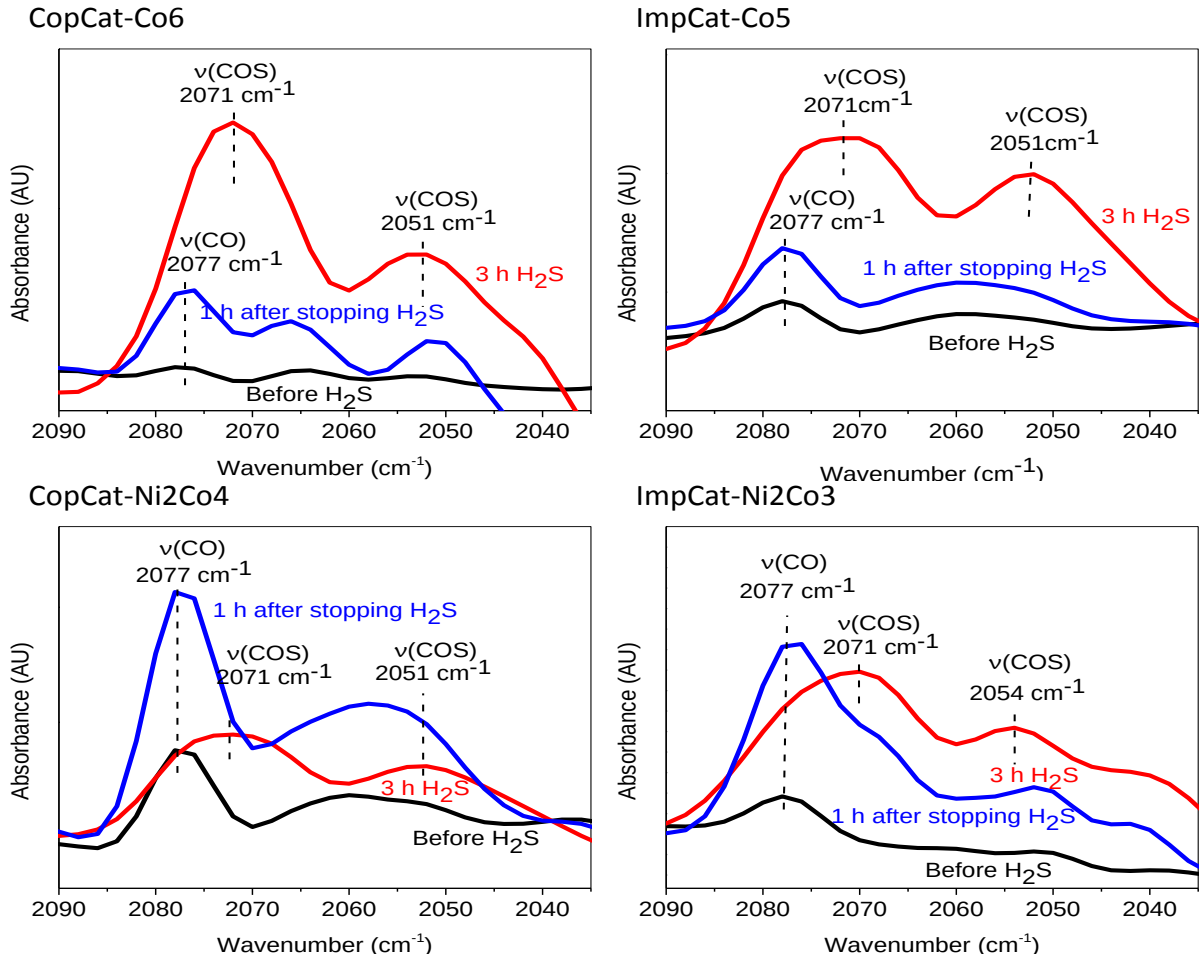

Figure 4-20. Carbonyl sulfide instead of carbonyl produced in the presence of H_2S.

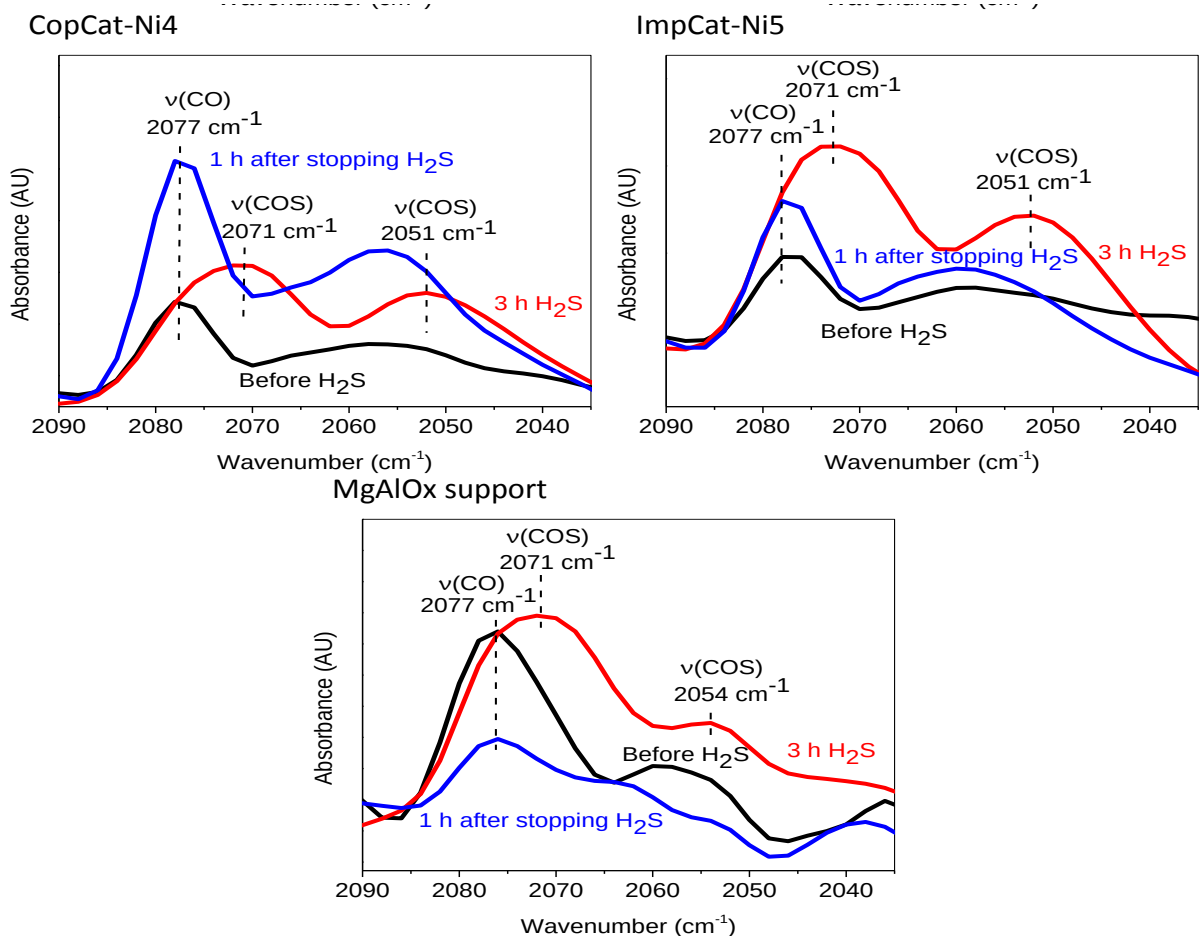

Figure 4-20. Carbonyl sulfide instead of carbonyl produced in the presence of H_2S (continued).

Czekaj et al. (2011) found from theoretical calculations that COS and H_2S are the most stable adsorbates on Ni/Al_2O_3. Carbonyl sulfide might not be a stable chemical species formed on the surface of the catalysts, this is suggested by the disappearance of COS bands after stopping the H_2S flow. Therefore, carbonyl sulfide must not be responsible for the poisoning of the catalysts.

4.4.4 Proposed mechanism for H_2S poisoning

By reconciling the observation of hydroxyl consumption with the observation that CH_4 and CO_2 adsorptions were decreased on nickel monometallic catalysts, suggesting that H_2S attacks nickel active sites, the following mechanism is proposed for poisoning of the nickel active sites:

$$Ni(OH)_2 + H_2S \rightarrow NiS + 2H_2O \quad (4.4)$$

The observation of OH^- consumption occurred not only for nickel monometallic catalysts, but also for cobalt monometallic catalysts, suggesting that sulfidation could occur on cobalt metal sites, or even on the support, by the following mechanisms:

$$Co(OH)_2 + H_2S \rightarrow CoS + 2H_2O \quad (4.5)$$

$$Mg(OH)_2 + H_2S \rightarrow MgS + 2H_2O \quad (4.6)$$

Summarizing the subsection 4.4, DRIFT spectroscopy did not show absorbance bands attributed to the fundamental vibrations of H_2S or SH^- species, but it showed carbonyl sulfide adsorbed on the surface instead of the linear carbonyl. The presence of carbonyl sulfide bands may indicate that the product selectivity is changed by H_2S. Also, there was a decrease in intensities of methane and CO_2 bands on nickel-containing catalysts in the presence of H_2S. This decrease was higher on coprecipitated catalysts (CopCat-Ni2Co4 and CopCat-Ni4) than on impregnated catalysts (ImpCat-Ni2Co3 and ImpCat-Ni5). The reduction in intensities of CH_4 and CO_2 bands in the presence of hydrogen sulfide was not observed on cobalt monometallic catalysts. The decline in hydroxyl groups after the interaction of H_2S with the catalysts suggests the formation of nickel sulfide and water.

4.5 Effect of SO_2 on dry reforming of methane

The purpose of this section is to elucidate the poisoning mechanism by SO_2 during the dry reforming of methane reaction. Firstly, to better understand the mechanism, the independent

adsorption of SO_2 was studied to try to understand how sulfur dioxide interacts with the catalysts and determine the chemical species formed on the catalyst surface.

Secondly, in another set of experiments, the dry reforming of methane reaction was carried out first. Then, SO_2 was introduced to understand its effect on the mechanism of the dry reforming of methane reaction and the poisoning mechanism. Finally, the SO_2 feed was stopped to understand the outcome of the chemical species produced (if any) during the poisoning period.

4.5.1 Independent interactions of SO_2 with the catalysts

For these experiments, the catalysts were reduced at 600 ^oC and a background spectrum was collected at the end of reduction as explained in chapter 3. Then, a mixture containing 1000 ppm of SO_2 in N_2 was introduced at the same temperature and a scan was collected 10 minutes after.

Peaks at 1374 and about 1348 cm^{-1}, approximately, were detected on every catalyst after SO_2 was fed to the reaction cell. Bands at 1374 and 1360 cm^{-1} are attributed to gaseous SO_2 (Padley et al., 1994). Also, a band at about 1358 cm^{-1} was seen as shown in Figure 4-21. Bands at near wavenumbers are attributed to aluminum sulfates (Gracia et al., 2005) or less explicitly to SO_4^{2-} species (Liu et al., 2006). Since most of the spectra in Figure 4-21 are expressed in KM units, it is not possible to compare spectra to obtain quantitative information.

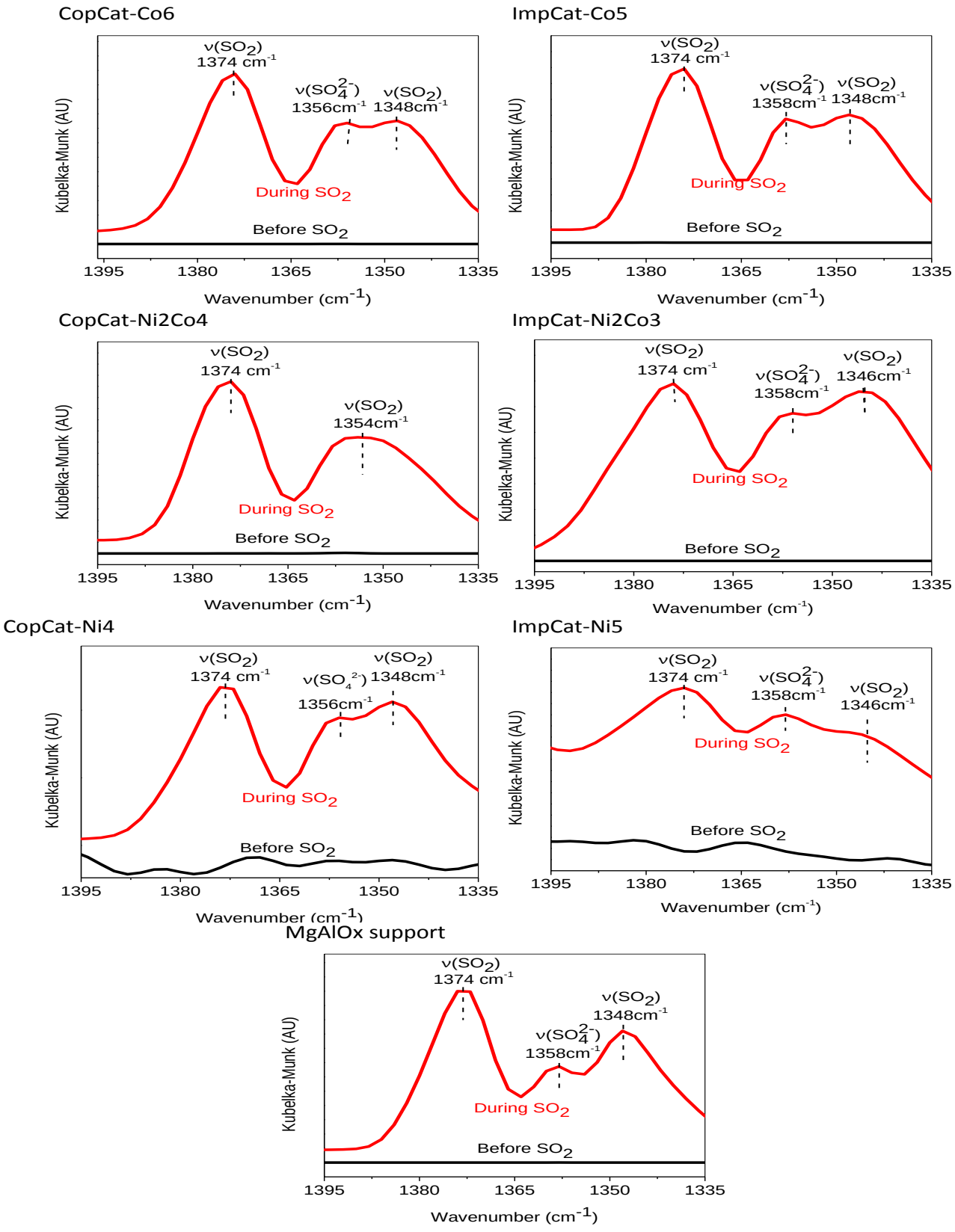

Figure 4-21. Bands attributed to physisorbed SO_2 and sulfate species.

It can be seen in Figure 4-21 that the band attributed to SO_4^{2-} for the support is smaller than the other two bands ascribed to adsorbed SO_2. The presence of nickel or cobalt makes the SO_4^{2-} band higher with respect with the two bands attributed to adsorbed SO_2. For cobalt monometallic catalysts, CopCat-Co6 and ImpCat-Co5, the preparation method did not have any effect on the intensity of the three different peaks since the peaks appear almost similar. This could be explained by the similar catalytic surface since Co was not able to be reduced by H_2. For the coprecipitated bimetallic catalyst, CopCat-Ni2Co4, the SO_4^{2-} peak at 1358 cm^{-1} and the peak attributed to adsorbed SO_2 at 1348 cm-1 seemed to form a new peak. For the nickel impregnated monometallic catalyst, ImpCat-Ni5, the SO_4^{2-} band was higher than the band attributed to adsorbed SO_2 at about 1348 cm^{-1} and for the nickel coprecipitated monometallic catalyst, the SO_4^{2-} band was smaller than the band attributed to adsorbed SO_2. The difference in the intensity of the bands caused by SO_2 adsorption in Figure 4-21 at least indicates the changing electronic properties on the catalyst surfaces.

Also, during the independent interaction of SO_2 with some catalysts, the observation of the peak pointing downwards at about 3742-3720 cm^{-1} (Figure 4-22), similar to the effect produced by H_2S, may also represent the interaction between SO_2 and the hydroxyl groups. According to Zhao et al. (2011) and Abdulhamid et al. (2006) this negative peak could indicate that hydroxyl groups were consumed in the presence of SO_2. Datta and Cavell (1985) reported that infrared bands of non-hydrogen-bonded hydroxyls disappeared in the presence of SO_2, suggesting hydroxyl perturbation by SO_2.

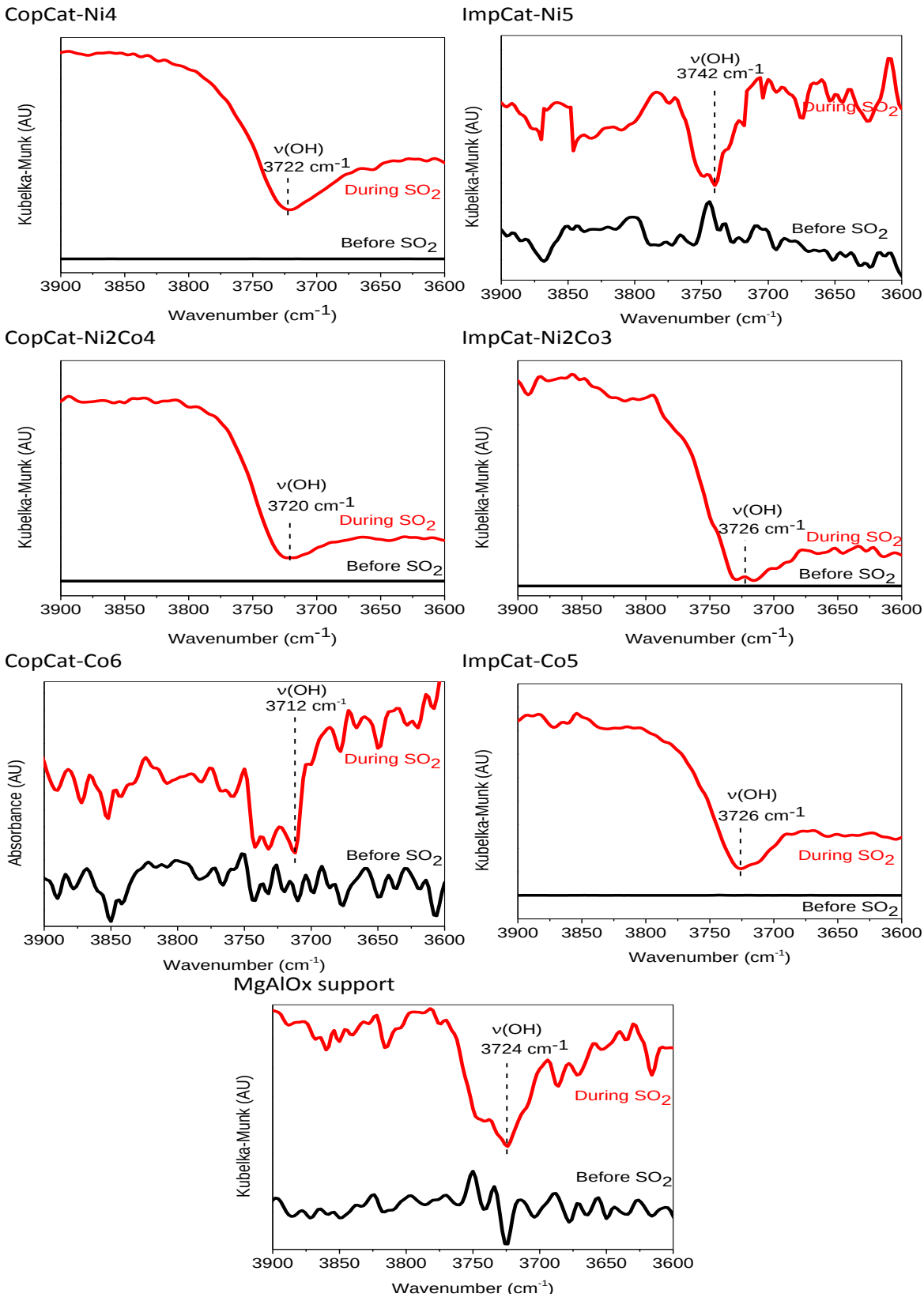

Figure 4-22. Negative peak at the OH^- region seen after the interaction of SO_2.

There are differences in the positions of these negative bands shown in the presence of SO_2. For impregnated catalysts either bimetallic, nickel monometallic or cobalt monometallic, the negative peaks occurred at higher wavenumbers than for coprecipitated catalysts. The negative peak was located at higher wavenumbers on nickel monometallic impregnated catalyst than on cobalt monometallic impregnated catalyst. Similarly, the negative peak was found at higher wavenumber on nickel monometallic coprecipitated catalyst than for cobalt monometallic precipitated catalyst. The reason for these discrepancies is not clear.

4.5.2 Adsorptions of CH_4 and CO_2 in the presence of SO_2

To determine how SO_2 affects the methane, CO_2 and its related bands (carbonates and carbonyl bands), spectra were taken at different intervals: 1) after 15 minutes of DRM (black spectrum); 2) three hours after the introduction of SO_2 during DRM (red spectrum) and; 3) one hour after stopping the SO_2 flow (blue spectrum). Figures 4-23 to 4-29 show the comparison of bands produced by carbon dioxide: a) and methane: b) 3012 cm^{-1} (asymmetrical stretching); c) 2823 and 2599 cm^{-1} (combination band and overtone respectively) and; d) 1540 and 1302 cm^{-1} (in-plane bending and out-of-plane bending, respectively). The bands attributed to sulfates and adsorbed SO_2 also appear in d) for Figures 4-23 to 4-29 and were also compared.

For the impregnated monometallic nickel catalyst (ImpCat-Ni5), the methane and CO_2 bands considerably decreased in height in the presence of SO_2 and remained almost the same after 1 hour of stopping the SO_2 flow. This decline in intensity could indicate that SO_2 blocks the catalytic active sites irreversibly, preventing new methane and CO_2 adsorptions (Figure 4-23). It could also be seen for this catalyst in the presence of SO_2 a peak attributed to SO_2 at 1358 cm^{-1} and two bands ascribed to adsorbed SO_2 at 1374 and 1342 cm^{-1}. These bands greatly decreased

in intensity one hour after stopping the flow of SO_2, suggesting that the formation of sulfates is reversible.

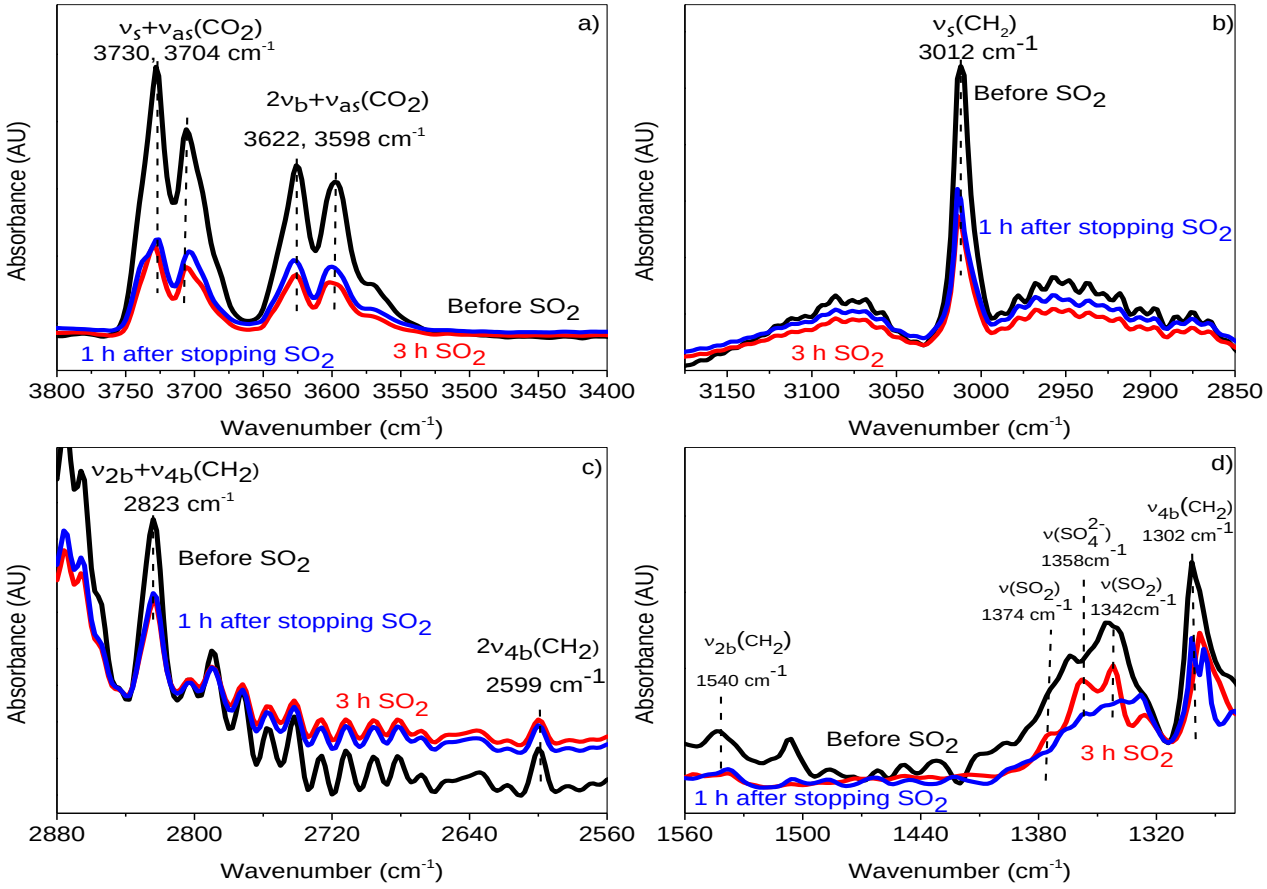

Figure 4-23. Bands attributed to CO_2 (a) and CH_4 (b, c, d) displayed before introducing SO_2, 3 hours after introducing SO_2 and 1 hour after stopping the SO_2 flow for ImpCat-Ni5.

For the coprecipitated monometallic nickel catalyst (CopCat-Ni4), the methane and CO_2 bands did not seem to change noticeably in the presence of SO_2, except the band at 3730 cm^{-1} that slightly decreased. After stopping the SO_2 flow, all the bands did not change in intensity (Figure 4-24), suggesting that poisoning by SO_2 did not occur. During the interaction of SO_2 with this

catalyst, bands attributed to adsorbed SO_2 and sulfates were detected. The sulfates disappeared after stopping the SO_2 feed but the adsorbed SO_2 remained.

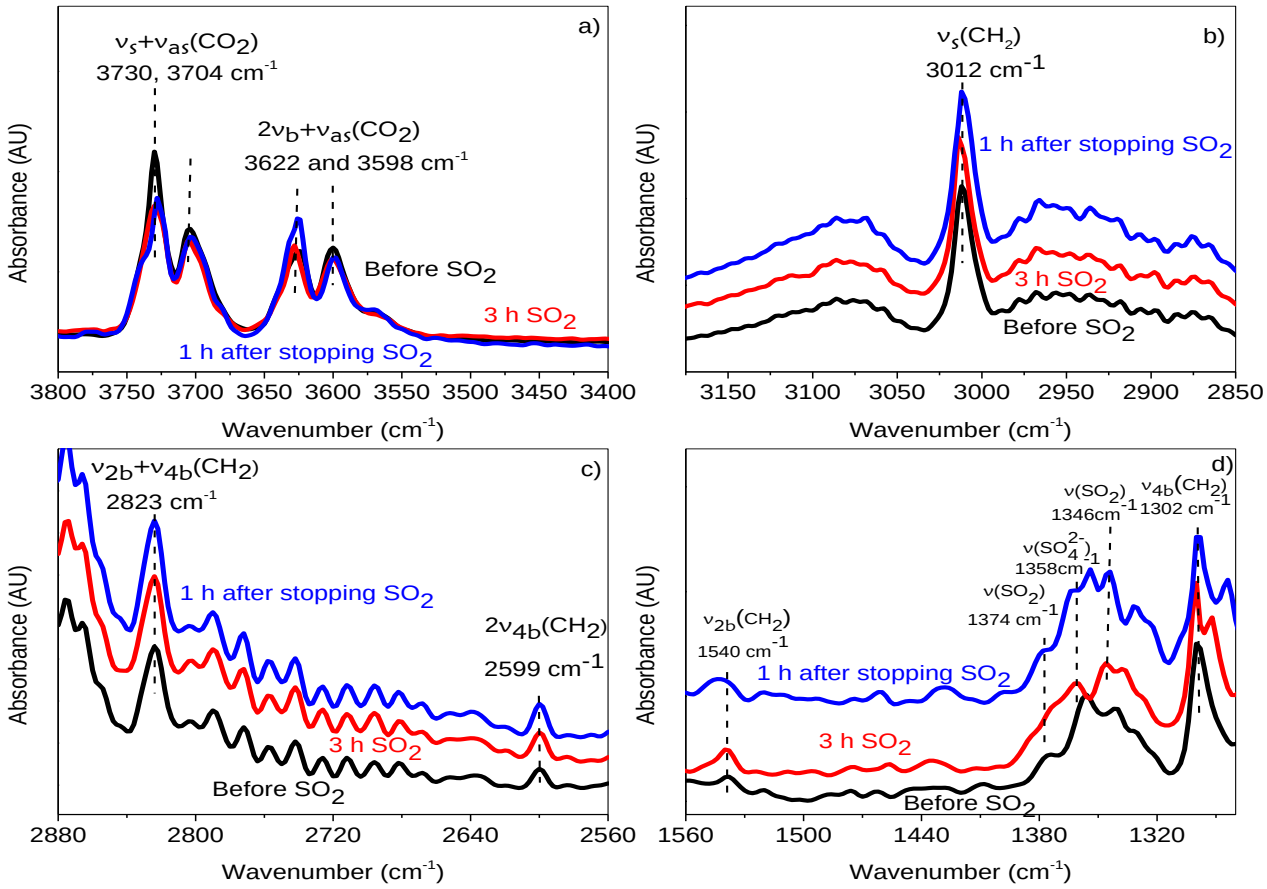

Figure 4-24. Bands attributed to CO_2 (a) and CH_4 (b, c, d) displayed before introducing SO_2, 3 hours after introducing SO_2 and 1 hour after stopping the SO_2 flow for CopCat-Ni4.

For CopCat-Co6, the noticeable change was the intensity decrease for the bands at 3012 and 1302 cm^{-1} after stopping the feed of SO_2. If poisoning occurred, the poisoning was still effective even after the SO_2 had been stopped. Sulfate and adsorbed SO_2 were seen in the presence of SO_2 and the bands were also visible after stopping the SO_2, confirming that the poisoning was still effective.

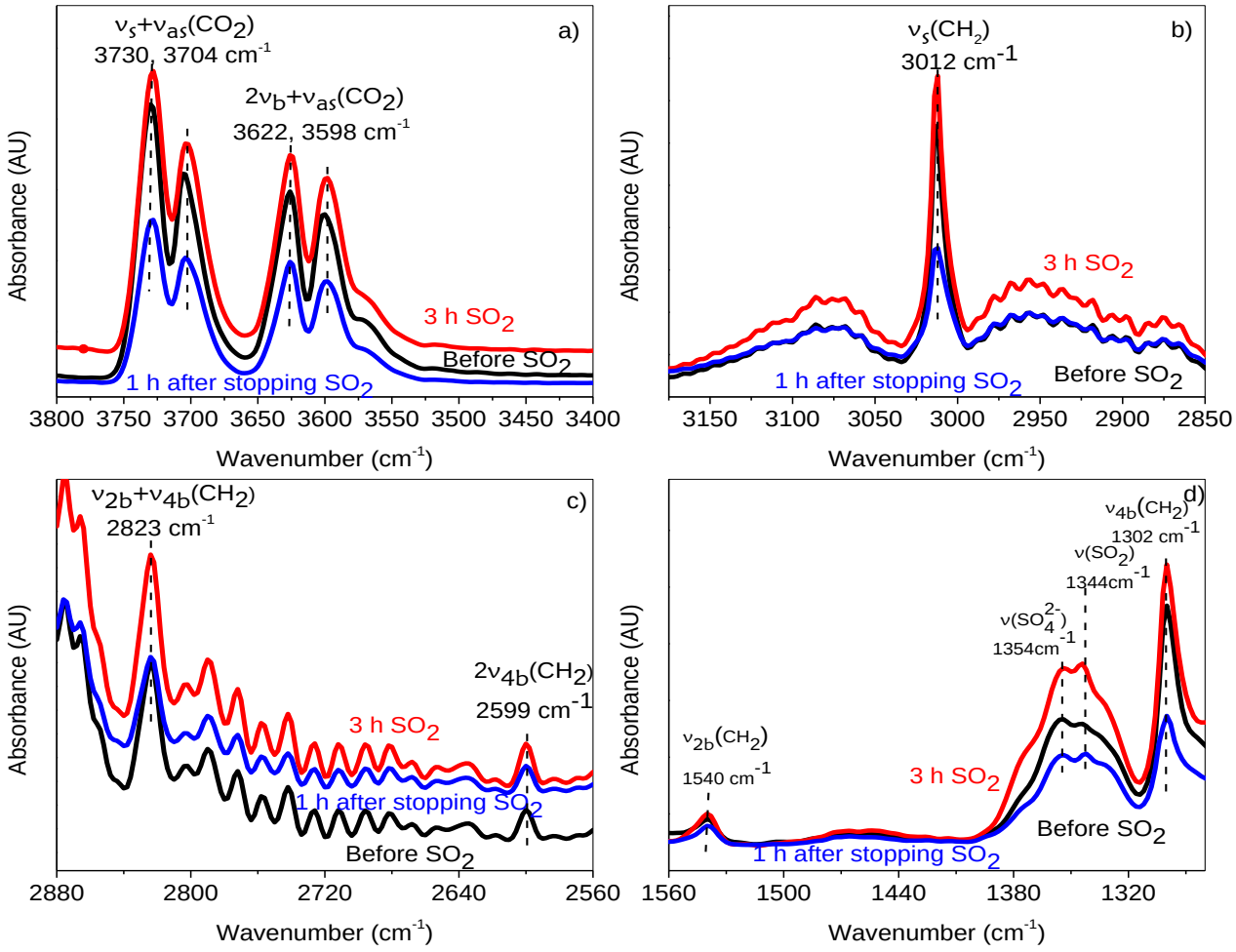

Figure 4-25. Bands attributed to CO_2 (a) and CH_4 (b, c, d) displayed before introducing SO_2, 3 hours after introducing SO_2 and 1 hour after stopping the SO_2 flow for CopCat-Co6.

For ImpCat-Co5, there were no significant changes in the bands attributed to CH_4 and CO_2. SO_2 on the surface of the catalysts was confirmed by two bands at 1374 and 1344 cm^{-1}. Also, a band at 1356 cm^{-1} indicated the presence of sulfate. After SO_2 was stopped, only a big band remained located at lower wavenumber compared to the sulfate peak. The reason for the appearance of only this shifted band is unclear.

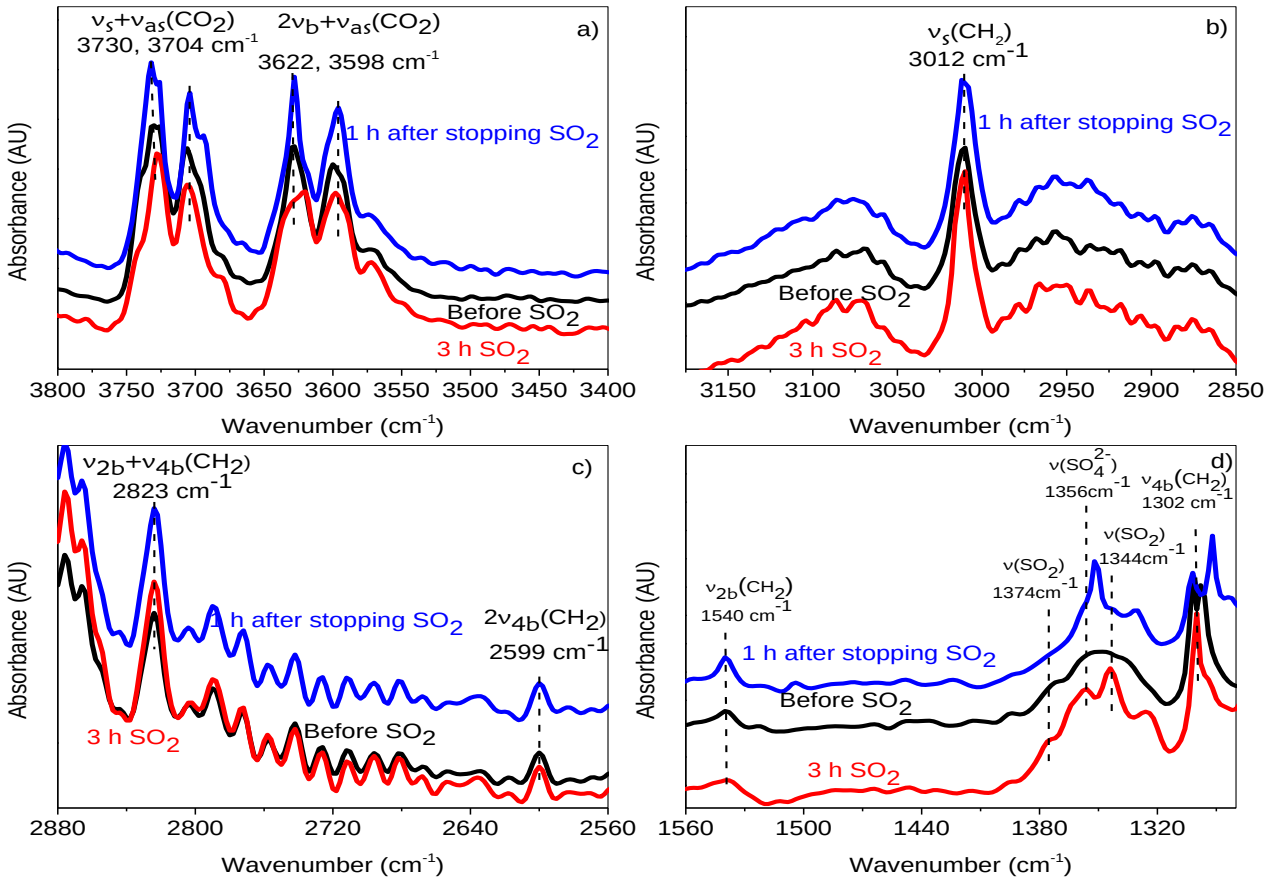

Figure 4-26. Bands attributed to CO_2 (a) and CH_4 (b, c, d) displayed before introducing SO_2, 3 hours after introducing SO_2 and 1 hour after stopping the SO_2 flow for ImpCat-Co5.

For CopCat-Ni2Co4 (Figure 4-27) and ImpCat-Ni2CO3 (Figure 4-28) bimetallic catalysts, the bands attributed to CO_2 at 3730 and 3704 cm^{-1} decreased in the presence of sulfur dioxide but the intensity recovered after SO_2 was stopped. The bands attributed to the vibration of CH_2 groups did not vary much in the presence of SO_2 for the bimetallic catalysts

For the coprecipitated bimetallic catalyst, CopCat-Ni2Co4, similar to the observation for ImpCat-Co5, it was possible to observe a band attributed to sulfates in the presence of SO_2 that disappeared after stopping the feed of SO_2. It seems as if the sulfate band is shifted to lower

wavenumber after stopping the SO_2 flow and whatever this band is attributed to it increased in intensity after stopping SO_2.

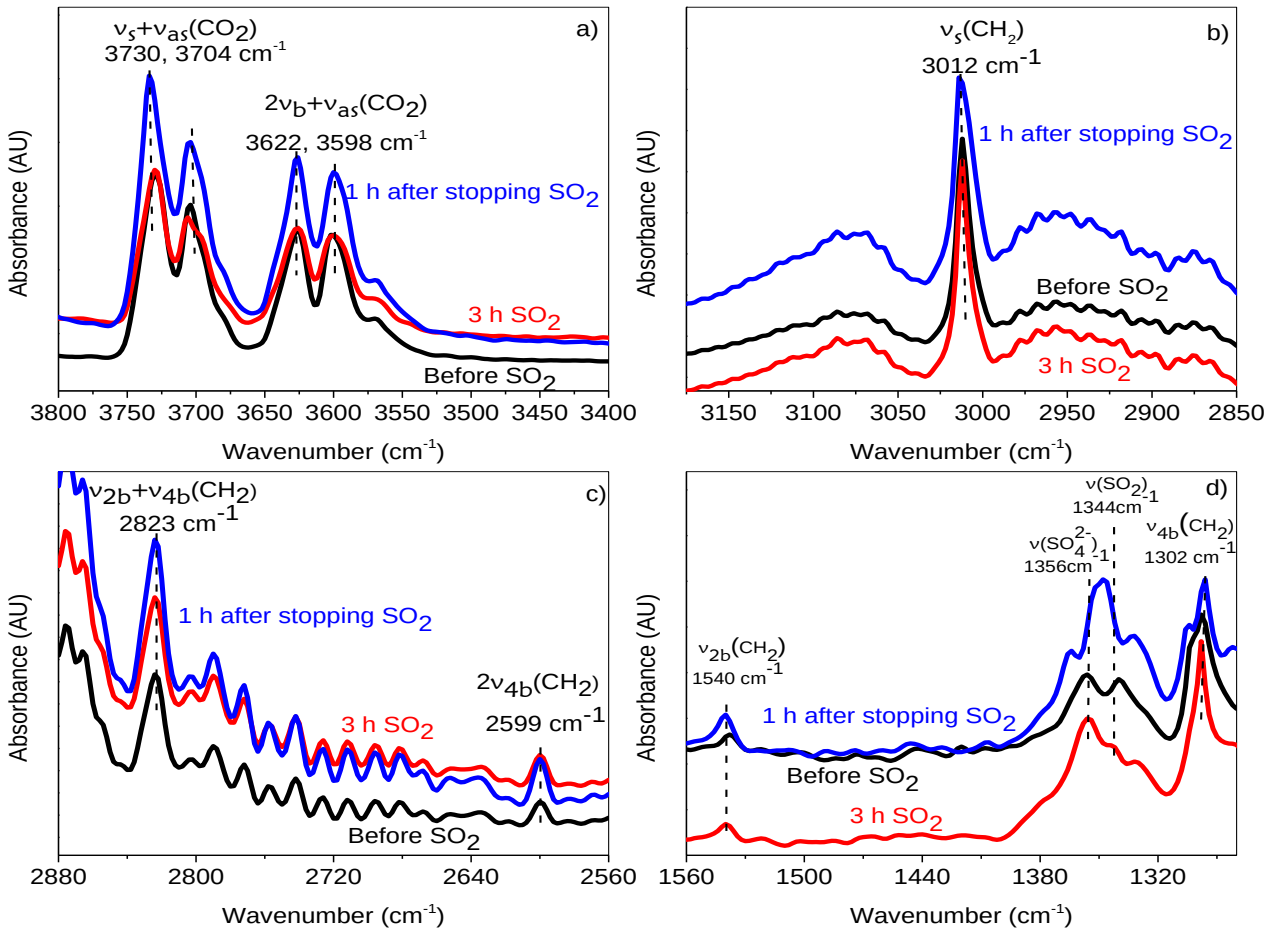

Figure 4-27. Bands attributed to CO_2 (a) and CH_4 (b, c, d) displayed before introducing SO_2, 3 hours after introducing SO_2 and 1 hour after stopping the SO_2 flow for CopCat-Ni2Co4.

For ImpCat-Ni2Co3, sulfate seen in the presence of SO_2 disappeared one hour after stopping the flow of SO_2, suggesting that the formation of sulfate is reversible. A band attributed to adsorbed sulfur dioxide at 1344 cm^{-1} remained after stopping the SO_2 feed.

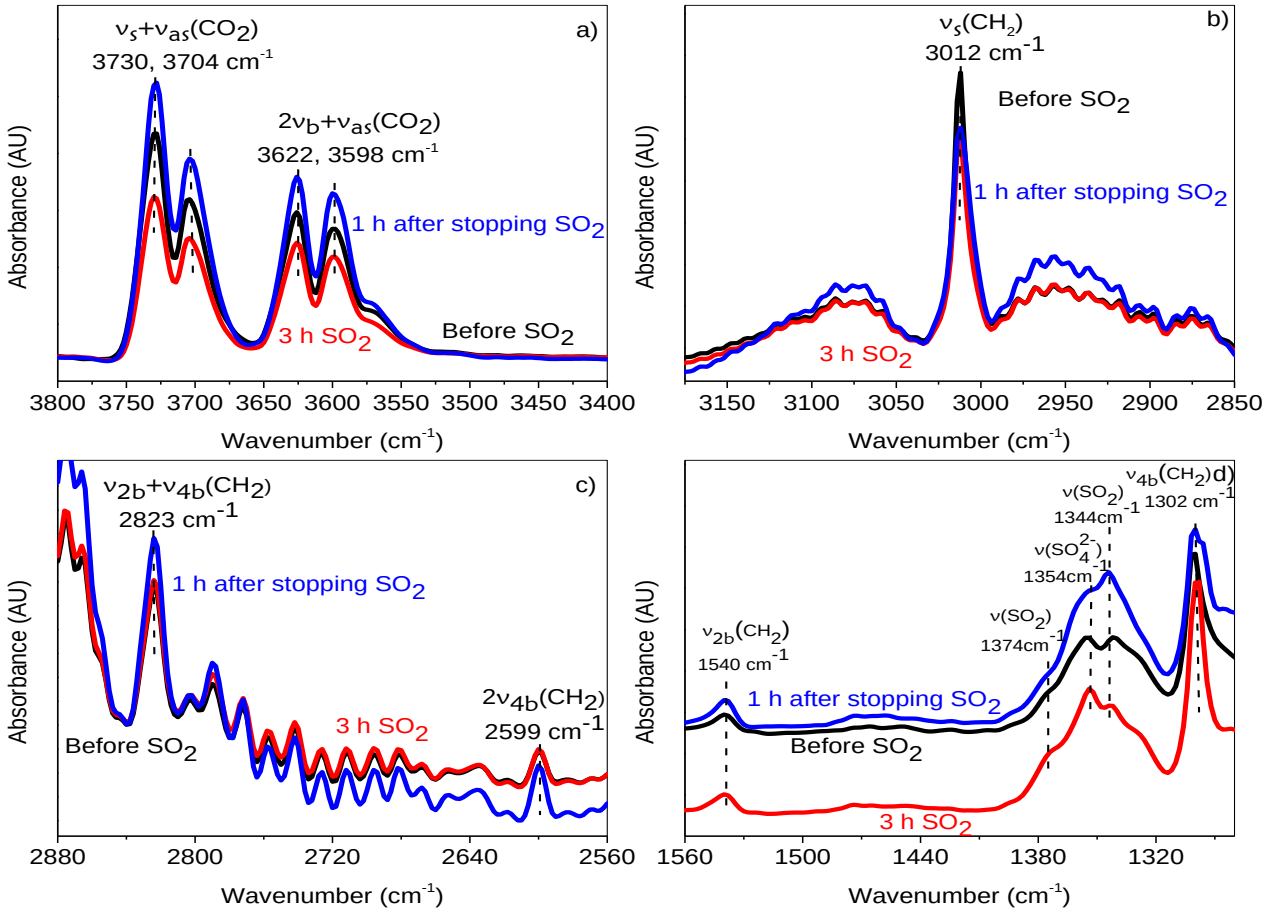

Figure 4-28. Bands attributed to CO_2 (a) and CH_4 (b, c, d) displayed before introducing SO_2, 3 hours after introducing SO_2 and 1 hour after stopping the SO_2 flow for ImpCat-Ni2Co3.

For MgAlOx support, the CO_2 and methane bands increased in intensity in the presence of SO_2 and increased even more after SO_2 removal (Figure 4-29), suggesting that magnesium and aluminum oxides present on the support are not attacked by SO_2. Therefore, the adsorptions of methane and CO_2 were not interfered. SO_2 adsorbed on the surface of the support was detected by two obvious bands at 1374 and 1342 cm^{-1}, sulfates were confirmed by the presence of a band at 1352 cm^{-1}. After discontinuing the flow of SO_2, these species significantly decreased in intensity. Suggesting that the poisoning on the support is reversible.

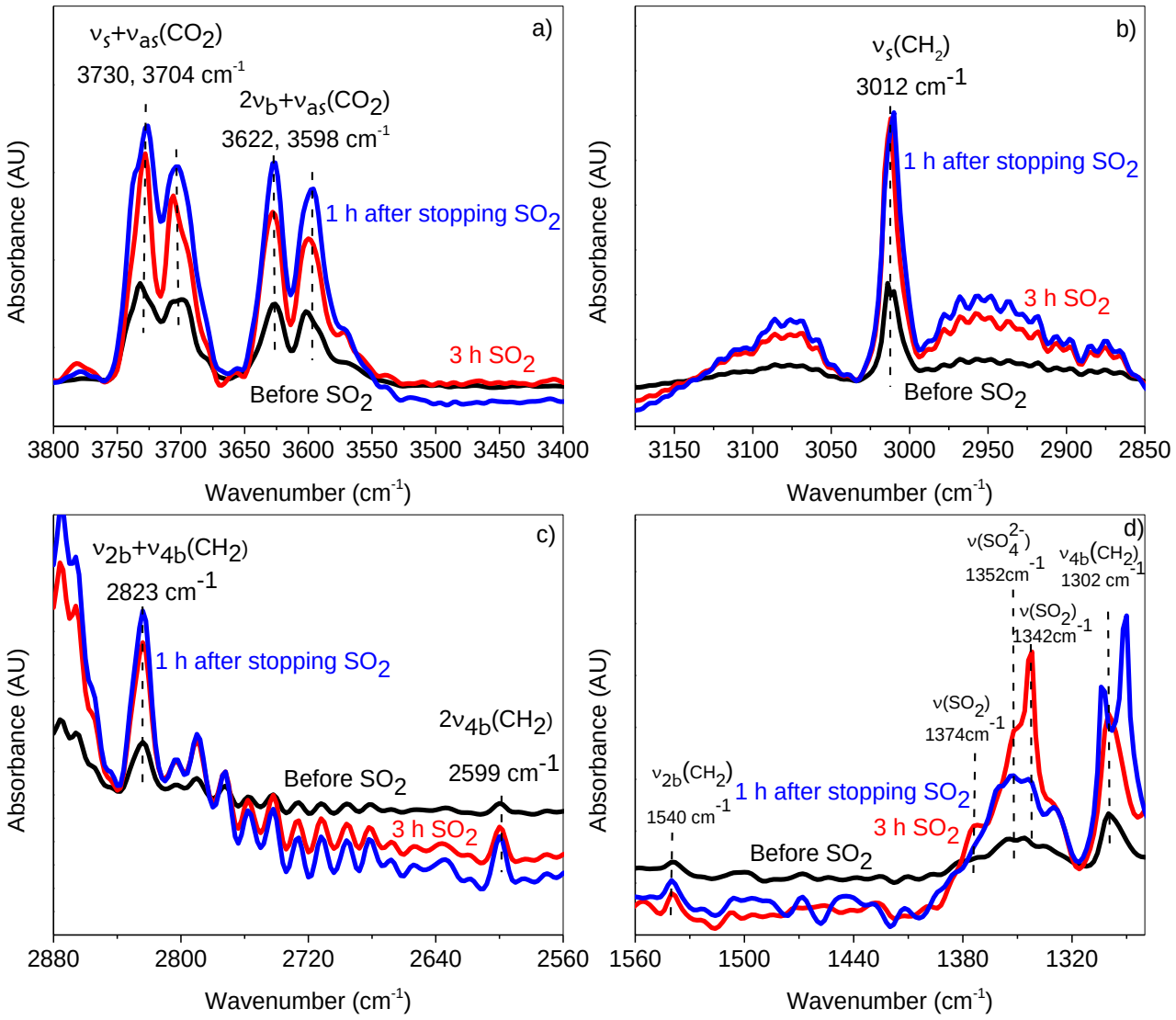

Figure 4-29. Bands attributed to CO_2 (a) and CH_4 (b, c, d) displayed before introducing SO_2, 3 hours after introducing SO_2 and 1 hour after stopping the SO_2 flow for $MgAlO_x$ support.

It is important to determine if SO_2 hinders the formation of CO or carbonyl on the catalyst surface. From this point of view, it was observed on Figure 4-30 that the intensity of CO decreased on every catalysts when SO_2 was introduced except for ImpCat-Co5 and the support. The intensity of CO can be recovered to various extent, except for ImpCat-Ni5 and CopCat-Co6. On CopCat-Co6, the intensity of CO further decreased after stopping the SO_2 feed. Fig 4-30

basically imply that SO_2 forms $SO_4^{(2-)}$ species on the catalyst surfaces and hinders the formation of CO during reforming reaction.

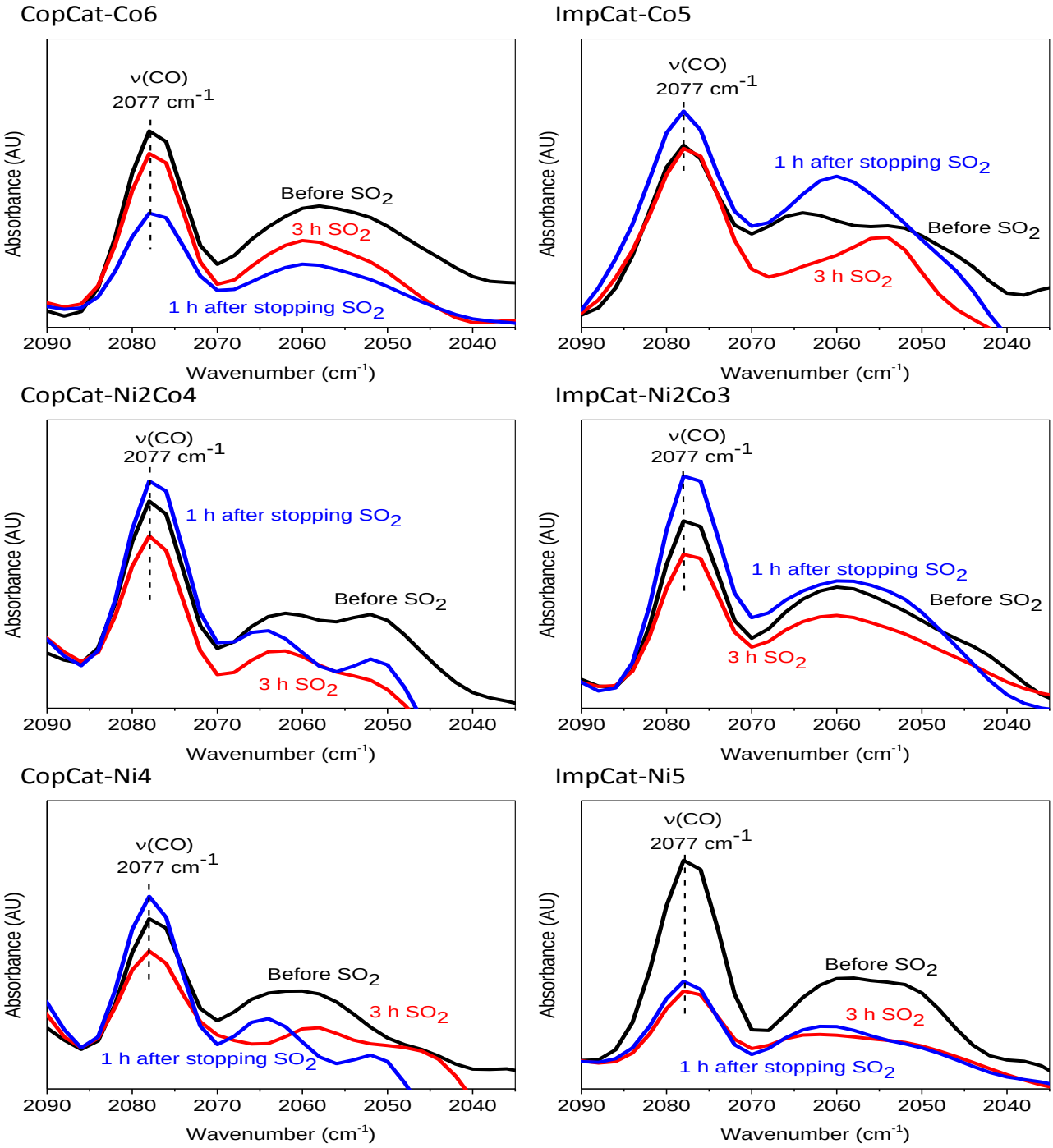

Figure 4-30. The impact of the presence of SO_2 on CO species for various catalysts

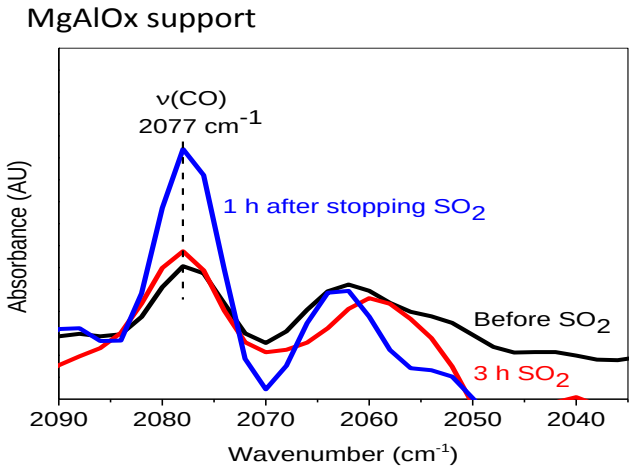

Figure 4-30. The impact of the presence of SO_2 on CO species for various catalysts (continued).

As seen in section 4.3, there is a correlation between the concentration of adsorbed CO and the concentration of carbonates. Since the formation of sulfates seen in Figures 4-23 to 4-29 might be responsible for the decrease in the concentration of CO during SO_2 poisoning seen on Figure 4-30. It is suggested that the formation of sulfates is also responsible for the decrease in the concentration of carbonates observed in Figure 4-31. It can also be seen that the concentration of carbonates was recovered after stopping SO_2, especially for the support, since the concentration of carbonates was even higher than before the introduction of SO_2.

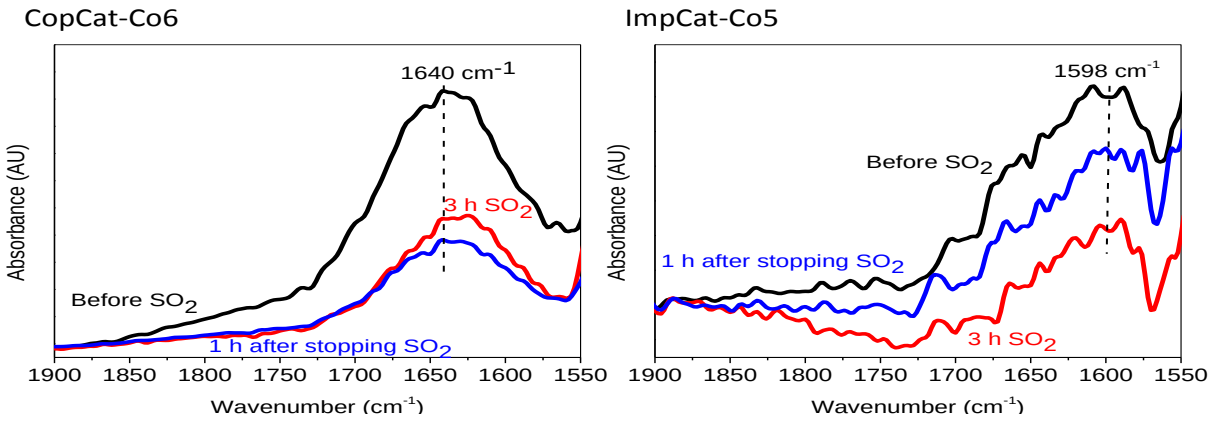

Figure 4-31. Concentration of carbonates before, in and after the presence of SO_2.

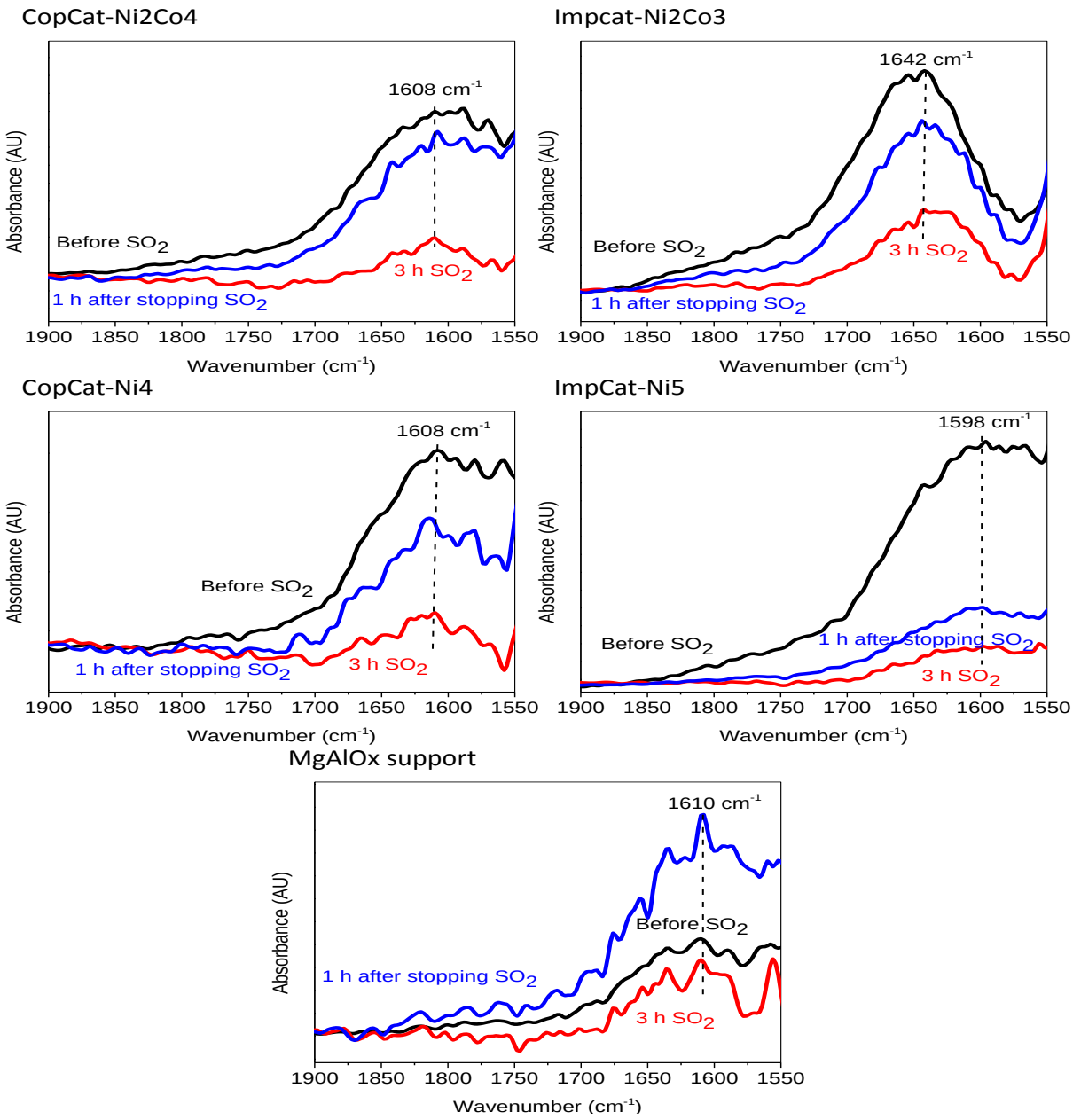

Figure 4-31. Concentration of carbonates before, in and after the presence of SO_2 (continued).

The capacity of catalysts to form carbonates is associated with a better catalyst activity for DRM (Bitter et al., 1997; Nakamura et al., 1994). The decrease in the carbonates band is higher for CopCat-Ni4 than for CopCat-Co6, suggesting than cobalt catalysts are harder to poison by SO_2 than nickel catalysts. Similarly, the decrease in the concentration of carbonates was higher for

CopCat-Ni2Co4 than for ImpCat-Ni2CO3, suggesting that impregnated catalysts are more resistant to SO_2 poisoning than coprecipitated catalysts.

The formation of sulfates involves attachment of SO_2 to oxygen, similar to the attachment of CO_2 or CO to oxygen to form carbonates. The formation of sulfates might compete with the formation of carbonates. For this reason, experiments were conducted to determine if the concentration of carbonates produced by CO is reduced by the presence of SO_2. It was confirmed that carbonates disappeared or, at least, were substantially reduced by the presence of SO_2 (Figure 4-32). Kylhammar et al. (2011) also observed the removal of surface carbonates upon introduction of SO_2. Therefore, it is suggested that the formation of sulfates scavenge the oxygen available on the catalyst surface, preventing the formation of carbonates by CO_2 and CO. The previous suggestion is in agreement with Anderson et al. (2006) who reported that SO_x species restrained the formation of carbonates on $Pt/Ba/Al_2O_3$ catalysts.

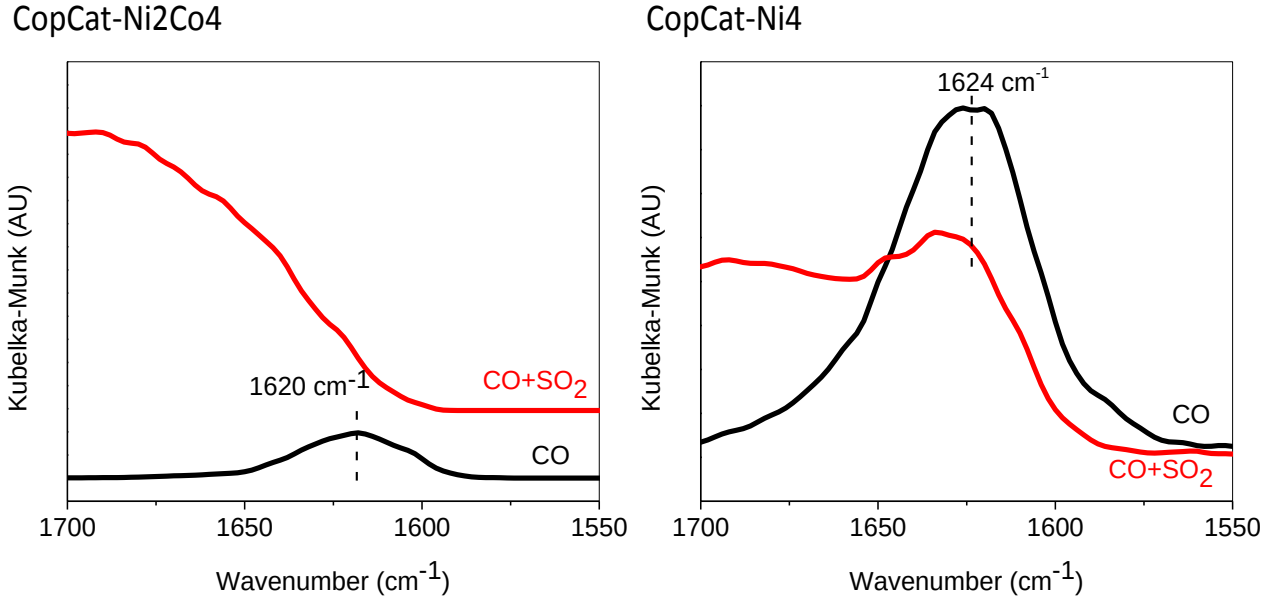

Figure 4-32. Decrease of the concentration of carbonates after the introduction of SO_2.

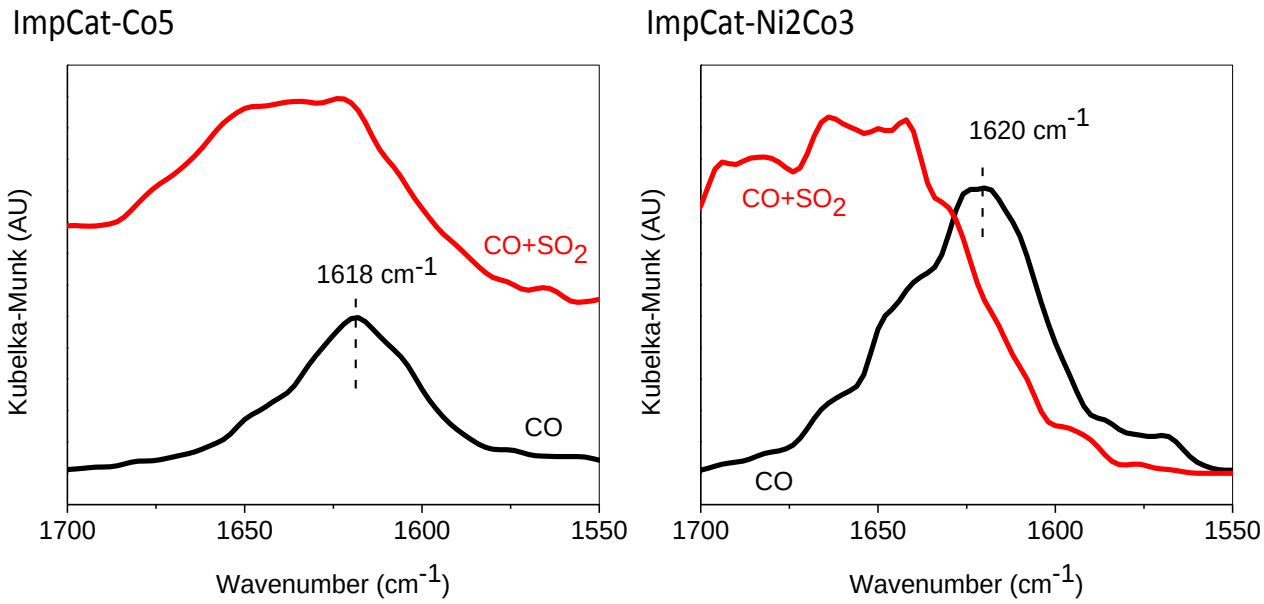

Figure 4-32. Decrease of the concentration of carbonates after the introduction of SO_2

(continued)

It is not clear what causes the position of the carbonates. Neither is clear if the sulfates attack firs to the carbonates and that produces a reduction in the concentration of adsorbed CO or viceversa. However, it has been proved that both species are decreased in the presence of sulfur dioxide.

4.5.3 Proposed mechanism for SO_2 poisoning

The presence of SO_2 does not seem to have caused significant change on species associated to CH_4 and CO_2 adsorption. Its impact on the formation of sulfate, carbonate and CO on all the catalyst samples including the support should be analyzed.

Reconciling the two observations of the negative peak (OH^- consumption) and the peak at about 1358 cm^{-1} (sulfate formation), it is suggested that the formation of sulfates occur on Ni or Co metal sites as well on the support by the following mechanisms:

$$Ni(OH)_2 + SO_2(g) \rightarrow Ni(SO_3) + H_2O \quad (4.7)$$

$$NiO + SO_2 \rightarrow Ni(SO_3) \quad (4.8)$$

$$Ni(SO_3) + 2OH^- \rightarrow NiSO_4 + H_2O \quad (4.9)$$

$$Co(OH)_2 + SO_2(g) \rightarrow Co(SO_3) + H_2O \quad (4.10)$$

$$CoO + SO_2 \rightarrow Ni(SO_3) \quad (4.11)$$

$$Co(SO_3) + 2OH^- \rightarrow CoSO_4 + H_2O \quad (4.12)$$

$$Mg(OH)_2 + SO_2(g) \rightarrow Mg(SO_3) + H_2O \quad (4.13)$$

$$MgO + SO_2 \rightarrow Mg(SO_3) \quad (4.14)$$

$$Mg(SO_3) + 2OH^- \rightarrow MgSO_4 + H_2O \quad (4.15)$$

To recapitulate, hydroxyl consumption was shown by the presence of SO_2. The proposed mechanism suggests that sulfites are formed first, and sulfates are formed in the further step. The peak at about 1358 cm^{-1} for all catalysts confirm the presence of sulfates. These sulfate species seem to interfering with the formation of carbonates and carbonyl on the surface of the catalysts.

CHAPTER 5. CONCLUSIONS AND RECOMMENDATIONS

5.1 CONCLUSIONS

The conclusions that can be drawn from this study are the following:

5.1.1 Mechanism of dry reforming of methane

The mechanism of dry reforming of methane on Ni-Co/AlMgOx catalysts was observed to occur by the following steps:

-Methane adsorption and possibly dissociation into C, CH_x and H_2. The presence of bands at the OH^- region could have been caused by dissociated hydrogen bonding to oxygen present in the catalysts, suggesting methane dissociation.

- Carbon dioxide adsorption and dissociation into CO.

- Formation of carbonates (all the catalysts tested showed the ability to form carbonates).

-It was observed a relationship between the concentration of carbonates and the concentration of CO adsorbed on the catalysts surfaces.

The catalyst preparation method affects the reducibility of the catalysts and the oxides content. Formation of carbonates was higher in catalysts with higher oxygen content, such as the support and Copcat-Co6.

5.1.2 Effect of H_2S on dry reforming of methane

When H_2S interacted with the catalysts, it was observed a negative band in the region between 3730-3720 cm^{-1}, suggesting OH^- consumption.

For nickel-containing catalysts, either monometallic or bimetallic, the methane and CO_2 adsorption bands decreased in the presence of H_2S. Interestingly, the catalysts containing only cobalt (CopCat-Co6 and ImpCat-Co5) showed the opposite trend: the methane and CO_2 adsorption intensities increased in the presence of hydrogen sulfide, this might suggest that H_2S helps to reduce cobalt.

The concentration of carbonates was reduced in the presence of H_2S. For the cobalt monometallic catalyst, ImpCat-Co5, the decrease in the carbonates band during H_2S feed was not as obvious as for nickel-containing catalysts CopCat-Ni4, CopCat-Ni2Co4 and ImpCat-Ni5, suggesting that the monometallic cobalt catalyst ImpCat-Co-5 is harder to poison by H_2S than the nickel-containing catalysts. For coprecipitated catalysts CopCat-Ni2CO4 and Copcat-Ni4, the decrease in the concentration of carbonates in the presence of H_2S was higher than for the impregnated catalyst ImpCat-Ni5. This suggests that impregnated catalysts are more resistant to H_2S poisoning than coprecipitated catalysts.

Carbonyl sulfide, instead of adsorbed CO, was found on all catalysts after the interaction with H_2S during dry reforming of methane. Carbonyl sulfide was reversible upon stopping H_2S feed.

5.1.3 Effect of SO_2 on dry reforming of methane

When SO_2 interacted with the catalysts, a negative band was observed, suggesting OH^- consumption. Sulfates were also detected in the presence of SO_2. The mechanism proposed is that the consumption of OH^- functional groups by SO_2 leads to formation of sulfates. Sulfates might be responsible for the decrease in concentration of CO and carbonates. The decrease in the concentration of carbonates band was higher for CopCat-Ni4 than for CopCat-Co6, suggesting than cobalt catalysts are harder to poison by SO_2 than nickel catalysts. Similarly, the decrease in the concentration of carbonates was higher for CopCat-Ni2Co4 than for ImpCat-Ni2CO3, suggesting that impregnated catalysts are more resistant to SO_2 poisoning than coprecipitated catalysts.

5.2 RECOMMENDATIONS

1. To determine by X-ray absorption spectroscopy the formation of sulfides such as NiS, CoS and MgS. Also, to determines the types of sulfates formed such as $NiSO_4$, $CoSO_4$, $Al_2(SO_4)_3$, $MgSO_4$.

2. To determine how the mechanism of poisoning by H_2S and SO_2 changes at actual reaction temperature for DRM (700 ^oC and higher).

3. To study the simultaneous interaction of H_2S and SO_2. However, this could form elemental sulfur (S) that could block the reactor and piping, unless precautions are taken to prevent this problem.

4. To determine the effect of other sulfur compounds found in natural gas such as mercaptans, dimethyl sulphide, carbonyl sulphide, etc.

5. To determine the effect of H_2S or SO_2 at actual concentrations in feedstock for DRM after desulfurization process.

6. To obtain integral information about the poisoning mechanism using operando spectroscopy. This would allow to determine the activity and spectroscopic information at the same time for DRM in the presence of H_2S and SO_2.

REFERENCES

Aasberg-Petersen, K., Christensen, T. S., Nielsen, C. T. & Dybkjaer, I. "Recent developments in autothermal reforming and pre-reforming for synthesis gas production in GTL applications." Fuel Processing Technology 83, 253-261 (2003).

Abdulhamid, H., Fridell, E., Dawody, J. & Skoglundh, M. "In situ FTIR study of SO_2 interaction with $Pt/BaCO_3/Al_2O_3$ NO*x* storage catalysts under lean and rich conditions." Journal of Catalysis 241, 200–210 (2006).

Agrawal, P. "Surface and reaction studies of the poisoning of transition metal methanation catalysts." (1979).

Anderson, J. A., Liu, Z., Fernandez Garcia, M. "Use of in situ FT-IR and XAS/XRD to study SO_2 poisoning over model $Pt/Ba/Al_2O_3$ NO_x storage and reduction (NSR) catalysts." Catalysis Today 113, 25-33 (2006).

Armaroli, T., Becue, T. & Gautier, S. "Diffuse Reflection Infrared Spectroscopy (DRIFTS): Application to the in situ analysis of catalysts." Oil and Gas Science and Technology. Vol 9, 215-237 (2004).

Aoki, K., Yamawaki, H. & Sakashita, M. "Phase study of solid CO_2 to 20 GPa by infrared-absorption spectroscopy." Physical Review B. Volume 48, Number 13 (1993).

Ashcroft, A. T., Cheetham, A. K., Green, M. L. H. “Partial oxidation of methane to synthesis gas using carbon dioxide.” Letters to Nature (1991).

Ashrafi, M., Pfeifer, C., Proll, T. & Hofbauer, H. “Experimental study of model biogas catalytic steam reforming: 2. Impact of Sulfur on the deactivation and regeneration of Ni-based catalysts.” Energy & Fuels, 22, 4190-4195 (2008).

Ayabe, S., Omoto, H., Utaka, T., Kikuchi, R., Sasaki, K., Teraoka, Y., Eguchi, K. “Catalytic autothermal reforming of methane and propane over supported metal catalysts.” Applied Catalysis A: General 241, 261-229 (2003).

Bachiller-Baeza, B., Mateos-Pedrero, C., Soria, M. a., Guerrero-Ruiz, a., Rodemerck, U., & Rodríguez-Ramos, I. “Transient studies of low-temperature dry reforming of methane over Ni-CaO/ZrO_2-La_2O_3.” Applied Catalysis B: Environmental, 129, 450–459 (2013).

Barnes, I., Becker, K. H., Patroescu, I. “FTIR product study of the OH initiated oxidation of dimethyl sulphide: Observation of carbonyl sulphide and dimethyl sulphoxide.” (1995).

Barrai, F., Jackson, T., Whitmore, N., Castaldi, M. J. “The role of carbon deposition on precious metal catalyst activity during dry reforming of biogas.” Catalysis Today 129, 391-396 (2007).

Bartholomew, C. H. “Mechanisms of catalyst deactivation.” Applied Catalysis A: General, *212*(1-2), 17–60 (2001).

Bitter, J. H., Seshan, K., & Lercher, J. A. “On the contribution of X-ray absorption spectroscopy to explore structure and activity relations of Pt / ZrO_2 catalysts for CO_2/CH_4 reforming.” *10*, 295–305 (2000).

Bitter, J. H., Seshan, K., Lercher, J. A. “The state of zirconia supported platinum catalysts for CO_2/CH_4 reforming.” Journal of catalysis 171, 279-286 (1997).

Bradford, M. C. J., & Albert, M. V. A : "Catalytic reforming of methane with carbon dioxide over nickel catalysts II. Reaction kinetics". (1996).

Bradford, M. C. J. & Vannice, M. A. "CO_2 reforming of methane." Catalysis Reviews: Science and Engineering. (2007).

Buekens, A. "Energy recovery from residual waste by means of anaerobic digestion technologies." Conference: "The future of residual waste management". (2005).

Cengel, Y. U. & Boles, M. A. "Thermodynamics. An engineering approach." Seventh edition. Mc Graw Hill, (2011).

Centi, G. & Perathoner, S. "Opportunities and prospects in the chemical recycling of carbon dioxide to fuels." Catalysis Today 149, 191-205. (2009).

Cheekatamarla, P. K. & Lane, A. M. "Catalytic autothermal reforming of diesel fuel for hydrogen generation in fuel cells. I. Activity tests and sulfur poisoning." Journal of Power Sources. (2005).

Chen, Y., Xie, C., Li, Y., Song, C. & Bolin, T. B. "Sulfur poisoning mechanism of steam reforming catalysts: an X-ray absorption near edge structure (XANES) spectroscopic study." Phys. Chem. Chem. Phys. 12, 5707-5711 (2010).

Choudhary, T. V., Aksoylu, E. & Goodman, D. W. "Nonoxidative oxidation of methane." Catalysys Reviews Vol. 45, No. 1, pp. 151–203 (2003).

Choudhary, T. V. & Goodman, D. W. "Methane decomposition: Production of hydrogen and carbon filaments." Catalysis, 19, 164–183 (2006).

Choudhary, T. V., Sivadinarayana, C., Goodman, D. W. "Production of COx-free hydrogen for fuel cells via step-wise hydrocarbon reforming and catalytic dehydrogenation of ammonia." Chemical Engineering Journal 93, 69-80 (2003).

Christensen, T. S., Christensen, P. S., Dybkjaer, I., Hansen, J. H. B. & Primdahl, I. I. "Developments in autothermal reforming." Studies in Surface Science and Catalysis. Vol 119. (1998).

Cui, Y., Zhang, H., Xu, H., & Li, W. "Kinetic study of the catalytic reforming of CH_4 with CO_2 to syngas over Ni/α-Al_2O_3 catalyst: The effect of temperature on the reforming mechanism." Applied Catalysis A: General, 318, 79–88 (2007).

Czekaj, I., Struis, R., Wambach, J. & Biollaz, S. "Sulphur poisoning of Ni catalysts used in the SNG production from biomass: Computational studies." Catalysis Today 176, 429-432 (2011).

Datta, A. & Cavell, R. G. "Adsorption of SO_2 on the alumina catalyst studied by FTIR and EPR spectroscopy." J. Phys. Chem. 89, 443-449 (1985).

Datta, A. & Cavell, R. G., "An FTIR Study of the sequential adsorption of SO_2 and H_2S on the alumina catalyst." J. Phys. Chem. 89, 454-457 (1985).

Davidson, J. M. & Sohail, K. "A DRIFTS study of the surface and bulk reactions of hydrogen sulfide with high surface area zinc oxide." Ind. Eng. Chem. Res. 34, 3675-3677 (1995).

Dowden, D.A., Schnell, C.R., and Walker, G.T., "The design of complex catalysts," Fourth International Congress on Catalysis, Rice University, Houston, pages 1120-1131 (1968).

Erdőhelyi, A., Fodor, K., & Solymosi F. "Reaction of CH_4 with CO_2 and H_2O over supported Ir catalyst." Studies in Surface Science and Catalysis (1997).

Erdőhelyi, A., Fodor, K., & Szailer, T. "Effect of H_2S on the reaction of methane with carbon dioxide over supported Rh catalysts." Applied Catalysis B: Environmental, 53(3), 153–160 (2004).

Epa.gov/climatechange/ghgemissions/usinventoryreport.html

Epa.gov/climate/climatechange/science/indicators/ghg/index.html

Figoli, N. S. & Argentiere, P. C. L. "Regeneration of Ni/SiO_2 poisoned with carbon disulfide." Catalysis Letters 38, 171-174 (1996).

Gangadharan, P., Kanchi, K. C., Lou, H. H. "Evaluation of the economic and environmental impact of combining dry reforming of methane with steam reforming of methane." Chemical Engineering Research and Design 90, 1956-1968 (2012).

Goula, M. A., Lemonidou, A. A., & Efstathiou, A. M. "Characterization of Carbonaceous Species Formed during Reforming of CH_4 with CO_2 over $Ni/CaO–Al_2O_3$ Catalysts Studied by Various Transient Techniques." *640*(0225), 626–640 (1996).

Gracia, F. J., Guerrero, S., Wolf, E. E., Miller, J. T. & Kropf, A. J. "Kinetics, operando FTIR, and controlled atmosphere EXAFS study of the effect of sulfur on Pt-supported catalysts during CO oxidation." Journal of Catalysis 233, 372-387 (2005).

Greene, E. F., Tauch, S., Webb, E. & Amarasiriwardena, D. "Application of diffuse reflectance infrared Fourier transform spectroscopy (DRIFTS) for the identification of potential diagenesis and crystallinity changes in teeth." Microchemical Journal 76, 141-149 (2004).

Haldor Topsoe. Steam reforming catalysts. www.haldortopsoe.com

Hashemnejad, S. M. & Parvari, M. "Deactivation and regeneration of nickel-based catalysts for Steam-methane reforming." Chinese Journal of catalysis 32, 273-279 (2011).

Hattori, S., Schmidt, J. A., Mahler, D. W., Danielache, S. O., Johnson, M. S., Yoshida, N. "Isotope Effect in the Carbonyl Sulfide Reaction with $O(^3P)$." The Journal of Physical Chemistry. (2012).

Hauchecorne, B. & Lenaerts, S. “Unravelling the mysteries of gas phase photocatalytic reaction pathways by studying the catalyst surface: A literature review of different Fourier transform infrared spectroscopy reaction cells used in the field.” Journal of Photochemistry and Photobiology C: Photochemistry Reviews 14, 72– 85 (2013).

Hickman, D. A. & Schmidt, L. D. “Production of syngas by direct catalytic oxidation of methane.” Science Magazine (2015).

Highfield, J., Prairie, M., Renken, A. “In-situ DRIFT spectroscopy in a continuous recycle reactor.” *9*, 39–46 (1991).

Hongbo, W., Xiao, W., Jianmin, C., Hongkun, Y., Huaxin, X., Xunxi, P., Huiqi, H. “Mechanism of the heterogeneous reaction of carbonyl sulfide with typical components of atmospheric aerosol.” Chinese Science Bulletin. (2004).

Hu, Y., Liu, Z., Xu, J., Huang, Y., & Song, Y. “Evidence of Pressure Enhanced CO_2 Storage in ZIF - 8 Probed by FTIR Spectroscopy.” (2013).

Hubbard, C. P., Otto, K., Gandhi, H. S., Ng, K. Y. S. “Effects of support material and sulfation on propane oxidation activity over platinum.” Journal of Catalysis, 144, 484-494 (1993).

Huber, S. & Knozinger, H. “FTIR spectroscopic studies of methane adsorption on sodium and cesium containing Y-zeolites.” Chemical Physics Letters 244, 111-116 (1995).

Jones, J. M., Dupont, V. A., Brydson, R., Fullerton, R. J., Nasri, N. S., Ross, A. B. & Westwood, A. V. K. “Sulphur poisoning and regeneration of precious metal catalysed methane combustion.” Catalysis Today 81, 589-601 (2003).

Joseph, J. & Jemmis, E. D. “Red-, Blue-, or No-Shift in Hydrogen Bonds: A Unified Explanation.” JACS Articles (2007).

Jones, J. M., Dupont, V. A., Brydson, R., Fullerton, D. J., Nasri, N. S., Ross, A. B., Westwood, A. V. K. "Sulphur poisoning and regeneration of precious metal catalyzed methane combustion." Catalysis Today, 589-601 (2003).

Kathiraser, Y., Wang, Z. & Kawi, S. "Oxidative CO_2 reforming of methane in $La_{0.6}Sr_{0.4}Co_{0.8}Ga_{0.2}O_{3-\delta}$ (LSCG) Hollow Fiber Membrane Reactor." Environmental Science and Technology 47, 14510−14517 (2013).

Kitla, A., Safonova, O. V., Fottinger, K. "Infrared studies on bimetallic copper/nickel catalysts supported on zirconia and ceria/zirconia." Springerlink.com (2013).

Kroll, V. C. H., Swaan, H. M., Lacombe, S., & Mirodatos, C. "Methane Reforming Reaction with Carbon Dioxide over Ni / SiO_2 Catalyst." (1997).

Kylhammar, L., Carlsson, P-A. & Skoglundh, M. "Sulfur promoted low-temperature oxidation of methane over ceria supported platinum catalysts." (2011).

Liu, J., Yu, Y., Mu, Y. & He, H. "Mechanism of Heterogeneous Oxidation of Carbonyl Sulfide on Al_2O_3: An *in Situ* Diffuse Reflectance Infrared Fourier Transform Spectroscopy Investigation." J. Phys. Chem. B, 110, 3225-3230 (2006).

Luo, T. & Gorte, R. J." Characterization of SO_2-poisoned ceria-zirconia mixed oxides." Applied Catalysis B: Environmental 53, 77–85 (2004).

Matsumura, Y. & Nakamori, T. "Steam reforming of methane over nickel catalysts at low reaction temperature." Applied Catalysis A: General 258, 107-114 (2004).

Mescia, D., Hernandez, S. P., Conoci, A., Russo, N., "MSW landfill biogas desulfurization." Science Direct. (2011).

Morlanés, N. “Reaction mechanism of naphtha steam reforming on nickel-based catalysts, and FTIR spectroscopy with CO adsorption to elucidate real active sites.” International Journal of Hydrogen Energy, 38(9), 3588–3596 (2013).

Nakamura, J., Aikawa, K., Sato, K. & Uchijima, T. “Role of support in reforming of CH_4 with CO_2 over Rh catalysts.” Catalysis Letters 25, 265-270 (1994).

Padley, M. B., Rochester, C. H., Hutchings, G. J. & King, F. “FTIR spectroscopic study of thiophene, SO_2, and CO adsorption on Cu/Al_2O_3 catalysts.” Journal of Catalysis 148, 438-452 (1994).

Pakhare, D., Schwartz, V., Abdelsayed, V., Haynes, D., Shekhawat, D., Poston, J. & Spivey, J. “Kinetic and mechanistic study of dry (CO_2) reforming of methane over Rh-substituted $La_2Zr_2O_7$ pyrochlores.” Journal of Catalysis 316, 78–92 (2014).

Pan, Q., Peng, J., Sun, T., Wang, S. & Wang, S. “Insight into the reaction route of CO_2 methanation: Promotion effect of medium basic sites.” Catalysis Communications 45, 74-78 (2014).

Pichas, C., Pomonis, P., Petrakis, D., Ladavos, A. “Kinetic study of the catalytic dry reforming of CH_4 with CO_2 over $La_{2-x}Sr_xNiO_4$ perovskite-type oxides.” Applied Catalysis A; General 386, 116-126 (2010).

Poulston, S. & Rajaram, R. R. “Regeneration of NO_x trap catalysts.” Catalysis Today 81, 603-610 (2003).

Priya, K. S., Abatzoglou, N., Blais, S. “Inhibition of carbon formation during steam reforming of methane over ethyldisulfide-impregnated metallic nickel catalysts.” Catalysis Today 207 21-27 (2012).

Rahemi, N., Haghighi, M., Babaluo, A. A., Jafari, M. F., & Estifaee, P. "Synthesis and physicochemical characterizations of $Ni/Al_2O_3–ZrO_2$ nanocatalyst prepared via impregnation method and treated with non-thermal plasma for CO_2 reforming of CH_4." Journal of Industrial and Engineering Chemistry, 19(5), 1566–1576 (2013).

Rahemi, N., Haghighi, M., Babaluo, A. A., Jafari, M. F., & Estifaee, P. "Syngas production via CO_2 reforming of methane over plasma assisted synthetized $Ni-Co/Al_2O_3-ZrO_2$ nanocatalysts with different Ni loadings." International Journal of Energy Research. (2013).

Rangan, M., Yung, M. M., & Medlin, J. W. "Experimental and computational investigations of sulfur-resistant bimetallic catalysts for reforming of biomass gasification products." Journal of Catalysis, 282(2), 249–257 (2011).

Reding, F. P., & Hornig, D. F. "Vibrational Spectra of Molecules and Complex Ions in Crystals. X. H_2S and D_2S." The Journal of Chemical Physics, 27(5) (1957).

Rest, A. J., Warren, R., Murray, S. C. "Assignment of the overtones and combination bands for liquid methane across the near infrared spectrum." (1996).

Rodrigues, L. M. T. S., Silva, R. B., Rocha, M. G. C., Bargiela, P., Noronha, F. B., Brandao, S. T. "Partial oxidation of methane on Ni and Pd catalysts: Influence of active phase and CeO_2 modification." Catalysis Today 197, 137-143 (2012).

Rodriguez, J. A., Jirsak, T., Hrbek, J. "Reaction of SO_2 with cesium and cesium-promoted ZnO and MoO_2." J. Phys. Chem, 103, 1966-1976 (1999).

Rostrup-Nielsen, J., Hansen, J. "CO_2 Reforming of methane over Transition metals." Journal of Catalysis, 144, 38-49 (1993).

Rostrup-Nielsen, J. R. "Promotion by poisoning." Catalyst Deactivation (1991).

Rostrup-Nielsen, J. R., "Sulfur-passivated nickel catalysts for carbon-free steam reforming of methane." Journal of Catalysis, 85, 31-43 (1984).

Rostrup-Nielsen, J. R., "New aspects of syngas production and use." Catalysis Today 63, 159-164 (2000).

Ruckenstein, E., & Hu, Y. H. "Carbon dioxide reforming of methane over nickel/alkaline earth metal oxide catalysts." Applied Catalysis A: General, 133(1), 149–161 (1995).

Ruckenstein, E. & Wang, H. Y. "Carbon dioxide reforming of methane to synthesis gas over supported cobalt catalysts." Applied Catalysis A: General 204, 257-263 (2000).

Saha, B., Khan, A., Ibrahim, H. & Idem, R. "Evaluating the performance of non-precious metal based catalysts for sulfur-tolerance during the dry reforming of biogas." Fuel 120, 202–217 (2014).

San-José-Alonso, D., Juan-Juan, J., Illán-Gómez, M. J., & Román-Martínez, M. C. "Ni, Co and bimetallic Ni–Co catalysts for the dry reforming of methane." Applied Catalysis A: General, 371(1-2), 54–59 (2009).

Sato, K., & Fujimoto, K. "Development of new nickel based catalyst for tar reforming with superior resistance to sulfur poisoning and coking in biomass gasification." Catalysis Communications, 8(11), 1697–1701 (2007).

Scarano, D., Bertarione, S., Spoto, G., Zecchina, A., & Arean, C. O. "FTIR spectroscopy of hydrogen, carbon monoxide and methane adsorbed and co-adsorbed on zinc oxide." (2001).

Schuurman, Y., Marquez-Alvarez, C., Kroll V. C. H., Mirodatos, C. "Unraveling mechanistic features for the methane reforming by carbon dioxide over different metals and supports by TAP experiments." Catalysis Today 46 185-192 (1998).

Schwack, P., Hamilton, N., Eichelbaum, M., Thum, L., Lunkenbein, T. & Schlogl, R. "Structure sensitivity of the oxidative activation of methane over MgO model catalysts: II. Nature of active sites and reaction mechanism." Journal of Catalysis 329, 574-587 (2015).

Sehested, J. "Sintering of nickel steam-reforming catalysts." Journal of Catalysis, 217, 417–426 (2003).

Sehested, J. "Sintering of nickel steam-reforming catalysts: effects of temperature and steam and hydrogen pressures." Journal of Catalysis, 223(2), 432–443 (2004).

Shakouri, M. "Effects of preparation, Ni/Co ratio and sulfure poisoning of Ni-Co bimetallic catalysts for dry reforming reaction." A thesis submitted to the College of Graduate Studies and Reearch. University of Saskatchewan. (2011).

Silverstein, R. M., Webster, F. X., Kiemle, D. J. "Spectrometric identification of organic compounds." 7ed- Webster & kiemle.pdf. John Wiley & Sons, Inc. (2005).

Smith, B. C. "Infrared spectral interpretation." A Systematic Approach. CRC Press. (1999).

Song, C. & Pan, W. "Tri-reforming of methane: a novel concept for catalytic production of industrially useful synthesis gas with desired H_2/CO ratios." Catalysis Today 98, 463-484 (2004).

Sun, H. "Preparation and Evaluation of Sol-Gel Made Nickel Catalysts for Carbon Dioxide Reforming of Methane." University of Saskatchewan MSc thesis. (2005).

Takanabe, K., Nagaoka, K., Nariai, K., & Aika, K. "Titania-supported cobalt and nickel bimetallic catalysts for carbon dioxide reforming of methane." Journal of Catalysis, 232(2), 268–275 (2005).

Taleghani, G., Kia, A. S. "Technical-economical analysis of the Saveh biogas power plant." Renewable Energy 30, 441-446 (2005).

Tang, S., Ji, L., Lin, J., Zeng, H. C., Tan, K. L., & Li, K. "CO_2 Reforming of Methane to Synthesis Gas over Sol–Gel-made Ni/γ-Al_2O_3 Catalysts from Organometallic Precursors." Journal of Catalysis, 194(2), 424–430 (2000).

Teuner, S. C., Neumann, P., Von Linde, F. "The Calcor standard and Calcor economy processes." OIL GAS European Magazine (2001).

Toops, T. J. & Crocker, M. "New sulfur adsorbents derived from layered double hydroxides II. DRIFTS study of COS and H_2S adsorption." Applied Catalysis B: Environmental 82 , 199–207 (2008).

Tsipouriari, V. A., Verykios, X. E. "Carbon and oxygen reaction pathways of CO_2 reforming of methane over Ni/La_2O_3 and Ni/Al_2O_3 catalysts studied by isotopic tracing techniques." Journal of Catalysis 187, 85-94 (1999).

Tsipouriari, V. A., & Verykios, X. E. "Kinetic study of the catalytic reforming of methane with carbon dioxide to synthesis gas over Ni/La_2O_3 catalyst." Catalysis Today 64, 83–90 (2001).

Udengaard, N.R.; Hansen, J.-H. B.; Hanson, D. C.; Stal, J. A., "Sulfur passivated reforming process lowers syngas H_2/CO ratio", Oil & Gas Journal, 90, 62 (1992).

Wang, H., Miller, J. T., Shakouri, M., Xi, C., Wu, T., Zhao, H., Akatay, M. C. "XANES and EXAFS studies on metal nanoparticle growth and bimetallic interaction of Ni-based catalysts for CO_2 reforming of CH_4." Catalysis Today 207, 3-12 (2013).

Wilhelm, D. J., Simbeck, D. R., Karp, A. D., Dickenson, R. L. "Syngas production for gas-to-liquids applications: technologies, issues and outlook." Fuel Process Technology 71, 139-148 (2001).

Yadav, L. D. S. "Organic spectroscopy." Springer-Science+Business Media, B.V. (2005).

Zhang, J., "Research and development of nickel based catalyst for carbon dioxide formation of methane." PhD thesis, department of chemical engineering, University of Saskatchewan (2008).

Zhang, J., Wang, H., & Dalai, A. "Development of stable bimetallic catalysts for carbon dioxide reforming of methane." Journal of Catalysis, 249(2), 300–310 (2007).

Zhang, J., Wang, H. & Dalai, A. K. "Effects of metal content on activity and stability of Ni-Co bimetallic catalysts for CO_2 reforming of CH_4." Applied Catalysis A: General 339, 121-129 (2008a).

Zhang, J., Wang, H. & Dalai, A. K. "Kinetic Studies of Carbon Dioxide Reforming of Methane over Ni-Co/Al-Mg-O Bimetallic Catalyst". Ind. Eng. Chem. Res. 2009, 48, 667-684 (2009b).

Zhang, J., Wang, H., Xi, C., Shakouri, M., Hu, Y. & Dalai, A. K. "Design and Preparation of Ni-Co Bimetallic Nanocatalyst for Carbon Dioxide Reforming of Methane." American Chemical Society (2012).

Zhao, L., Li, X., Quan, X. & Chen, G. "Effects of Surface Features on Sulfur Dioxide Adsorption on Calcined NiAl Hydrotalcite-like Compounds." Environ. Sci. Technol. 45, 5373–5379 (2011).

APPENDIX A: FUNDAMENTALS OF FTIR SPECTROSCOPY

Since FTIR spectroscopy was the main technique used to conduct this research, it will be described the fundamentals of this technique in the following paragraphs,

Infrared spectroscopy is the recording of the absorption of photons in the infrared region of the electromagnetic spectrum. The infrared radiation is a range in the electromagnetic spectrum between 14000-4 cm^{-1} as shown in Figure A-1.

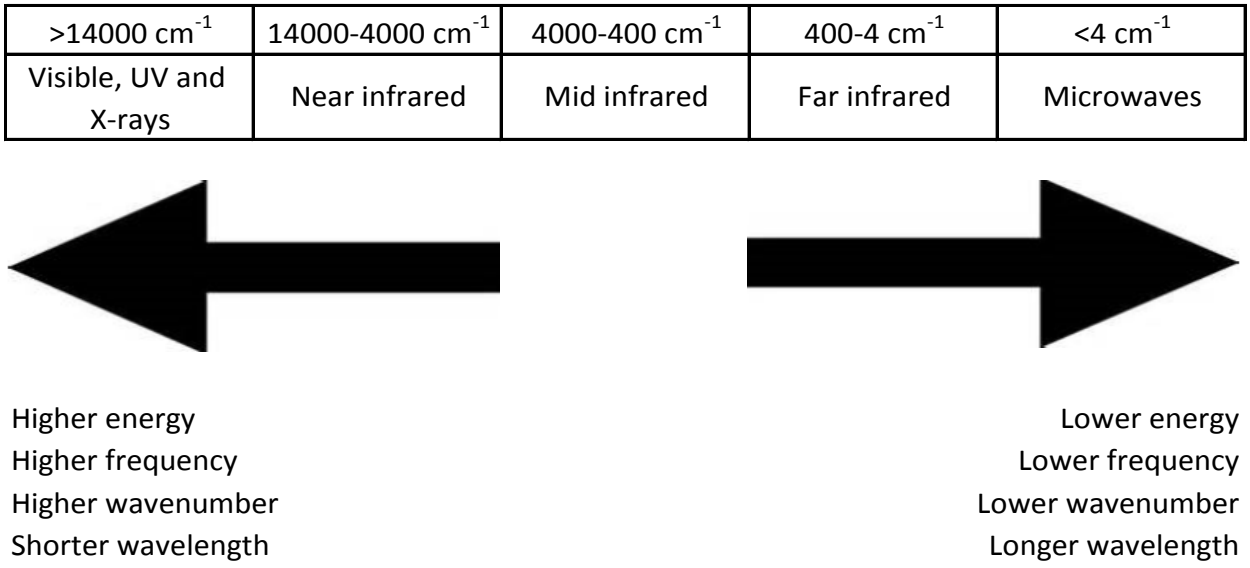

Figure A-1. The electromagnetic spectrum.

The conversion between wavenumber, energy, frequency and wavelength can be carried out with the following formulas (Smith, 1999).

Wavenumber to wavelength.

$W=1/\lambda$ (A-1)

where W=wavenumber in cm^{-1} and λ= wavelength in cm^{-1}.

Wavelength to frequency.

$\lambda=c/\nu$ (A-2)

where c=the speed of light ($3x10^{10}$ cm/second) and ν= frequency in Hertz (sec^{-1}).

Energy to wavelength.

$E=hcW$ (A-3)

where E= photon energy in eV and h= Planck´s constant ($4.14x10^{-15}$ eV-second).

Infrared radiation causes quantized vibrational and rotational changes when it is absorbed by molecules. Therefore, infrared spectroscopy is also called vibrational-rotational spectroscopy (Yadav, 2005). Infrared radiation below 100 cm^{-1} causes transitions in the rotational energy of the molecule, producing discrete lines in the spectra. On the contrary, infrared radiation in the range 100-10000 cm^{-1} produces transitions in the vibrational energy levels. In this case, the vibration of the molecules are noticed in the spectra as bands rather than as lines. Most of the chemists employ infrared spectroscopy in the range 4000-667 cm^{-1} (Yadav, 2005).

Vibration in a molecule is caused when a photon with the necessary energy impinges a molecule. This vibration, or mode, is generally of two types: stretching vibration or bending vibration.

(Yadav, 2005). Stretching vibrations involve the contraction or lengthening of two atoms in the same original bond axis. Stretching vibrations can be of two types: symmetric and antisymmetric. Symmetric stretching vibrations occur when the movements of two atoms with respect to the same common atom is in the same direction along the same bond axis. On the contrary, antisymmetric vibration involves the movement of two different atoms with respect to the same common atom in different directions (Figure A-2).

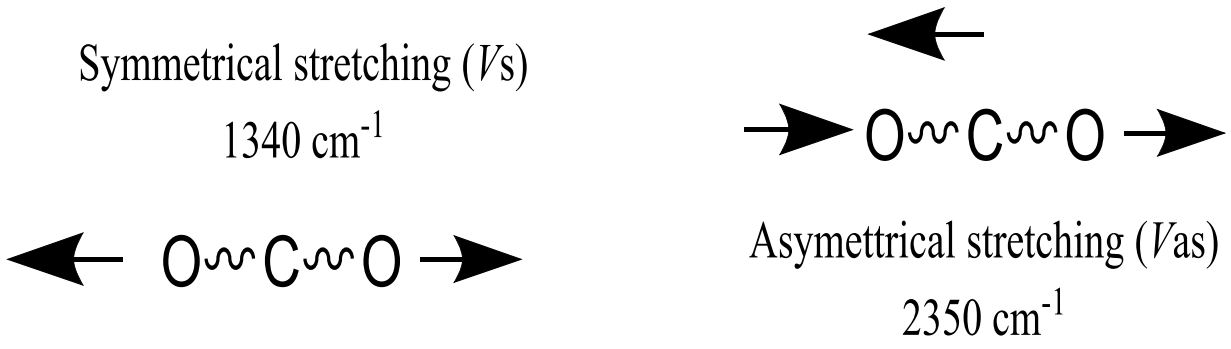

Figure A-2. Stretching vibrations (symmetrical and asymmetrical) of the CO_2 molecule (Silverstein et al., 2005).

Bending vibration occurs when two atoms in a bond change of position with respect to the original bond axis. There are four types of bending vibrations: scissoring, rocking, wagging and twisting (Figure A-3).

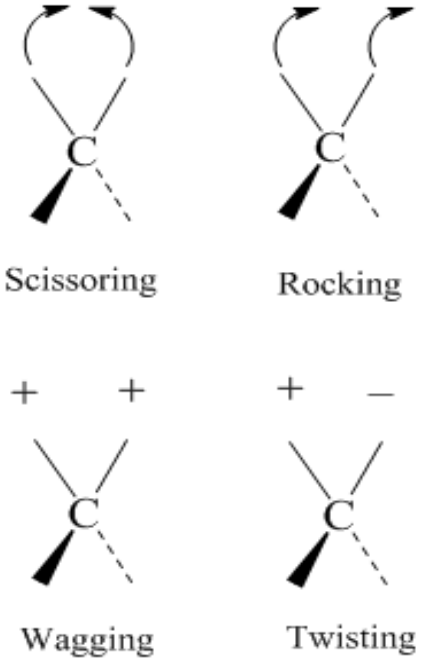

Figure A-3. Bending vibrations for a CH_2 group (+ and – denote movements perpendicular to the plane of the sheet) (Yadav, 2005).

Infrared spectra display only vibrations that result in a change in the dipole moment in a molecule. In some cases bands cannot be observed such as fundamental vibrations that coalesce and appear as one; very weak bands or; degenerate bands caused by various absorptions of the same frequency in symmetrical molecules (Silverstein et al., 2005).

Different Fourier Transform Infrared Spectroscopy Techniques exist such as Transmission-Absorption Spectroscopy and Diffuse Reflectance Infrared Spectroscopy.

Transmission-Absorption spectroscopy is useful only if the sample absorbs infrared radiation weakly. In this method, the radiation is transmitted through a sample, and the molecules in the sample will absorb part of the energy. The negative logarithm of the ratio of the energy received

over the transmitted energy (Equation A-4) generates a spectrum in absorbance units. In this technique, the spectra follow the Lambert-Beer Law and therefore it is possible to obtain quantitative information.

$$\text{Absorbance}=-log_{10}\left(\frac{\Phi^{i}}{\Phi^{t}}\right) \quad \text{(A-4)}$$

where ϕ^{i} is the radiant energy received by the sample and ϕ^{t} is the radiant energy transmitted by the sample.

Other FTIR spectrometric technique is Diffuse Reflectance Infrared Fourier Transform Spectroscopy (DRIFTS). The radiation focused on a molecule could either be absorbed, directly reflected (in a specular manner for polished surfaces) or diffused in all directions. This last effect is exploited by Diffuse Reflectance Infrared Fourier Transform Spectroscopy (Armaroli et al., 2004). For DRIFTS, the Lambert-Beer law used in Transmission-Absorption spectroscopy is not applicable and instead the Kubelka-Munk equation is applied (Hauchecorne and Lenaerts, 2013):

$$\text{KM}=\frac{(1-R_{\infty})^{2}}{2R_{\infty}}=\frac{k}{s}=\frac{2.3\varepsilon c}{s} \quad \text{(A-5)}$$

where KM is the Kubelka-Munk dimensionless unit, R_{∞} is the reflectance of an infinitely thick layer, k is the absorption coefficient, s is the diffusion or scattering factor, ε is the molar absorptivity and, c is the sample concentration. The scattering coefficient depends on the wavelength of the photon, particle size and shape. It is possible to obtain quantitative information by DRIFTS when the scattering coefficient is constant. However, this condition is hardly achieved (Hauchecorne and Lenaerts, 2013). Other properties of the sample that affect the

DRIFTS spectra are the refractive index, packing density, homogeneity, concentration and absorption coefficients (Armaroli et al., 2004). If the sample is very absorbent, it could significantly affect the spectra, making it necessary to dilute the sample in KBr or another non-absorbent matrix.

DRIFTS, although less used than transmission infrared spectroscopy, is a very valuable technique to characterize non-transparent materials in situ at elevated temperatures. One advantage of this method is the easiness of sample preparation (Armaroli et al., 2004). DRIFT spectra can be collected in absorbance units as well as in Kubelka-Munk units (Greene et al., 2004). The main disadvantages of this technique are the difficulty in obtaining quantitative measurements and repetitive measurements due to differences in sample preparation in different experiments. Since the temperature affects the bandwidth and intensity, it is important to collect the spectra at the same temperature if samples need to be compared (Armaroli et al., 2004).

In the present work, some of the spectra are expressed in absorbance units and others are expressed in Kubelka-Munk (KM) units.

3.4.1 Factors that affect the vibrational frequencies

Symmetric vibrations can be approximately calculated by the Hooke's law when two atoms and their connecting bond are treated as two masses united by a spring. The Hooke's law relates the frequency of the vibration, the force constant of the connecting bond and the two atomic masses united by the bond according to Equation A-6.

$$\bar{\nu} = \frac{1}{2\pi c}\sqrt{\frac{f}{(MxMy)/(Mx+My)}} \qquad \text{(A-6)}$$

where $\bar{\nu}$ is the vibrational frequency in cm^{-1}; *c* is the speed in light in cm/s; *f* is the force constant of the bond in dyne/cm; *Mx* and *My* represent the mass in grams of the atoms x and y, respectively. The force constant (*f*) is approximately $5x10^5$ dyne/cm for single bonds and nearly twice and thrice for double and triple bonds, respectively (Silverstein et al., 2005).

Sometimes there are differences between the frequencies of bands in a spectrum and the expected frequencies calculated by the Hooke Law. Electronic and steric effects of other groups in a molecule can change the force constants of a bond. Some factors responsible for the shifts in a vibrational frequency can be:

Coupled vibrations: This is caused by two or more of the same bonds in a molecule. For example, there are differences between C-H, CH_2 and CH_3 functional groups. For a C-H group, only one symmetric vibration should occur. However, for CH_2, symmetric and asymmetric vibrations can occur (Yadav, 2005).

Hydrogen bonding: When hydrogen bonds to a functional group, there is a considerable decrease in the frequency of the resulting bond. Hydrogen bonding also changes the shape and intensity of a vibration band, causing the bands to appear more intense and broader. If the hydrogen bond is stronger, the O-H stretching frequency is lower.

In infrared spectra, besides the fundamental vibrational frequencies of the molecules (transition from v=0 to v=1), it is common to find additional peaks that could be caused by combination bands, overtones or Fermi resonance.

Combination bands could appear on the infrared spectra if two or more fundamental vibrations are excited at the same time. A combination band can be found at wavenumbers approximately equal to the sum of different frequencies. However, difference bands are also possible, and the vibration frequencies are subtracted.

Overtones occur when a molecule is excited from v=0 to v=2 or from v=0 to v=3. However, the possibility of overtone decreases as $v=\pm n$ increases. The energy necessary for an overtone transition will be n times the fundamental transition for harmonic oscillator approximation or usually less than a multiple of the fundamental wavenumber according to anharmonic oscillator calculations.

Fermi resonance results in the splitting of two vibrational bands that have nearly the same energy and symmetry in both IR and Raman spectroscopy. The two bands are usually a fundamental vibration and either an overtone or combination band. The wave functions for the two resonant vibrations mix according to the harmonic oscillator approximation, and the result is a shift in frequency and a change in intensity in the spectrum. As a result, two strong bands are observed in the spectrum, instead of the expected strong and weak bands. It is not possible to determine the contribution from each vibration because of the resulting mixed wave function.

Enrico Fermi observed this phenomenon for the first time in a CO_2 molecule. The explanation for this is that the molecule transfers its energy from fundamental vibration to overtone or combination band level back and forth, causing a pair of transitions of almost equal intensity. Therefore, the resulting absorption bands appear as a doublet or as two bands.

APPENDIX B: WAVENUMBERS OF FUNCTIONAL GROUPS

A list of the wavenumbers for the vibrations of the functional groups relevant to this study is presented in the following tables.

Table B-1. Vibrations attributed to OH^- functional groups.

Wavenumber cm^{-1}	Vibration	References
3707, 3682, and 3641	Ni-OH	Kroll et al., 1997
3615	NiO-OH	Bradford and Albert, 1996

Table B-2. Vibrations attributed to carbonates.

Wavenumber cm-1	Vibration	References
1653, 1434 and 1227	Hydrogen carbonate	Pan et al., 2014
1650-1300	Carbonate species	Morlanés, 2013
1640	Carbonates on support in NiMgAl.	Morlanés, 2013
1560, 1450, 1267, 1181, 1010, and 903	Carbonates, presumably produced in a reaction of CO_2 with surface oxide ions.	Kathiraser et al., 2013

Table B-3. Vibrations attributed to H_2S or species produced by H_2S.

Wavenumber cm^{-1}	Vibration	References
2570	Chemisorbed H_2S and HS^-	Toops and Crocker, 2008
2535	SH^-	Reding and Hornig, 1957
2532	H_2S	Reding and Hornig, 1957
2530	SH^-	Davidson and Sohail, 1995
1349	H_2S	Reding and Hornig, 1957

Table B-4. Vibrations attributed to SO_2 or species produced by SO_2.

Wavenumber cm^{-1}	Vibration	References
1374 and 1360	Gaseous SO_2	Padley et al., 1994
1360, 1290, 1170 and 1045	Aluminum sulfate	Gracia et al., 2005
1354	SO_4^{2-} species	Liu et al., 2006
1335	$\nu_{as}(SO_2)$	Padley et al., 1994
1330-1300	Physisorbed SO_2	Toops and Crocker, 2008
1220 and 980	Surface sulfites and hydrogen sulfites SO_3^{2-}	Luo and Gorte, 2004
1149	ν_s (SO_2)	Padley et al., 1994
1135-1189	Physisorbed SO_2	Toops and Crocker, 2008
1055	SO_2 adsorbed on alumina.	Datta and Cavell, 1985

Table B-5. Vibrations attributed to carbonyl sulfide.

Wavenumber cm^{-1}	Vibration	References
2071	Carbonyl sulfide	Hattori et al., 2012
2070	Carbonyl sulfide	Barnes et al., 1995
2069 and 2046	Carbonyl sulfide	Hongbo et al., 2004

Table B-6. Vibrations attributed to CH_4.

Wavenumber cm^{-1}	Vibration	References
3850	$3\nu_4$ overtone of methane	Rest et al, 1996
3020	υ_3 Free methane	Scarano et al, 2001
3010	$\upsilon 3$ mode of methane	Rest et al, 1996
2853	Symmetrical stretching (ν_s CH_2)	Silverstein et al, 2005
2815	$\upsilon_2+\upsilon_4$ combination band	Rest et al., 1996
2594	Overtone peak of methane $2\nu_4$	Rest et al., 1996
1535	υ_2 mode of methane	Rest et al., 1996
1308	ν_4 bending mode	Scarano et al., 2001
1300	υ_4 mode of methane	Rest et al., 1996

Table B-7. Vibrations attributed to CO_2.

Wavenumber cm^{-1}	Vibration	References
3700	$\upsilon_3+\upsilon_1$ Combination modes	Hu et al., 2013
3600	$\upsilon_3+2\upsilon_2$ Combination modes	Hu et al., 2013
2359 and 2330	CO_2 gas phase	Kroll et al., 1997
2350	Assymmetrical stretching (υ_{as} o υ_3 CO_2)	Silverstein et al., 2005
1384	Adsorbed gaseous CO_2	Kathiraser et al., 2013
1340	Symmetrical stretching (υ_s o υ_1 CO_2) IR inactive	Silverstein et al., 2005
665	Scissoring (bending) (δ_s o υ_2 CO_2)	Silverstein et al., 2005

Table B-8. Vibrations attributed to CO.

Wavenumber cm^{-1}	Vibration	References
2181 and 2121	Gaseous CO	Bachiller Baeza et al., 2013
2175 and 2115	Gaseous CO	Kroll et al., 1997
2100-1900	Strong CO-metal bound carbonyl peaks either in linear or bridged form	Kathiraser et al., 2013
2072-2056	Linear carbonyl	Morlanés, 2013
2050	Linear CO	Bradford and Albert, 1996
2050 and 1935	Linear and bridged CO	Bradford and Albert, 1996
2040	CO adsorbed linearly on reduced Ni sites	Bachiller-Baeza et al., 2013
2034, 1950	Linear and bridged carbonyl, respectively	Morlanés, 2013
Around 2030	Linear CO	Bachiller-Baeza et al., 2013
2012 and 1855	CO, linear and multibonded, respectively	Kroll et al., 1997
Around 1905	Bridge CO	Bachiller-Baeza et al 2013
1801	CO on cobalt metal sites	Kathiraser et al., 2013